EFFECTS OF THERMOMECHANICAL PROCESSING ON THE MICROSTRUCTURE, TENSILE STRENGTH AND PLASTICITY INDICES OF 6063 ALUMINIUM ALLOY

BY

OMOTOYINBO JOSEPH AJIBADE

M.Sc (Metallurgical & Materials Engineering)

A THESIS IN THE DEPARTMENT OF METALLURGICAL AND MATERIALS ENGINEERING SUBMITTED TO THE SCHOOL OF POSTGRADUATE STUDIES IN PARTIAL FULFILMENT OF THE REQUIREMENTS FOR THE AWARD OF DOCTOR OF PHILOSOPHY (Ph.D) DEGREE IN METALLURGICAL AND MATERIALS ENGINEERING OF THE FEDERAL UNIVERSITY OF TECHNOLOGY, AKURE, NIGERIA.

FEBRUARY 2008.

CERTIFICATION

We certify that Engr. J.A. Omotoyinbo of the Department of Metallurgical and Materials Engineering, Federal University of Technology Akure, carried out this study.

Prof. J.S.O. Adeniyi

(Major Supervisor)

Prof. J.O. Borode

(Co-Supervisor)

Dr. J.O.T. Adewara

Head of Department/ (Co-Supervisor)

DEDICATION

This work is dedicated to the GOD ALMIGHTY, whose grace sustained my life until today. He lifted me up severally from the valley of death and often silently reminded me, "to succeed you must not quit, I am a God that never fails."

ACKNOWLEDGMENT

I would like to thank Professor J.S.O Adeniyi (the Major Supervisor of this work), whose supervision has been invaluable. The assistance he provided in the form of advice and fruitful discussions was always useful and sometimes a source of inspiration. Likewise my sincere appreciation goes to Prof. J.O. Borode (the Co-Supervisor of this work), for his moral and academic support. I will forever be grateful for all the pains you endured in ensuring that this work came to a logical conclusion.

I am also indebted to my Head of Department, Dr. J.O.T.Adewara for his numerous and far-reaching contributions to the success of this project.

My profound gratitude goes to Prof. K. Ipinmoroti of the Department of Chemistry, who in his capacity as the Deputy Vice Chancellor (Academics) encouraged me to put more effort towards the successful completion of the work.

The assistance of Prof. P.A. Akinola of the Department of Mathematics, Obafemi Awolowo University, Ile-Ife in modeling is very much appreciated, and I sincerely thank him for his encouragement.

I would like to seize this opportunity to remember Late Prof. O.T. Adepoju, the Foundation Dean of the School of Engineering and Engineering Technology (SEET) and the most senior colleague in the department of Metallurgical and Materials Engineering, Federal University of Technology, Akure. The legacy of hard work and togetherness he left behind continues to thrive.

I do acknowledge the contributions of the subsequent Deans of the School of Engineering and Engineering Technology for sustaining the enabling environment that allowed the school to progress, and in particular, I must thank the current Dean of SEET, Prof. A.S. Ogunlowo for his unalloyed encouragement.

My thanks go to Dr A.M. Oguntuase, Dr M.O. Alatise and Prof O.T. Fapetu for their encouragements. I would also like to express particular appreciation to Dr B.O. Adewuyi, Prof. John Ade Ajayi, and all other academic and non-academic staff members of the Metallurgical and Materials Engineering department for their prayers and moral support. Same goes to my colleagues and friends in other departments in SEET.

I wish to acknowledge the materials assistance received from the Nigerian Aluminium Extrusion Company (NIGALEX), and Tower Aluminium Rolling Mills both in the Lagos metropolis.

Deformation and heat treatment facilities as well as technical assistance were generously made available by the Federal University of Technology, Akure (FUTA), Engineering Materials Development Institute (EMDI), Akure, Obafemi Awolowo University, (OAU), Ile-Ife, University of Lagos,(UNILAG), and SCUBA METALS, a privately owned heat treatment outfit in Lagos.

The immense contributions of my friends and colleagues in the diasporas are particularly recognized, Prof. AB Ogwu of the University of Paisley, Paisley, Scotland, and Dr A.G. Odeshi of the University of Manitoba, Winnipeg, Canada.

I thank the Federal University of Technology, Akure for granting me the opportunity for this research through the Staff Development Programme. Mr. Muyiwa Babafemi is appreciated for his assistance in word processing.

My gratitude goes to my wife, Rose and my children, for their understanding, patience and pains throughout the period of this work.

Finally, I commit all those that contributed to the success of this work in one form or the other to the mercy and blessings of God Almighty.

J.A. Omotoyinbo

February 2008.

TABLE OF CONTENT

LIST OF TABLES

LIST OF FIGURES

LIST OF PLATES

LIST OF SYMBOLS

Symbol	Definition
"G-P Zones"	Guinier-Preston zones
β''	fully coherent precipitate
β'	semi coherent precipitate
β	stable, incoherent precipitate
σ_{UTS}	Ultimate tensile strength (N/mm^2)
$\sigma_{0.2}$	Proof Stress (N/mm^2)
σ_0	Nominal yield strength of matrix.
$\%\varepsilon$	Percentage elongation
ω_{exp}	Experimental Impact energy (J)
ω_{imp}	Model Impact energy (J)
T^oC	Temperature in degree Celsius
F	Free energy
ΔF_{ir}	Energy barrier of nucleation.
S	Surface area (m^2)
γ	Free energy per unit area
γ_{eff}	Effective interface energy
$\Delta F_{cr}^{GP}, \Delta F_{cr}^{\beta'}, \Delta F_{cr}^{\beta}$	Energy barrier of nucleation of GP-zones, β' and β precipitates respectively.
J	Rate of precipitate nucleation
Q	Activation energy of passage of an atom through an interface
e	Exponential constant
K	Boltsmann constant
A	Experimental Constant
G	Shear modulus
E_L	Energy of dislocation per unit length.

r_p	Radius of particle
γ_α	Staking fault energy of matrix
γ_β	Stacking fault energy of precipitated phase
r_c	Radius of semicircular dislocation.
ψ	Poisson's ratio
b	Burger's length
$\gamma_{\alpha\beta}$	Energy of particle-matrix interface
Fmax	Repulsive force (per unit length)
l_i^0	Distance between dislocation-pinning precipitates
τ	Resolved shear stress
η	Scaling factor
l_f	Friedel length
τ_{eq}	Equilibrium shear stress
Ca	Concentration of particles in the glide plane
T_m	melting temperature
λ	interparticle spacing
α	stress dependent parameter
ρ	density of dislocation
α –sss	supersaturated solid solution
P_b	gain in boundary energy
P_a	gain in surface energy
P_{dr}	gain in free energy/mole
M	mobility of grain boundary
J	rate of precipitates nucleation in an ageing alloy
$T_{G.P}$	solvus temperature for G.P zone
V	rate of boundary migration of grain boundary.
t_r'	recrystallization temperature

ABSTRACT

An investigation has been carried out on the effect of the variation of thermomechanical processing parameters on the microstructure, tensile strengths and plasticity indices of 6063 Aluminium alloy. It is intended to determine the possibility of developing a high tensile strength-plasticity indices alloy through refining of microstructure by thermomechanical ageing route, thereby expanding the horizon of its applications in machine building, automobile, architecture and civil engineering industries. The as received alloy samples were solution heat treated (SHT) at 530^0C for 2hours and quenched in water to room temperature. The study involved initial characterization of the thermoplastically worked Al-Mg-Si alloy, after solution heat treatment, as a singular operation employing varying degrees of plastic deformation (10%-50%) at different working temperatures (28^0C, 160^0C, 180^0C, 200^0C, 220^0C and 240^0C). Similarly, artificial ageing of the solution heat treated alloy samples was carried out at different ageing times (1-20hrs) and temperatures (160^0C, 180^0C, 200^0C, and 220^0C), followed by the characterization of the aged alloy samples. Both thermoplastic working and artificial ageing were carried out as preliminary studies. Finally, the solution heat treated alloy was subjected to various thermomechanical ageing treatments in order to give room for a exhaustive assessment of the effects of process variables (degree of preageing, % deformation, deformation temperature, final ageing time and temperature) on the microstructure, tensile strengths and plasticity indices of the 6063 Aluminium alloy. Tensile and impact tests were carried out on the processed alloy samples as means of property assessment, as well as microstructural examinations using the optical and transmission electron microscopes. Attempt was also made to develop mathematical models capable of relating tensile strength and plasticity as a function of processing parameters. The

results show that thermomechanical processing has significant effect on the microstructure, tensile strengths and plasticity of the alloy.

Precisely the properties were enhanced within certain ranges of the values of the processing parameters, while same properties were impoverished within some ranges of the values of the processing variables. However, thermomechanical ageing processing route TMAIIIC(9hrs preageing time, 30% warm deformation, 10hrs final ageing time and water quenched to room temperature), produced the best results in terms of tensile strength-plasticity indices of the alloy. It is therefore concluded that thermomechanical ageing techniques could be a highly useful tool for developing higher strength-plasticity property in age-hardenable alloys, as demonstrated in the studied 6063 Aluminium alloy. Likewise, improved understanding of the fundamental mechanisms of alloy strengthening by thermomechanical ageing can by appropriate process control, help in the creative task of alloy development. The success of an alloy development effort, of course, always depends on the competition with existing materials, and on the search for new demanding applications on the part of industrial alloy users. Scientifically and technologically, thermomechanical ageing is ready for such a challenge, in particular for age-hardenable alloys.

1.0 INTRODUCTION

The evolution of new engineering materials has opened the way for new designs and structures, especially in machine building, automobile, and civil engineering industries. Among these new materials are various Aluminium alloys and Aluminium matrix composites. Because of their lightweight and high strength-to-weight ratio, they are employed extensively in aircrafts, machine building, automobiles and structural works.

An understanding of how these materials behave in service life is essential for their continued application in industry, and everyday life since their lifetime depend on the level or pattern of response to service conditions. The materials must *ab initio* possess good properties, such that the level of damage experience by them is significantly low during normal service life. By damage, any irreversible change to the thermomechanical properties of the material (Melvin, 1991) is intended.

Very important service factors are load and temperature. Both factors can separately or jointly bring about appreciable change in shape and size of materials. Essentially, thermomechanical processing changes the grain size, grain boundary structure, dislocation structure, and other substructures. It is well known that mechanical deformation causes temperature changes, but they go unnoticed if the loading is slow, resulting in an isothermal process. Under fast loading conditions and extensive deformation, considerable heating can occur leading to localized melting, and this may contribute to fatigue failure. Analysis of the temperature response to deformation provides information on the structural state of a material, i.e. its thermomechanical history.

It is the object of this thesis to discuss the changes in structure and properties occurring in Al-Mg-Si alloy following the exposure to various regimes of thermoplastic working and thermomechanical ageing treatments.

1.1 AIM AND OBJECTIVES

The aim of this research work is to investigate the possibility of developing a high tensile strength-plasticity indices Al-Mg-Si alloy through refining of microstructure by thermomechanical ageing route, thereby expanding the horizon of its applications in machine building, automobile, architecture and civil engineering industries.

Specific objectives of the research are to;

(a) determine the properties of the Al-Mg-Si alloy prior to thermomechanical ageing;

(b) evaluate the effect of thermomechanical ageing processing variables on 6063 Aluminium alloy;

(c) examine the relationship between the microstructure and the properties of the processed alloy;

(d) establish an optimum value for the thermomechanical ageing processing variables; and

(e) develop a model describing tensile strength and plasticity as a function of processing parameters.

The research work on completion is envisaged to;

(i) Provide an established framework for the understanding of the thermomechanical ageing mechanisms in a typical 6063 Aluminium (Al-Mg-Si) alloy;

of the metal's unique range of properties which, without doubt are still undervalued. In the same vein a series of educational programmes on Aluminium have been embarked upon in Europe, Japan and America, for the next generation of designers and specifiers, aimed at all levels from primary schools to universities and polytechnics.

Furthermore, and borrowing the words of Byko (2000), "Aluminium has sided our houses and contained our beer. Since the 1940s, it has had its place in the everyday landscape of modern living".

In a World-wide exhibition tagged "Sheen of Silver, Weight of Air", opened in October 28, 2000 and continued through February 11,2001 at the Schneider Museum of Art, Southern Oregon University, USA, over 350 items covering all facets of Aluminium were displayed, including its place in architecture, jewelry, the automobile industry and day-to-day life.

Marvelled, by the versatility of Aluminium, one of the participants in the exhibition, Sarah Nichols remarked that, "there are two new materials that have sort of revolutionized how we lived in the 20th century; they are Aluminium and plastic".

Based on the versatility of Aluminium, the world of science and technology is interested in harnessing for the benefit of mankind this ubiquitous material, and has necessitated researches into the development of aluminium alloys for engineering applications.

In 1906, Wilm developed and patented the Aluminium-Copper-Magnesium alloys, which then became well known as duralumin, based on their age hardening properties. This phenomenon was previously unknown and although the alloys were used

during the First World War, the explanation and exploitation of age hardening was not forth coming until the early 1920s (West, 1986).

Better strength Aluminium alloys were again developed in the 1940s, the Aluminium-Zinc-Magnesium types. These are however, susceptible to corrosion and it is only recently that their application has become extensive.

By 1950, the Fulmer Research Institute, Sweden, investigated the Aluminium-Copper-Cadmium group as this type showed a very much slower response to reheating after ageing, hence making them somewhat more suitable for welded assemblies. The development of more aluminium alloys had continued over the years such that today we can find a very long list of Aluminium alloys, which have been broadly divided into two groups of heat treatable and non-heat-treatable alloys (Woodward, 1981).

Al-Mg-Si and Al-Si alloys were patented about 1930s, and were initially applied for marine and structural purposes. The level of success recorded led the way to much wider usage in the post-1945 years, including the packing and building industries. Today the application has extended to the automotive industry.

The improvement of the properties of these alloys by numerous working or processing techniques is a subject of current research, especially with regard to the ever-increasing field of Aluminium alloy applications. One of the novel techniques of enhancing the quality of alloys is thermomechanical processing.

Thermomechanical processing of metals is a way of improving the quality of metals by subjecting the metal to plastic deformation at a specified elevated temperature,

such that there is increase in the density of defects and thus affecting the formation of the structure in the phase transformations occurring during the thermal action.

Consequently, not every combination of straining, heating and cooling can be called thermomechanical processing. For example, if plastic deformation is carried out after all operations of heat treatment, we are dealing with common heat treatment followed by plastic deformation, not thermomechanical working or processing. Such treatment has no effect on the structure formed, through phase transformation since the phase transformations have taken place before plastic deformation was applied. In thermomechanical treatment or processing, it is only important that phase transformations take place under the conditions of increased density of the lattice defects formed through plastic deformation. Dobatkin (1965), worked on the structural strengthening of Aluminium alloys. He employed the method of preliminary thermomechanical treatment on Duralumin rods and found a gain in the yield and ultimate tensile strength, in ageing the alloy, due to the retention of unrecrystallised structure.

Bernstein (1968), reported that the strengthening effect produced by high temperature thermomechanical processing is inherited upon repeated heat treatment. However, his findings concerned steel profiles. Consequently, the phenomenon of inherited strengthening in repeated short time heating can be investigated in new materials, as it may widen the range of application of high temperature thermomechanical treatment. Rabinovich (1972) carried out some investigation on the dependence of impact toughness of Aluminium on the mode of thermomechanical processing and established a dependence, which is clearly dictated by the temperature of processing.

Singh and Goel (1990), examined the influence of thermomechanical ageing on tensile properties of 2014 Aluminum alloy, and confirmed that the general strengthening of the alloy is due mainly to the existence of θ", θ' precipitate phases and dislocation-precipitate tangles. They also concluded that dislocation-precipitate structure is the most effective in stabilizing the tensile properties at elevated temperature.

Hodgson et.al, (1993) employed a mathematical model to simulate the thermomechanical processing of steel. The model was developed to follow the thermal and microstructural evolution of steel during thermomechanical processing. It was reported that the model has a wide application, such that it could possibly be used to design new compositions and processing route to achieve a given package of properties.

Jonas (2000), and Hutchinson (2000); presented a report each, on the thermomechanical processing of steel, with a unifying conclusion that thermomechanical processing is an important scientific and technological field, which must be vigorously exploited in the new millennium in order to increase the horizon of the applications of metals, especially steel and Aluminium alloys.

CHAPTER TWO

2.0 LITERATURE REVIEW

2.1 HISTORY OF ALUMINIUM

Aluminium is the most abundant metallic element in the Earth's crust and constitutes about 8% by mass. In nature, however, it only exists in very stable combinations with other materials (particularly as silicates and oxides) and it was not until 1808 that its existence was first established. Its principal ore is Bauxite which occurs predominantly in equatorial region. The concentrated form of the ore contains 20-30% Aluminium as oxide and hydroxide (Meyers, 1989).

Key dates on Aluminium are briefly reviewed below.

1808: Sir Humphrey Davy (Pontian) established the existence of Aluminium and named it.

1821: P. Berthier (a French chemist) discovered hard, reddish, clay-like material containing 52% Aluminium oxide near the village of Les Baux in Southern France. He called it Bauxite, the most common ore of Aluminum (Encyclopedia Americana, 1989).

1824: Han Christian Oersted produced metallic Aluminium by passing Chlorine into a heated mixture of charcoal and alumina; the Aluminium chloride vapour formed condensed in a cooler region of the system protected from air. He then reacted it with potassium amalgam to produce aluminium amalgam. By distilling off the mercury in a vacuum, he was able to obtain a small quantity of metallic Aluminium which he described as having a resemblance to tin in colour and luster.

1827: Friedrich Wöhler (Germany) carried out an experiment, reacting metallic potassium with anhydrous Aluminium Chloride in a porcelain crucible and obtained Aluminium metal (John 1988).

1845: Friedrich Wöhler established the specific gravity (density) of Aluminium and one of its unique properties- lightness.

1854: Henri Ste Claire Deville extracted Aluminium from halide salts by reduction with metallic Sodium and this process was equally used with some degree of commercial success until about 1887 (West, 1986). This is the date accepted internationally as the discovery date for Aluminium because this process cleared all doubts about the metal.

1855: A bar of Aluminium, the new precious metal was exhibited at the Paris exhibition.

1883-84: William Frishmuth; extracted Aluminium from Corundum, producing about 51kg in 1884.

1886: Processing pure Aluminium from alumina using reactant such as Potassium was a very expensive process, until 1886 when Charles Martins Hall in USA and Paul L.T. Heroult in France devised almost simultaneously and completely independently, a process of electrolytic reduction of alumina which was relatively cheaper; the method involved the electrolysis of a molten solution of alumina in the mineral cryolite ($Na_3 AlFe_6$) at a temperature of about 950°C (West 1986).

1888: The first Aluminium firms were founded in France, Switzerland, and U.S.A.

1889: Karl Bayer invented a process for extracting high-grade alumina from bauxite ore. Pure Aluminium of about 99% and above purity can be gotten from the high-grade alumina.

The significance of these inventions is that the production of Aluminium metal has continued to experience upward trend since 1890, as exemplified by the world Annual output below;

1900: Annual output, 8,000 tones

1913: Annual output, 60,000 tones

1920: Annual output, 128,000 tones

1946: Annual output, 681,000 tones

1999: Annual output, 24 million tones (Cornell & Bhadeshia 1999).

2006: Annual output 26.4 million tones. (JOM; Nov.2006)

2.2 GEOLOGY OF ALUMINIUM

In the various parts of the world, Aluminium is produced from Bauxite, in particular its morphological form called gibbsite. Prominent among the producers of Aluminium are USA, Europe, CIS, China, Australia, and Asia, all accounting for about 79% of world production, while the rest of the world, including Africa account for 21% of world production of primary Aluminium in the same year. The most common form of commercial alumina in soils is gibbsite. This is however not found to a large extent in Nigerian soils. The condition for the formation of gibbsite requires considerable leaching. Field determination of pore waters associated with gibbsitic and kaolinitic laterite from Sierra Leone suggests that equilibrium is maintained between the two mineral species

when the dissolved silica concentration is in the range of 2.1-2.6ppm SiO2 at 22-24^{0}C (Gaskin 1975). Under conditions of good drainage, where this concentration is exceeded, kaolinite is the stable mineral formed. The rate of silica removal from the zone of chemical weathering must therefore be high, such that kaolinite is either not allowed to be formed, or if formed, it degrades immediately into gibbsite.

Ojanuga (1979) is of the opinion that leaching in savannah soils is just high enough for the prevention of montmorillonite/illite, but not quite high as to lead to the degradation of kaolinite or the formation of Bauxite i.e. gibbsite. Amorphous alumina could, however, be present in small amounts, usually under 5% and this is the situation in Nigeria.

2.3 MINERALOGY OF BAUXITE FOR PRODUCING SMELTER-GRADE ALUMINA

Bauxite is the principal Aluminium ore from which Aluminium hydroxide (also called trihydrate), Al (OH) $_3$ is extracted by the Bayer Process. A generalized schematic diagram of the Bayer Process is shown in Figure 2.1. Four to Seven tons of Bauxite is required to produce two tons of alumina, which produce one ton of Aluminium.

According to Authier-Martin et. al. (2001), approximately 90% of the world production of Bauxite is destined to manufacture alumina. That alumina is then dissolved in a molten bath of natural or synthetic cryolite (Na_3AlF_6) to produce Aluminium via the Hall-Heroult process.

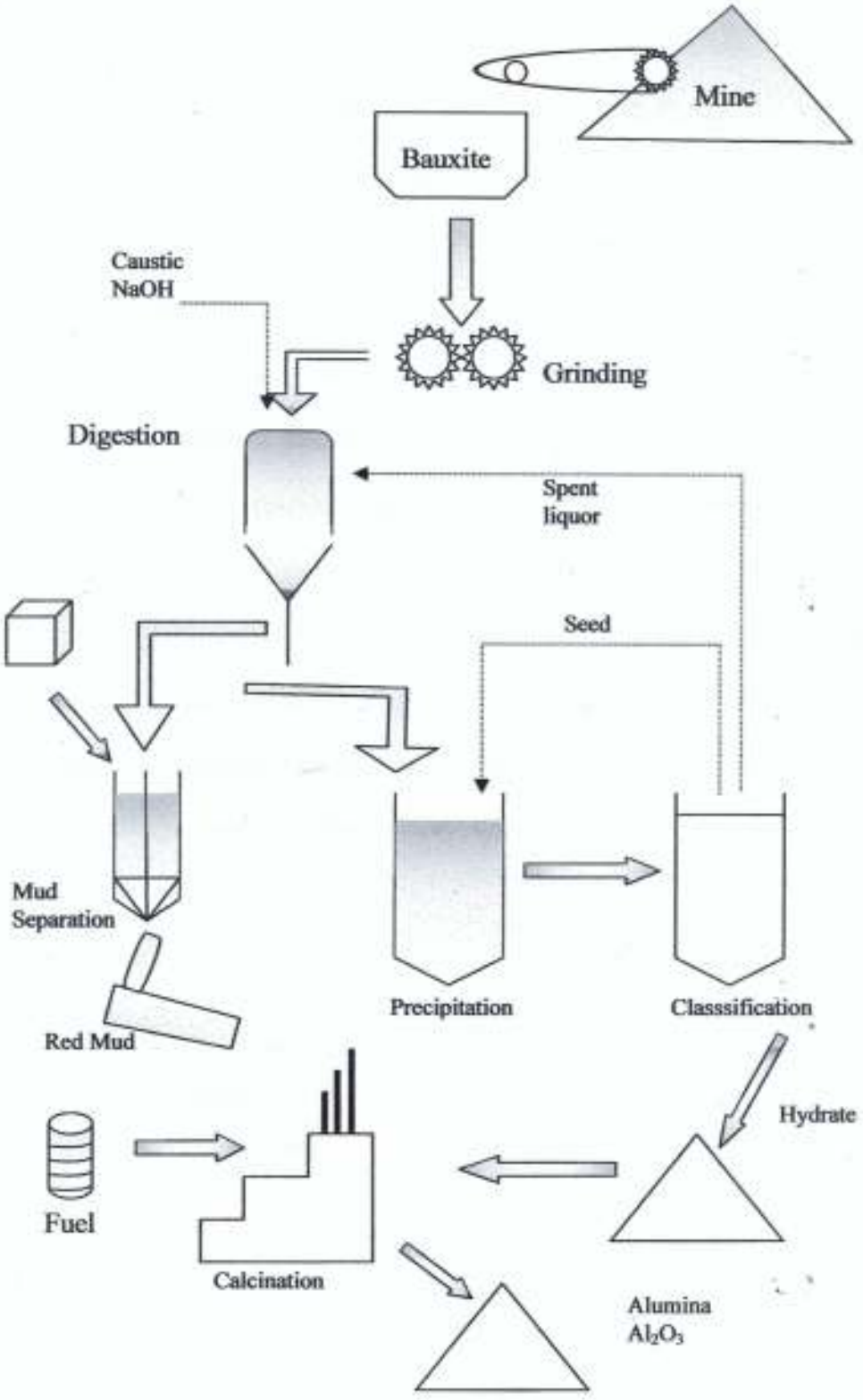

Figure 2.1. A schematic diagram of the Bayer process. (After Authier-Martin et.al, 2001)

Bauxite deposits are known to occur in at least 50 countries, with estimated world reserves of approximately 25 billion tones. World Bauxite production in year 2000 was 127 million tones, which rose to 140 million tones in 2002. Four countries account for 68% of the world production (Sehnke, 1996): Australia, 37%; Guinea, 12%; Jamaica10% and Brazil 9%.

Bauxite deposits are generally divided into two major groups according to their host rock; karst and laterite bauxites (Bardossy and Aleva, 1990), and are predominant throughout tropical and equatorial regions. Regardless of their geographical origin, their mineralogy can generally be represented by Table 2.1, (Webers and Misra 1987). Bauxite is the end product of millions of years of aggressive weathering of primary Aluminium silicates (e.g. feldspars) and clay minerals, resulting in the dissolution of silica, iron compounds, bases, and other constituents from alumina-bearing minerals.

Table 2. 1. Mineralogical Composition of Tropical Bauxites (After Authier-Martin et.al, 2001)

Elements	Mineral	Chemical Composition
Major		
Aluminium	Gibbsite	$Al(OH)_3$ or $Al_2O_3.3H_2O$
	Boehmite	$AlOOH$ or $Al_2O_3.H_2O$
Silicon	Quartz	SiO_2
	Kaolinite/Halloysite	$Al_2Si_2O_3(OH)_4$ or $Al_2O_3.2SiO_2.2H_2O$
Iron	Hematite	Fe_2O_3
	Aluminium Geothite	$(Fe_3Al)OOH$ or $Fe_2Al)_2O_3.H_2O$
Titanium	Anatase	TiO_2
	Rutile	TiO_2
Minor		
Carbon	Organic carbon	Humic materials
Phosphorus	Wavellite	$Al_3(PO_4)_2(OH)_3.5H_2O$
	Crandallite-H	$CaAl_3(PO_4)(PO_3OH)(OH)_6$
Calcium	Calcite	$CaCO_3$
	Crandallite-H	$CaAl_3(PO_4)(PO_3OH)(OH)_6$
Potassium	Illite	$KAl_2(Si_3AlO_{10})(OH)_2$
Manganese	Lithiophorite	$(Al,Li)MnO_2(OH)_2$
Magnesium	Magnesite	$MgCO_3$
	Dolomite	$CaMg(CO_3)_2$
Sodium	Dawwsonite	$NaAlCO_3(OH)_2$
Strotium	Celestite	$SrSO_4$
Sulphur	Woodhouseite	$CaAl_3(PO_4)(SO_4)(OH)_6$
	Pyrite	FeS_2
Zinc*	Gahnite	$ZnAl_2O_4$
Chromium*	Chromite	$FeCr_2O_4$

Elements	Mineral	Chemical Composition
Minor		
Vanadium*	Schubnelite	$Fe_2(V_2O_4).2H_2O$
Zirconium	Zircon	$ZrSiO_4$

**At least some of the zinc, chromium, and vanadium have been established to be present in the Aluminium goethite lattice.*

The principal Aluminium-ore minerals in tropical bauxite exist as several forms of hydrated Aluminium oxides: gibbsite ($Al_2O_3.3H_2O$) also known as hydrargillite (or trihydrate) and boehmite ($Al_2O_3.H_2O$), also known as the monohydrate. Gibbsite is present as the gamma form of Aluminium hydroxide, γ-$Al(OH)_3$, and boehmite is the gamma form of an Aluminium-oxide hydroxide, γ-AlOOH. Diaspore, the alpha form of Aluminium-oxide hydroxide, α-AlOOH, requires much higher temperatures of extraction as well as concentrated caustic solutions.

Bauxites vary in chemical composition (Table 2.2) according to the geology of the deposits and their geographical localization (Ostap 1984). Trihydrate bauxites contain mostly gibbsitic alumina, with less than 2% boehmitic alumina. Monohydrate bauxites are predominantly boehmitic, sometimes containing some diaspore.

Mixed bauxites are primarily gibbsitic but contain 2% or more boehmitic alumina. Two other alumina trihydrate forms exist: nordstrandite, which has occasionally been identified in Jamaica bauxites, and bayerite, a man-made product. Other significant Aluminium-bearing minerals in bauxite are the clay minerals, kaolinite and hallogisite ($Al_2O_3.2SiO_2.2H_2O$), and Aluminium goethite $(Fe,Al)_2O_3.H_2O$. Gibbsite occurs as a loosely aggregated mix of tablets and prisms in Guyanese bauxite, and as elongated hexagonal prisms in Australian Bauxite, and as massive interlocking prisms in Amazon (Trombetas) bauxite, with a gibbsite crystal size about the same as in Boke (Guinea) bauxite.

The silicon-bearing minerals are clays, kaolinite and halloysite ($Al_2O_3.2SiO_2.2H_2O$), and quartz (SiO_2). The iron minerals are mostly responsible for Bauxite's colour; red indicates the presence of heamatite (Fe_2O_3) while yellow indicates aluminium goethite [$(Fe,Al)_2O_3.H_2O$]. Heamatite is present as the alpha form of ferric oxide (α-Fe_2O_3), and Aluminium goethite is present as alpha form of goethite [α- (Fe,Al)OOH]. Most Bauxite ores contain a mix of the two iron minerals. Along with heamatite and goethite, some bauxite ores may contain minor or trace amounts of black magnetite (Fe_3O_4).

The Titanium minerals occur as two simple oxides, Anatase and Rutile (TiO_2). Gallium and Zinc are present, to some extent in all bauxites. Phosphorus is present in all bauxites as either crandallite or wavelite. All Bauxites contain objectionable amounts of caustic-soluble phosphate minerals (Ostap, 1984).

2.4 ALUMINIUM AND ITS ALLOYS

Aluminium is the most abundant metal and the third abundant chemical element in the earth's crust comprising over 8% of its weight. Only Oxygen and Silicon are more prevalent. Yet until about 150 years ago Aluminium in its metallic form was unknown to man. The reason for this is that Aluminium unlike Gold, Copper, Iron or Silver, does not exist as a metal in nature. Because of its chemical activity and its affinity for Oxygen, Aluminium is always found combined with other elements, mainly as Aluminium oxide. As such it is found in nearly all clays and many minerals. Rubies and sapphires are Aluminium oxide coloured by impurities, and Corundum, also Aluminium oxide, is the second hardest naturally occurring substance on earth- only Diamond is harder. It was not until 1886 that scientists learned how to economically extract Aluminium from

Aluminium oxide via electrolytic reduction. Yet in the more than 100years since that time, Aluminium has become the second most widely used of the approximately 60 naturally occurring metals, behind only iron.

Aluminium is a light-weight, silver-coloured metal that can be formed into almost any shape. It can be rolled into thick plates for armoured tanks or into thin foil for chewing gum wrappers. It may be drawn into wire or made into cans. Aluminium does not rust, and it resists wear from weather and chemicals. Pure Aluminium is soft and has little strength. For this reason, Aluminium producers almost always alloy (mix) it with small amounts of Copper, Magnesium, Zinc, Silicon and other elements to form Aluminum alloys. The added elements give Aluminium strength and other properties that make it a very useful metal.

The largest share of Aluminium alloy production goes to the packaging industry for use in such items as beverage cans, bottle caps, foil pouches, foil wrappers, and food containers. The construction industry uses alloys for gutters, panel, roofs and sides of buildings, tubes for electric wires, and window/door frames. Manufacturers of transportation equipment use huge amounts of Aluminium in aeroplanes, cars, boats, and railway carriages. Aluminium is used widely in electrical equipment, including light bulbs, power lines, and telephone wires. Many other products also contain Aluminium. These products include cooking utensils, golf clubs, knitting needles, paints refrigerators, rocket fuel, toasters, and zip fasteners. While commercially pure Aluminium (defined as at least 99% Aluminium) does find application in electrical conductors, chemical equipment and sheet metal work, it is a relatively weak material, and its use is restricted to applications where strength is not an important factor. Some strengthening of the pure

to ship because the containers weigh less than those made of other metals. To make Aluminium alloys lighter, the lightest metal, Lithium, is added to the Aluminium.

2.5 PRODUCTION OF PRIMARY ALUMINIUM.

Aluminium, which has a strong affinity for oxygen, is never found in its pure state. Aluminium is obtained from bauxite which is the name given to ores usually containing 40-60% hydrated Aluminium, together with impurities such as iron oxides, silica and Titanium. Production of primary Aluminium from bauxite involves two distinct processes. First high grade alumina called Aluminium hydroxide or Aluminium trihydrate ($Al_2O_3.3H_2O$), especially written as Al $(OH)_3$) is extracted from bauxite almost exclusively by the Bayer process. The process essentially, involves digesting crushed bauxite with strong caustic soda solution at temperatures up to 240°C (Polmear, 1989). Most of the alumina is extracted leaving an insoluble residue known as "red mud", consisting largely of iron oxide and silica, which is removed by filtration. After cooling, the liquor is seeded with crystals of alumina trihydrate being precipitated and the caustic soda recycled. The whole process can be represented by the chemical reaction;

$$Al(OH)_3 + NaOH = NaAlO_2 + 2H_2O \quad (1)$$

The alumina trihydrate [Al $(OH)_3$] is then calcined in a rotating kiln at 1200°C to remove water of crystallization and alumina (Al_2O_3) is produced as a fine powder.

Alumina has a melting point of 2400°C and is a poor conductor of electricity. In fact, it is a ceramic or refractory material.

The key to the successful production of Aluminium lies in dissolving the alumina in molten cryolite (Na_3AlF_6), and a typical electrolyte contains 80-90% of this compound and 2-8% alumina, together with additives such as Aluminium and calcium fluorides.

The alumina is then electrolyzed in a multi-anode (outer casing). The bath runs at around 950°C and cells are arranged in series so called "Pot lines". This electrolytic technology of extracting Aluminium from high grade alumina was developed by Charles Martin Hall in the United States and Paul Heroult in France, more than 118years ago. This technology, while different in design today, has changed little since it was discovered and developed in 1886. Currents loading are now as high as 250,000A with a voltage drop of approximately 5V across each cell. In electrolytic process, metals in the liquid state, sinks to the bottom of the cell and is periodically tapped off. The cell-tapped Aluminium has iron and silicon as major impurities. The overall reaction can be written as:

$$2Al_2O_3 + 3C \rightarrow 4Al + 3CO_2\uparrow \qquad (2)$$

Aluminium from the electrolytic cell is taken to large refractory-lined furnaces where it is refined before casting. Alloying elements may be added with the furnace charges here.

In the refining operation, the liquid metal is usually purged with chlorine gas to remove dissolved hydrogen gas, which is followed by skimming of the liquid metal surface to remove oxidized metal. Afterwards, it is screened and cast into ingots for further processing (Polmear, 1993).

It is worth noting that despite research work to develop an alternative production route, the Hall-Heroult process remains the foundation of the Aluminium industry.

Today, there are over 136 Aluminium smelters in the world producing approximately 23.3 million tones of primary metal annually (Hale, 2000). The smelters are of two basic types; Prebake Cells, where the anodes are produced outside the cell in a designated area of the plant, make up73% of the cells in the world, while cells called Soderberg produce the balance. These differ from the Prebake version in that the anode is produced in the cell through a self-manufacturing process, in which a petroleum coke and coal tar pitch mixture is calcined to an electrical conducting anode by the heat of the process. While the technology has a multiplicity of anodes numbering from six (6) to thirty-two (32), which are changed out on a periodic basis as the anode carbon is consumed, the Söderberg design has one large anode that stays in the cell. The anode is replenished with new material periodically when the semi-liquid paste is applied to the top of the existing anode. The Söderberg cell has two variations, the horizontal and vertical studs. These variations differ by the way the electrical conducting elements, or "pins" are inserted into the anode.

Few new smelters are planned, and existing smelters are ageing. This fact relates to the capital-intensive nature of the industry and the ability for the operators to incrementally improve the process of an existing plant through building new capacity on an existing site (brownfield) or increasing the capacity of the installed equipment (capacity creep).

However, work by several larger aluminium companies and engineering firms shows that the installed cost of a new plant could drop to below ₦448,000.00 ($3,200)

per tonne with innovations in cell design, building construction, and plant layout. This could be the catalyst for the next wave of plant installations- lean design and organization, built for purpose but not overbuilt.

2.6 PROPERTIES AND APPLICATIONS OF PURE ALUMINIUM

Pure Aluminium is relatively soft and has a low strength. It has a tensile strength of no more than $90N/mm^2$ in the annealed condition and for most engineering purpose is used in the alloyed form to enhance strength.

Aluminium has a low density ($2.70g/cm^3$) and a low melting point (660^oC).

Pure Aluminium is used widely as a conducting material. It shows a high electric conductivity when it is almost free from impurities and crystal lattice defects. High-purity Aluminium (with a total of impurities of 0.002%) and commercially pure Aluminium (with a total impurities of 0.2% - 0.5%) are widely used as conducting materials in electrical engineering. High-purity Aluminium has a high ductility and is suitable for making thin foil (6-7μm) for capacitors. Commercially pure Aluminium is used in the manufacture of wires for cables and current-carrying conductors.

Aluminium is inferior to copper as regards the electric conductivity and strength, but it is substantially lighter and more common in nature. When Aluminium is used in wires as a substitute for copper, the diameter of wires must be increased 1.3 times, but their mass will then be only 50% of that of copper wires. Like copper, Aluminium is employed in the annealed or work-hardening state.

Current-carrying wires of aerial power lines are produced from Aluminium alloys (of the Al-Mg-Si system), which are stronger than pure Aluminium. Aluminium

and its alloys have no temperature limit of cold brittleness and remain tough even at temperatures of -253°C to -269°C. On cooling, their tensile strength (σ_{uts}) increases by 35-60%, $\sigma_{0.2}$ by 15-25%, and the impact strength decreases monotonously to 0.5-0.2 MJ/m^2 (Hale,2000).

The failure toughness Kic, is not practically diminished, which means that Aluminum alloys on cooling have a lower notch sensitivity than at 25°C. In view of the high thermal expansion and substantial thermal conductivity of Aluminium, high thermal stress inevitably appears in rigidly fixed Aluminium structural elements.

One other property of Aluminium that is responsible for the wide use of the metal is its corrosion resistance. It readily forms an oxide film on its surface which protects the pure metal below from environmental attack.

2.7 CLASSIFICATION OF ALUMINIUM ALLOYS

The selection of Aluminium alloys for use in engineering has often been difficult because specification and alloy designation have differed from country to country. For this reason, the introduction of an International Alloy Designation System (IADS) for wrought and cast products was made. The system is based on the classification used for many years by the Aluminium Association of the United States of America.

These Aluminium alloys can be divided into two broad groups; wrought and cast alloys, based on the method of production (Timing 1989, Lakhtin 1990).

Wrought alloys are those alloys whose mechanical properties allow them to be formed by a variety of processes including forging, rolling, extrusion and drawing. They may be heat-treatable or non-heat treatable. On the other hand, cast Aluminium alloys are

alloys which can be used successfully for casting by a variety of processes including sand-casting and die casting. They may be heat-treatable or non-heat treatable.

2.7.1 WROUGHT ALUMINIUM ALLOY

Aluminium alloys produced in the wrought form (i.e. sheet, plate, extrusions, rod and wire) are classified according to the major alloying element(s) they contain. A four digit numerical designation is used to identify wrought aluminium alloys. The first digit is assigned on the basis of the major alloying elements. The second digit, if different from 0, denotes a modification in the basic or original alloy. The third and fourth digits form an arbitrary number which identifies the specific alloy in the series. A brief illustration of the nomenclature of wrought Aluminium alloy is given in Table2.3 and 2.4

Table 2.3. Nomenclature of Pure Wrought Aluminium Alloy (Robert, B, Ross 1992)

1	0	35
Aluminium purity at least 99.00%	No special alloying procedure	Aluminium Purity of 0.35% above 99.00%.

Table 2.4. Wrought Aluminium Alloy of Al-Mg-Si composition (Robert, B. Ross 1992)

6	0	61
Mg and Si are used as the major alloying elements	No special alloying procedure	Si and Mg added to the alloy according to the stated amount; 1%Mg & 0.6%Si

The table below shows the designation system for wrought aluminium alloys.

Table 2.5. Designation System for Wrought Aluminum alloys. (After Polmear, 1995)

Alloy Type	Designation
Aluminium, 99.00% minimum and greater purity.	1xxx
Aluminium alloy grouped by major alloying elements:	
Copper.....	2xxx
Manganese.....	3xxx
Silicon.....	4xxx
Magnesium	5xxx
Magnesium and Silicon	6xxx
Zinc	7xxx
Other elements	8xxx
Unused series	9xxx

2.7.2 CAST ALUMINIUM ALLOYS.

Cast alloys are those that are poured molten into sand (sand casting) or high-strength steel (permanent mould or die casting) moulds, and are allowed to solidify to produce the desired shape. The wrought and cast alloys are quite different in composition; wrought alloys must be ductile for fabrication, while cast alloys must on melting, be fluid enough for castability. A cast alloy is assigned a three-digit number followed by a decimal. Here again the first digit signifies the alloy series or principal addition; the second and third digits identify the specific alloy; the decimal indicates whether the alloy composition is

for the final casting (0.0) or for ingot (0.i or 0.2). A capital letter prefix (A, B, C. etc.) indicates a modification of the basic alloy.

The designation system for cast Aluminum alloys is shown in Table 2.6.

Table 2.6. Designation System for Cast Aluminum Alloys (After Polmear, 1995)

Description or Major Alloying Element	Designation.
99.00% minimum Aluminium	1xx.x
Copper	2xx.x
Silicon plus copper and /or magnesium	3xx.x
Silicon	4xx.x
Magnesium	5xx.x
Unused series	6xx.x
Zinc	7xx.x
Tin	8xx.x
Other element	9xx.x

2.7.3 TEMPER SPECIFICATION OF ALLUMINIUM ALLOYS

Specification of an Aluminum alloy is not complete without designating the metallurgical condition, or temper, of the alloy. A temper designation system, unique for Aluminum alloys, was developed by the Aluminum Association and is used for all wrought and cast alloys. The temper designation follows the alloy designation, the two being separated by a hyphen. Basic temper designation consists of letters; subdivisions, where required, are indicated by one or more digits following the letter. The basic tempers are:

F— *As Fabricated.* Applies to the products subjected to shaping processes in which no special control over thermal conditions or strain hardening is employed. For wrought products there are no mechanical property limits.

O—*Annealed.* Applies to wrought products that are annealed to obtain the lowest strength, and to cast products that are annealed to improve ductility and dimensional stability. The figure 0 may be followed by a digit other than zero.

H—*Strain-Hardened.* Applies to wrought products that have their strength increased by strain hardening, with or without supplementary thermal treatments. The H is always followed by two or more digits.

W—*Solution Heat Treated.* An unstable temper condition applicable only to alloys that spontaneously age at room temperature after solution heat treatment. This designation is specific only when the period of natural ageing is indicated; for example: W $_{1/2hr.}$

T—*Thermally Treated to Produce Stable Tempers Other than F, O, or H.* Applies to products that are thermally treated, with or without supplementary strain hardening, to produce stable tempers. The T is always followed by one or more digits.

Apart from the above groupings, wrought Aluminum alloys are equally classified into two classes on the basis of heat treatment. The two classes are heat-treatable wrought Aluminium alloys and non heat-treatable wrought Aluminium alloys.

2.7.4 NON HEAT-TREATABLE WROUGHT ALUMINIUM ALLOYS

The non-heat-treatable wrought Aluminium alloys as the name implies are wrought alloys that do not respond significantly to heat treatment except annealing, but can only be strengthened by cold working. A typical non-heat treatable wrought

Aluminium alloy contains approximately 1.00 to 1.5 % Magnesia, this increases the tensile strength without materially affecting the excellent ductility of pure Aluminium.

Another non-heat-treatable-wrought Aluminium alloy contains Magnesium, which is highly corrosion-resistant, particularly in marine environment.

2.7.5 HEAT-TREATABLE WROUGHT ALUMINIUM ALLOYS

Heat-treatable wrought Aluminium alloys are wrought alloys that respond to strengthening by heat treatment, and in particular to the processes known as solution treatment and precipitation hardening. These alloys are covered by the three series: 2xxx (Al-Cu, Al-Cu-Mg); 6xxx (Al-Mg-Si) and 7xxx (Al-Zn-Mg, Al-Zn-Mg-Cu). All depends on age hardening to develop enhanced strength properties and they can be classified into two groups; those that have medium strength and are readily weldable (Al-Mg-Si and Al-Zn-Mg), and the high strength alloys that have been developed primarily for aircraft construction (Al-Cu, Al-Cu-Mg and Al-Zn-Mg-Cu) most of which have very limited weldability.

2.8 RECRYSTALLIZATION OF DEFORMED Al-Mg-Si ALLOYS

Primary recrystallization is the process that takes place during heating of cold worked Aluminium metal. In particular, it diminishes or fully eliminates the additional structural imperfections which have been caused by prior deformation.

It is then clear that the nature, density and distribution of imperfections, especially the dislocation structure of the deformed metal, should have the decisive effect on the trend of recrystallization. The structure of the deformed material depends on the mechanism of deformation. The principal mechanism of plastic deformation in metals,

and in all crystals in general, is the shear movement of some portions of a crystal (or crystallite) relative to other portions; it is effected through various dislocation movements, including movements along grain boundaries (Honeycombe,1993).

The dislocation and diffusion mechanisms determine the development of intragranular and intergranular deformation. Shear deformation can occur by a number of particular mechanisms, the principal ones being dislocation slip and cross-slip, twinning and kinking. In most cases, several mechanisms are operative at once, with one of them being predominant. The contribution of a particular mechanism (Gorelik, 1981) is determined by many factors, among which are;

1. Pattern and condition of deformation,
2. Type of crystal lattice,
3. Stacking fault energy,
4. Crystal orientation relative to the external stresses,
5. Size and shape of grains prior to deformation,
6. Chemical and phase composition of the Aluminium metal,
7. Size and plasticity of excess phase particles.

The phenomenon of structural changes in deformed metals is quite complicated. This is why many of the problems associated with the changes in structure and properties of plastically deformed metals have been analyzed only qualitatively.

Modern concepts of dislocations and their behaviour in metals and alloys, and structural analysis of stress-strain curves can be effectively used to study and interpret the structural changes in deformed Al-Mg-Si alloys.

These concepts have shown that plastic deformation by slip is the displacement by shear of individual dislocations on the crystal planes which are filled most densely with atoms and are respectively characterized by the largest interplanar distances. In Aluminium, dislocation slip usually occurs on {111} planes in [101] directions. The four octahedral planes of the type {111} and the three directions of the type [110] form 12 possible slip systems in Aluminium lattice.

In Aluminium and other alloys with an F.C.C lattice, slip on the planes of the cube can also occur along with slip on octahedral planes. At elevated temperatures, around 40% of slip lines belong to cube planes in Aluminium. When analyzing the process of slip under the action of an external stress, it should be remembered that shear is caused by a tangential stress operating on the slip plane in the slip direction. This is termed the resolved shear stress τ_r. Plastic deformation in a given slip system will occur when τ_r reaches the critical shear stress τ_{cr} the latter being an important characteristic of the mechanical properties of a material.

Direct studies of dislocation structures in deformed metals and alloys are associated with appreciable difficulties. In the first place, the methods used should provide for a very high resolution. On the other hand, this results in ever greater localization of the volumes being investigated and, therefore generates the need to resort to statistical analysis for higher reliability. In this connection, it is quite important to obtain data on the hardening effect produced by deformation. This remarkable peculiarity

of metals is directly associated with dislocation structure that forms on deformation and prevents further deformation of the metal. As a result, the critical shear stress τ_{cr} required for further deformation ε varies in the course of the process, and it does so more intensely when the dislocation structure formed by prior treatment offers an increased resistance to dislocation movement.

Novikov and Tiraspolsky (1970), remarked that stress-strain curves (hardening curves) actually show what amount of shear stress should be applied to cause further plastic deformation at a given dislocation density and dislocation distribution formed by prior treatment.

Plastic deformation is analyzed in the following way. The initial data are the hardening curves obtained for various metals and alloys under various conditions of deformation. These data are used to develop (construct) dislocation models and explain the τr- ε relationships established.

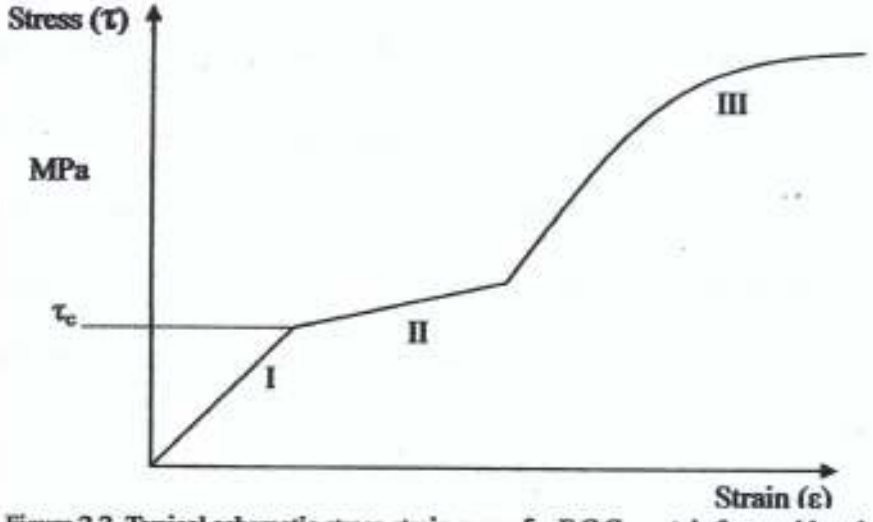

Figure 2.2. Typical schematic stress-strain curve for F.C.C crystals favourably oriented for easy slip

(After Gorelik, 1981)

The curve for an F.C.C crystal is most typical of the structural changes at various stages of hardening. It shows clearly that hardening passes through three stages as shown in Figure 2.2.

Apart from the lattice type, other factors that affect the pattern of stress-strain curves are:

(1) The stacking fault energy;

(2) The purity of the material in respect of type and quantity of impurities and alloying additions;

(3) The temperature and the rate of deformation.

The three main stages of the stress-strain curve are understood or analyzed thus;

Stage I

The specific structural change at the first stage is that shear occurs through dislocation slip on a single primary slip system due to the sources that existed prior to deformation. There are no substantial obstacles to dislocation movement, and therefore the free path of dislocation as a rule long. Trials of a large number of dislocations, which have moved on one and the same plane, are revealed metallographically as slip lines. They can be defected on a polished surface of single crystals by optical microscopy. Electron microscope reveals rather uniformly distributed long lines with jogs of a relatively low height (50-100 x 10^{-8}cm)

The first stage has two portions; (a) the initial linear portion representing elastic deformation and (b) the portion of plastic deformation which is a bend as deformation progresses into stage II. According to Hooke's law, the work-hardening coefficient for the first portion is sequel to the shear modulus G. The work- hardening coefficient θ_1 for

the later part of this stage is very low and is of an order of 10^{-4} G for F.C.C metals. For this reason, the first stage can be called the stage of easy slip. The critical shear stress τ_{cr} and the highest shear strain ε_I are also important parameters of this stage.

Stage II

The second stage is also characterized by a linear relationship $\tau=F(\varepsilon)$, but the work-hardening coefficient at this stage is appreciably higher than θ_I by a factor of 30 (Cavaliere, 2002). This stage is less affected by various factors than the first. In particular, the work hardening coefficient θ_{II} is independent of temperature, though the moment at which the second stage passes to the third stage is variable.

Stage III

The portion of the curve corresponding to the third stage diminishes with increasing deformation, and the phenomenon is called dynamic recovery. The onset of stage three is especially sensitive to the temperature of deformation, T_d. As this temperature rises, the onset of stage III shifts towards lower values of ε.

2.8.1 Deformation of Single Crystals

The hardening effect obtained in such an ideal case is associated with long-range interaction of dislocation loops in the primary slip systems, which are spaced at a distance Ro apart. According to Seeger (1957), parallel dislocations of the same sign, which are located on parallel planes, produce a long-range stress field whose maxima, are separated by distances of an order of R_o^1. For a dislocation to move between two like -

dislocations, it should overcome the inverse long-range stress. To effect this, the stress applied to an edge dislocation must be,

$$\tau_{edge} = \frac{Gb}{2\pi(1-\nu)R_o^1}, \qquad (3)$$

where G is modulus of elasticity in shear, b Burger's length, ν Poisson's ratio and that to a screw dislocation,

$$\tau_{scr} = \frac{Gb}{2\pi R_o^1} \qquad (4)$$

with an increased number of dislocation loops, the inverse stress Y_{inv} that acts on dislocation sources grows. When Y_{inv} becomes equal to the increased shear stress, generation of dislocation loops ceases. The work-hardening coefficient is,

$$Q = \frac{8G}{9\pi}\left(\frac{L}{R_o^1}\right)^{3/4} \qquad (5)$$

where L is the length of dislocation.

From the results obtained from various investigations, an inference was drawn, that a reduction of test temperature prolongs stage I in F.C.C crystals,(Gorelik,1981) and reduces the rate of hardening θ_I. In metals where upper yield limit is experienced, the appearance is due appreciably to locking of dislocations by impurity atmospheres. In crystals of high stacking fault energy, γ_{sf}, such as Aluminium, the second stage is less pronounced. The second stage of hardening is less influenced by orientation than the first stage.

The third stage of hardening which has a parabolic stress-strain relationship is characterized by a reduced intensity of hardening. At this stage, Q_{III} is a variable that diminishes with increased strain. This stage is much less sensitive to most of the factors that are essential at stages I and II, such as crystal orientation, impurities, and the type of lattice. Exceptions are the temperature of deformation and the stacking fault energy; these two factors have a substantial effect on the onset of stage III hardening and on its contribution to the total deformation.

As the temperature of deformation rises, the third stage begins to act at lower strains and its contribution to the total deformation becomes progressively predominant. According to Kuhlmann-Wilsdorf (1962), the stress τ_{III} for the onset of the third stage diminishes with increasing temperature by a logarithmic law;

$$\ell n\left(\frac{\gamma_{III}}{G}\right) = \ell n\left(\frac{\gamma_{III\,(o)}}{G_{(o)}}\right) - BT \qquad (6)$$

where B is a coefficient, and $\tau_{III\,(o)}$ and $G_{(o)}$ are the stress and the shear modulus at ^0K respectively. This relationship has been verified experimentally for Aluminium alloys and many F.C.C metals.

The stacking fault energy γ_{sf} has a similar effect. In materials with high values of γ_{sf} such as Aluminium, the transition to the third stage occurs at lower temperatures than in materials with low γsf such as copper or silver. (Mott, 1956).

As it is known, the stacking fault energy is largely responsible for the ability of a material to develop thermally activated cross-slip. These facts, as expressed above, have

suggested a conclusion to the effect that the third stage begins when dislocations have the possibility to bow (by cross-slip) around the dislocation locks they have formed on their path at the second stage, in the first place, Lomer-Cottrel locks.

Seeger (1957) derived the following expression for the shear stress τ_{III} required to compress dissociated leading dislocations of a dislocation pile-up:

$$\tau_{III} = \frac{\left(\frac{2G^{1/2}}{4\pi} - 2\frac{\gamma}{b}\right)}{n} \qquad (7)$$

where n is the number of dislocations in a pile-up. Using this expression and experimental values of τ_{III} for Aluminium at 4K, it has been found that n ≈25.

Deformation twining is one of the mechanisms of plastic shear deformation. Twinning is usually a fast process and is often accompanied by energy release in the form of sound. On the stress-strain curve the portion corresponding to twining has a tooth or saw-like shape (Blewitt., et al, 1967). The onset of twining should evidently be pile-ups acting as local stress concentrators. On the other hand, $\tau_{cr\ (tw)}$ remains appreciably lower than the stress corresponding to the theoretical strength. On that ground, twining cannot be associated with simultaneous movement of all atoms in a twin and is probably realized through successive displacement of atoms, i.e. as in dislocation movements. In modern views, twining is associated with the movement of partial dislocations, resulting in a situation that the sites occupied by atoms on both sides of slip planes cease to be equivalent. The quantitative relationship between the twining shear stress $\tau_{cr\ (tw)}$ and stacking fault energy, as proposed by Duggan and Roberts (1975), is of the form

$$\tau_{cr(tw)} = \frac{\gamma_{sf}}{b} + \frac{Gb_1}{2a} \qquad (8)$$

where b is the Burger [8] vector of the twining dislocation, G is the shear modulus, and **a** is the radius of a half-loop of the twinning dislocation.

Twinning is realized when γ_{sf} is low and $\tau_{cr\,(tw)}$ is smaller than $\tau_{cr\,(sl)}$. This agrees well with the results of experimental observations. For instance, twins (and especially annealing twins) are observed very frequently in Copper ($\gamma sf \leq 6 \times 10^{-6} J/cm^2$) but are very rear in Aluminium ($\gamma sf > 2 \times 10^{-5} J/cm^2$).

Apart from slip and twinning mechanisms of plastic deformation in metals, other means or mechanisms also exist, causing structural changes in the metal. Deformation by irregular rotation of the crystal lattice is noted. However, deformation of this type has not been studied thoroughly. It was first discovered in compressed minerals and later in rock salt crystals. In 1952, E.Orowan, observed the formation of a knee-shape kink in a cadmium rod on its compression in a direction almost parallel to the slip plane. The region in the knee was much similar to the tilt regions in minerals and was called the kink band. Kink bands were later observed in Aluminium crystals on tension. Generally in f.c.c. crystals, kink bands form perpendicular to the planes and direction of slip. The crystal lattice is rotated in them relative to the remaining lattice around an axis in the slip plane and perpendicular to the slip direction. These bands contain local regions of curved lattice as represented in Fig.2.3, consisting of two zones of opposite curvature. On heavy deformations, kink bands become locks for dislocation movement (Honeycombe, 1993).

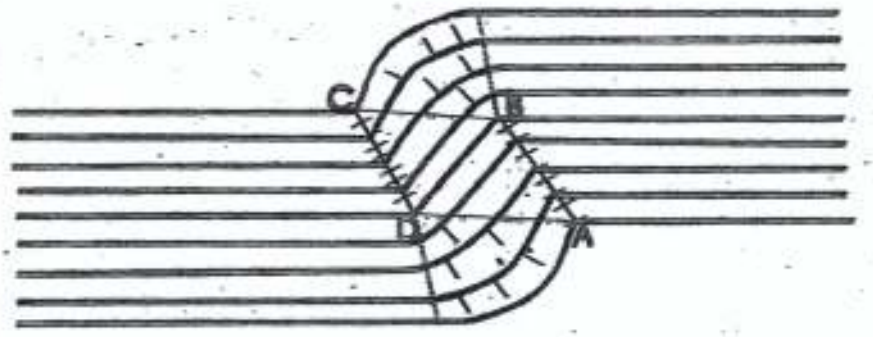

Figure 2.3 A kink band (Schematic) (After Gorelik, 1981)

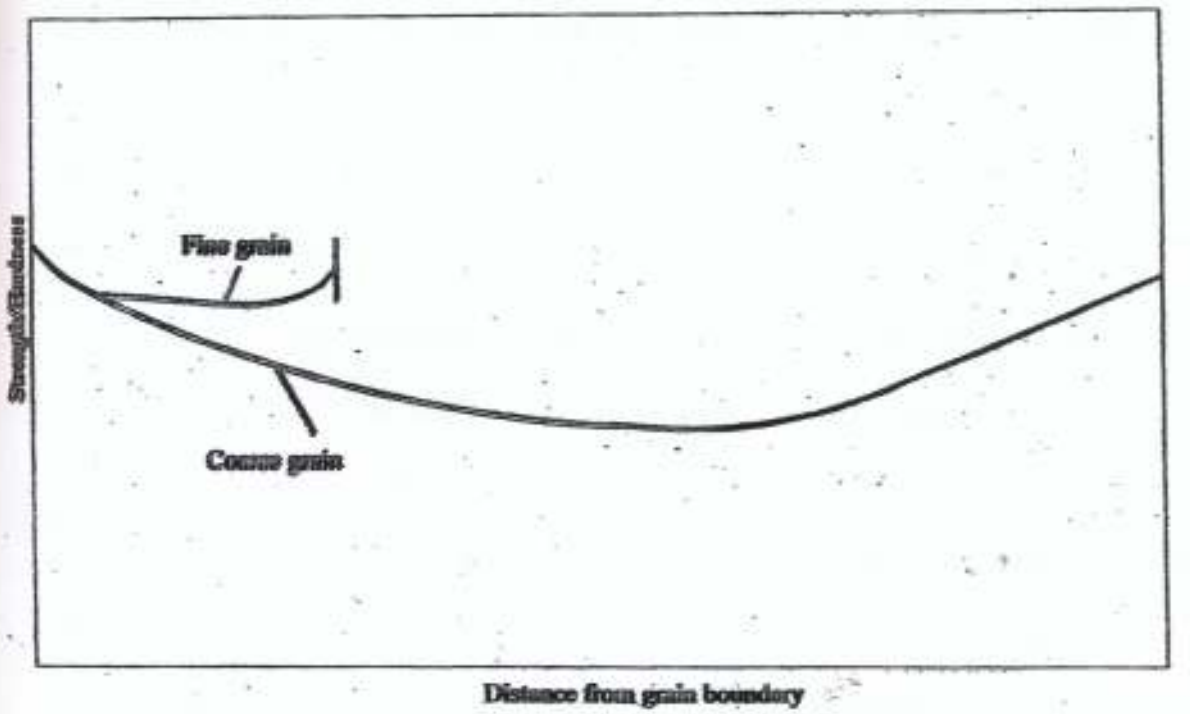

Figure 2.4 Effect of Grain size on microinhomogeneity of their deformation (schematic) (After Gorelik, 1981)

Regions of large curvature are sites where the formation of recrystallization nuclei occurs at the highest rate.

2.8.2 Deformation in Polycrystalline Aluminium Alloys.

In polycrystals, which are encountered most often in practice, the nature of deformation and the shape of τ-ε curve, especially at the initial stage of hardening, greatly differ from those in single crystals. On the other hand the principal features of the changes in single crystals in the second and third stages of work-hardening are essentially the same as in polycrystals.

The main changes result from the fact that every crystallite in a polycrystal is oriented in space, and therefore relative to external forces, in a different manner than are the surrounding adjacent crystallites from which the crystallite in question is separated by grain boundaries. Also every crystallite experiences the action of neighbouring crystallite which may have a different orientation. The nature and the result of the influence of adjacent crystallite on a given crystallite depend appreciably on the type of grain boundaries and their ability to impede the movement of dislocations.

In cases of cold deformation, grain boundaries are always stronger than the internal volumes of grains. At high temperatures, when the contribution of diffusion processes becomes tangible, boundaries turn out to be less strong than grains proper. The temperature at which boundaries and grain volumes have the same strength is called equicohesive temperature. In cold deformation, the strength of boundaries depends on the angle of misorietation, i.e. on the dislocation density at the boundaries.

Chalmers and Clark (1954) have demonstrated on bicrystals of Aluminium that the elastic limit and the yield limit increases appreciably (1.5 and 4 times respectively) with an increase in the angle of misorietation up to approximately 60°. This implies that grain boundaries grow in importance as barriers for dislocation movement and cause dislocation pile-up. This does not mean, however, that the deformation ceases as it reaches a grain boundary. The latter may be and usually is the site of a sharp deformation gradient. Usikov and Utevsky (1961), observed the excitation of dislocation sources on grain boundaries in f.c.c. polycrystalline materials such as Aluminium and nickel alloys under the effect of stresses that induce in a given grain the dislocations of an adjacent grain, which come to the boundary and stand arrested by it. The authors called this phenomenon the "relay race" (grain to grain) transmission of strain. The transmission not withstanding, slip systems on the two sides of a grain boundary are different.

Grain boundaries are responsible for a highly inhomogeneous deformation of grains that results, for example, in dislocation pile-ups on grain boundaries. In fine-grain materials, regions of multiple slip propagate from grain boundaries and extend into the bulk of crystallites. Furthermore, the interaction of dislocations moving from various boundaries of a grain can occur within the grain in such a material. The result is that fine-grained materials undergo a more intensive work-hardening than coarse-grained ones because the grain boundaries are closer in fine-grained alloys than in coarse-grained ones (fig.2.4).

Investigations have shown that polycrystals have a greater number of operative slip systems than are usually found in single crystals of the same materials. For instance, Boas and Ogilvie (1954) examined polycrystals of Aluminium and α-brass upon relatively light

deformations and detected trails of six slip systems in some grains, including on {111},{100} and {110} planes. Since different slip system may be operative in various volumes of a grain, polycrystals exhibit a non-uniform deformation in these volumes, which causes bending and local rotations of the lattice such as twinning, kink bands, strain bands and microbands. Cahn (1963) observed in polycrystalline Aluminium, deformed 40% by pressing, that the total misorientation within individual grains roughly 700μm in size reached 52°. At 50% deformation, each grain had at least one microband. Owing to sharp misorietations, microbands, like grain boundaries, become the preferable sites for the formation of recrystallization nuclei.

In addition to intragranular inhomogeneity, deformed polycrystals are characterized by an appreciable intergranular inhomogeneity, i.e. by non-uniform deformation of adjacent grains. This feature makes itself felt heavily at relatively low strains and substantially influences the nature of subsequent recrystallization.

According to Honeycombe (1993) elongation in some grains of coarse-grained Aluminium may vary from 2-14% or even more, with average elongation of a specimen amounting to about 5%. Similar variations are established for the values of microhardness in local regions. The almost complete absence of the first stage of the τ-ε curve in polycrystals is because multiple slip begins in crystallites upon relatively light deformations, in the first place, in boundary regions. According to Jaoul (1967), strain ε_l in Aluminum at the first stage of deformation does not exceed 2%. In many other metals, ε_l is still lower. However the second and third stages are more pronounced, and obey the same laws. A decrease in the stacking fault energy extends the

second stage (Fig. 2.2) to higher degrees of deformation and increases the absolute value and intensity of work-hardening. Consequently, in high-purity Aluminium, which has a high value of γsf and a relatively low melting point, the second stage is not detected at all on deformation at room temperature. The third stage is described by a parabolic curve (as with single crystals) and depends in a similar manner on the temperature of deformation and stacking fault energy.

Weissmann et. al. (1963), remarked that in pure aluminium, cell structure begins to form on rolling at a 5% deformation. At 30% deformation, cells become surrounded by a clear network of dislocation boundaries.

At heavy deformations of 70% or more, the dislocation density grows sharply, individual dislocations in cell walls usually cannot be resolved, but dislocation pile-ups in the walls are retained. He also demonstrated that small-angle boundaries of cells in heavily deformed aluminium become more asymmetrical and "twisted" and that the dislocation density in walls increases.

One of the most important consequences of plastic deformation in polycrystals is that their properties become anisotropic to some extent; i.e. grains which have been randomly oriented prior to deformation acquire a preferable crystallographic orientation which is called the texture.

During deformation of a metal specimen, its crystallites also change their shape and tend to orientate themselves definitely according to the external deforming forces. Practically, it is never possible to cause all crystallites in a body to line up on deformation strictly on the direction they tend to. Some subgrains and grains always remain more or

less disoriented relative to the ideal direction, in which case a scatter of texture is said to take place. In heavily deformed metals deformation textures are most pronounced, with texture scatter of 5 to 10 degrees. It should also be noted that owing to a complicated interaction with adjacent grains texture scatter may be appreciable not only between grains, but also within grains.

Dillamore and Roberts (1964), explained that metals of high stacking fault energy γ_{sf} such as Aluminium, give a {110}(112) + {112}(111) texture, which is called metal texture. However, the formation of rolling textures in f.c.c metals and alloys is found to be dependent on cross-slip. If a cross slip is impeded, a simple single component {110}(112) texture forms. As cross slip becomes easier, the {112}(111) orientation appears and its contribution becomes more and more important. This is why the {110}(112) texture, which is often called "alloy texture" or "brass texture", usually forms in f.c.c metals and alloys with low stacking fault energy γ_{sf}. Only materials of very low stacking fault energy γ_{sf} can retain a brass texture up to rather high temperatures of rolling (0.5Tm).

2.8.3. Presence of Macro and Micro inhomogeneity in deformed Alloys.

2.8.3.1 Inhomogeneities due to friction forces.

Under frictional forces acting between a deforming tool and the metals being deformed, the rate of plastic deformation and other parameters of metal flow may vary over the workpiece cross section. This involves differences in the structure, and texture over the cross section and the appearance of internal stresses between the surface and core layers of the metal. These microstructures, also called zonal stress or first order stress, are

counterbalanced in macrovolumes of the metal. Friction forces depend on the conditions of rolling, including the diameter and temperature of rolls, the temperature of the metal being rolled, the rate of deformation, the presence of scale or lubricant on metal surface and some other factors.

In f.c.c metals, such as aluminium, cold rolling forms the {001}(110) texture in surface layers of the metal, though no such textures appears in deeper layers. The depth to which this orientation penetrates increases with increasing coefficient of friction, μ, and the amount of deformation per pass. At very high values of μ, a weak component of the {111}(011) texture appears on the surface.

Other methods of deformation, such as drawing, extrusion, forging and stamping, can also produce texture inhomogeneity over the cross section. Non-uniform conditions of metal flow can cause the appearance of zonal stresses apart from the formation of textures.

The zone where the flow of metal during deformation has been more intensive (surface layers in rolling and core layers in extrusion) is subjected to the residual compressive stresses, and the zone with a lower rate of metal flow experiences residual tensile stresses.

2.8.3.2 Inhomogeneities due to excess phases.

The appearance of a secondary phase in an alloy may have an appreciable effect on the nature of the dislocation structure that forms on deformation. This effect is especially high if particles of the secondary phase are very hard and large in number.

Ashby (1964), Usikov and Utevsky (1964), Honeycomb (1993), and Bielder et. al. (2002) have given convincing evidences that dislocation density increases more quickly in alloys

which contain excess phase particles, and that these excess phase particles can serve not only as barriers to dislocation motion but also generate dislocations in heat treatment processes (heating, cooling, thermocyling) owing to the differences in thermal expansion and unit volume between these particles and the matrix.

2.8.3.3 Inhomogeneities due to the formation of point defects.

The above mentioned structural changes occurring during deformation are only associated with changes in the density and distribution of dislocations. The picture will be incomplete if we disregard the problem of how deformation affects the concentration and distribution of point defect, in the first place, of vacancies which play an important part in subsequent processes of recovery and recrystallization. Plastic deformation is accompanied by the formation of two types of point defects, vacancies and interstitial atoms, of concentrations a few orders of magnitude greater than the equilibrium concentration. The mobility of interstitial atoms in metals is quite high and their flow to dislocations and boundaries occur at rather low temperatures. For this reason, the effect of interstitial atoms on recrystallization can evidently be neglected, which is not the case with vacancies.

Though a major portion (about 70%) of vacancies is formed in deformation run off at a temperature below the recrystallization point, a certain fraction (20-30%) probably remains in the metal until the onset of recrystallization, and affects the conditions and the rate of the processes of dislocation climb and dislocation redistribution.

Further, vacancies, like impurities atoms, can form atmosphere around dislocations and thus lock them. This has been confirmed by the results of comparative mechanical tests of metals with various concentrations of vacancies. For instance, the critical shear stress

in hardened Aluminium, (having an elevated concentration of vacancies), has turned out to be five times that in Aluminium alloy slowly cooled down from a high temperature (Kaczorowski, 1984).

The particular mechanisms of the formation of point defects on the course of deformation have not been fully investigated due to certain experimental difficulties. Some of them can however, be specified from the geometrical analysis of the interaction of dislocations. Balluffi et al. (1963) suggested that one of the principal mechanisms is associated with non-conservative movement of dislocation jogs whose Burgers vector has a different orientation to that of the main dislocations. If stress is applied to a screw dislocation with jogs (which cannot slip), the dislocation will be bent between the locking jogs. Vacancies will form on the jogs owing to thermal activation, and this will enable the dislocation to slip forward. The vacancy so formed will diffuse into the volume of crystallite.

2.8.4. Processes Occurring in Deformed Al-Mg-Si Alloys on Heating

The elementary processes which can occur on heating of a deformed Aluminium alloy and decrease the activation energy are :

(1) Diffusion of point defects and their disappearance into dislocations and boundaries, resulting in partial annihilation of vacancies with interstitial atoms and deformation of complexes and groups of point defects;

(2) Redistribution of dislocations by formation of simple and cross-slip dislocations and by narrowing of dislocation loop.

(3) Redistribution of dislocations by climb, which, in combination with dislocation slip results in "flattering" or sometimes, on the contrary, on unraveling of dislocation arrays and their crystallographic orientation.

(4) Formation of low-angle boundaries associated with processes indicted in (2) and (3) above.

(5) Migration of low-angle boundaries and large-angle boundaries into the deformed matrix accompanied by annihilation (sweeping out) of defects;

(6) Migration of grain boundaries between recrystallized grains and coarsening of the grains.

(7) Dissolution of second phase particles

(8) Homogenization of dissolved second phase particles

It is, however, necessary to realize that the above categorization is only conditional and many of these elementary processes are not yet studied thoroughly. The above-mentioned elementary processes can occur either successively or superimposed in one another depending on the amount and nature of deformation, the rate and time of heating, the nature and purity of the material and some other factors.

As a result, the effects of cold work on the structure and properties of Aluminium alloy can be eliminated in different ways and to a different extent.

Summarily, the following stages are distinguished in the process of elimination of the effect of cold work on heating, (in order of increasing activation energy).

(1) Recovery:

(a) point defects annihilation;

(b) polygonization;

(2) Recrystallization:

(a) primary recrystallization;

(b) grain growth (uniform)

(c) Secondary recrystallization (often called "exaggerated grain growth")

Recovery should be understood as the process of structural perfection of a work-hardened metal by redistribution and annihilation of point defects and, besides by redistribution and partial annihilation of dislocations either without the formation of new boundaries (point defect annihilation proper) or with the formation and migration of low-angle boundaries only (polygonization).

Recrystallization is the process in which some grains of a given phase are replaced by the same phase grains of a higher structural perfection and lower energy. The process occurs through the appearance and motion of large-angle boundaries (primary recrystallization) or only through the motion of these boundaries (grain growth and secondary recrystallization). This definition makes a distinction between recrystalization and polygonization, which is associated with the formation and motion of low-angle boundaries. (Gorelik,1981). The rate of recrystallization at any of its stages is primarily determined by a gain in free energy ΔF. This gain serves as the driving force of the process. The gain in free energy related per mole is usually denoted as P_{dr}, and is a function of a number of other energies as represented below.

$$P_{dr} = \Sigma P_i = P_v + P_b + P_s \qquad (9)$$

Where P_v is gain in volume energy,

P_b is gain in grain-boundary energy

P_a is gain in surface energy.

Under real conditions, one should consider the factors which can lower the driving force of growth of nuclei and thus retard recrystallization. These include solute impurities, and excess-phase particles. The force that retards boundary migration is denoted as P_{ret}. All the stages of recrystallization except for the formation of recrystallization nuclei are realized through the migration of large-angle boundaries. The rate of boundary migration depends on P. which determines the direction of motion of a boundary, and also on mobility M of the boundary proper, which is determined by the structure of the boundary.

The rate of boundary motion and the rate of recrystallization can be written in a general form as, $V=M\Sigma Pi$. ----------(9a)

For primary recrystallization, $Vpr = MPv$; ----------(9b);

for grain growth, $V_{gr} = MP_b$; ----------(9c);

for secondary recrystallization, $V_{sec} = MP_h = MP_v = MP_a$, ----------(9d);

depending on the particular conditions. Regarding the retarding forces, the rate of boundary migration may be found as $V=M (P_{dr} - P_{ret})$.----------(9e).

Generally, on the basis of plastic deformation alone, recrystallization may be understood as a process which takes place in metals and alloys following distortion and fragmentation of constituent crystals by severe mechanical deformation, in which some fragments grow at the expense of others so that larger strain-free grains are formed; it progresses slowly at room temperature, but is greatly speeded by annealing. It is pertinent to mention here that the Al-Mg-Si alloy like most Aluminium alloys do not

undergo polymorphic changes during heat treatment or thermoplastic processing as clearly revealed by the pseudo-binary phase diagram of the alloy in Figure 2.5.

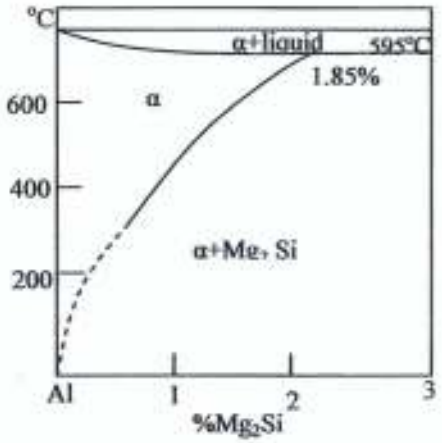

Figure 2.5 Pseudo-Binary Phase diagram for Al-Mg-Si alloy (After Polmear, 1989).

2.9 THERMOMECHANICAL PROCESSING

Thermomechanical working is a kind of processing involving plastic deformation and heat treatment, which increases the density of defects and affects the formation of the structures, as a result of phase transformations occurring during the thermal deformation actions. Plastic deformation causes a change in the pattern of distribution and an increase in the density of imperfections, such as dislocations, vacancies, stacking faults, low- and high-angle boundaries in an alloy. Since crystal lattice defects produce a strong effect on the formation of structure in alloys during phase transformations, plastic deformation before or during phase transformations can be used to form optimum structure in a heat-treated alloy.

Consequently, not every combination of straining, heating and cooling can be called thermomechanical processing. For example, if plastic deformation is carried out after all operations of heat treatment have been completed, then we are dealing with common heat treatment followed by plastic working rather than with thermomechanical

processing. Such is the case of plastic deformation after ageing, which will produce strain hardening and increase strength properties. However, this has no effect on the structure formed through phase transformations, since these transformations have taken place before the plastic deformation was applied.

If plastic deformation was effected prior to heat treatment and produced no decisive effect on the final structure formed in an alloy during phase transformations, it should be regarded as a simple combination of plastic working and heat treatment, rather than thermomechanical processing. This is the case of cold rolling followed by solution heat treatment, and both thermal transformation and deformation are not simultaneously causing significant structural changes. The process of plastic deformation and heat treatment in thermomechanical processing may be either combined in a single technological operation or made with a time interval of up to a few days one after the other. It is only important that phase transformations take place under the conditions if increased density of the lattice defects formed through plastic deformation (Novikov 1978).

At present, various methods of thermomechanical processing being employed in the industry are presented schematically in Figure 2.6. The first method is called low temperature thermomechanical treatment (LTMT), the second is high temperature thermomechanical treatment (HTMT), the third is high-low temperature thermomechanical treatment (HLTMT), and the fourth is preliminary thermomechanical treatment (PTMT). All of them include plastic deformations which produce the decisive effect on the formation of the structures in alloys on ageing or during polymorphic transformations.

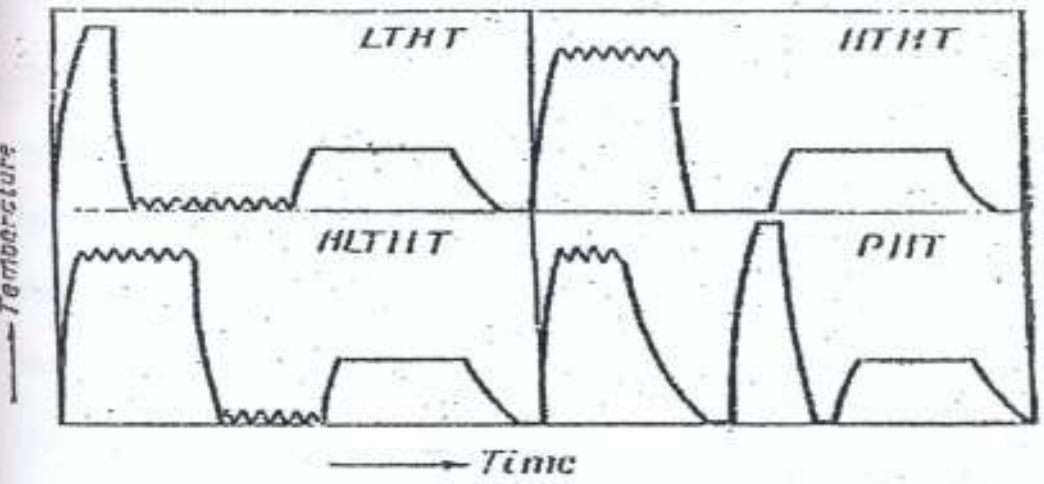

Fig. 2.6 Principal schemes of Thermomechanical processing of ageing alloys.
(After Novikov,1978)

Thermomechanical processing as applied to ferrous metals, steels in particular, consists of the following categories or types;

(1) **Controlled rolling**

(2) **Hot-cold working**

(3) **Ausforming**

(4) **Isoforming**

(5) **Marstraining**

(6) **Crysoforming and**

(7) **Thermomechanical annealing.**

Each of these operations involves heating, deformation at a particular temperature and eventual cooling to obtain a desired structure and properties. Details of each of these methods are found in literature; (Rajan et. al. 1988, Lakhtin 1990, and Gulaev, and Leshinskaya, 1980).

Thermomechanical processing of non-ferrous alloys is commonly applied to the age-hardenable alloys. The process consists of plastic deformation of alloys followed by ageing treatment. This is in contrast to thermomechanical treatments applicable to steel, which consist of plastic deformation and simultaneous phase transformation. However this is classified as a thermomechanical process because the mechanical working has been performed to effect and promote favourable ageing process. This is distinct from the case when the mechanical processing is carried out after no further ageing process can take place. Significant amount of work has been done on thermomechanical processing of non-ferrous alloys. Aluminium, Copper, and Nickel base precipitation hardenable alloys have been successfully subjected to thermomechanical treatment (Rabinovich, 1972; Singh andGoel, 1990; El-Baradie and El-Sayed, 1996; Celentano, 2002)

However, microstructural modeling of thermomechanical processing is well established as a valuable procedure for optimizing processing conditions in the steel industry (Beynon and Sellars, 1992) and is currently the subject of major research efforts in the Aluminium industry,(Vatne et.al,,1996). Depending on the temperature of deformation, the process can be divided into two major classes, namely, low temperature thermomechanical processing (LTMT) and high temperature thermomechanical processing (HTMT).

2.9.1 LOW-TEMPERATURE THERMOMECHANICAL TREATMENT (LTMT)

Low-temperature thermomechanical treatment of ageing alloys is the oldest, (introduced in the 1930s), and most widely used method of thermomechanical treatment. It is mainly used to enhance the strength properties of alloys.

With LTMT, an alloy is first quenched by a common technique and then subjected to cold deformation prior to ageing.

As compared with ageing without preliminary deformation, LTMT, yields higher values of ultimate tensile strength, yield strength, hardness and toughness but lowers ductility indices. Curve (1) in figure 2.7 shows how the degree of cold deformation affects the hardness of a quenched nickel alloy, a typical f.c.c alloy, while curve (2) is for deformation and ageing at 160°C for 16 hours.

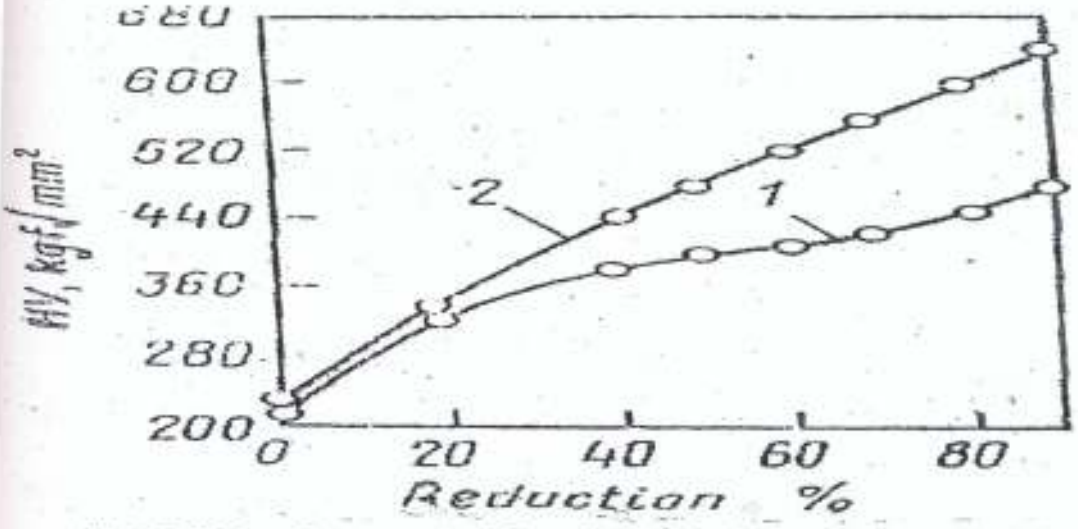

Fig.2.7 Effect of percentage deformation on hardness of typical metallic alloy under varied working conditions.

1- Cold drawn ; 2- Deformed and aged at 160°C for 16 hours (Novikov , 1978)

According to Bernstein, (1968), the hardening effect produced by LTMT may be explained by two principles. Firstly, the cold deformation produces strain hardening, so that the subsequent precipitation hardening begins from a higher initial hardness level of the alloy. Secondly and most important, cold deformation enhances the effect of precipitation hardening. With increasing degree of cold deformation, the hardening effect on ageing increases continuously (see the diverging curves 1 and 2 in Fig 2.7). With 90% reduction, the gain in hardness produced by ageing has amounted to 175kgf/mm^2 (1716MPa). Consequently, cold-working in the case considered has enhanced the hardening effect on ageing by one order of magnitude.

Experimental evidence and detailed analysis show that the effect of strain-hardening on ageing may be quite complicated. The nature of this effect depends on the

(a) structure of the alloy and type of precipitates,

(b) super saturation condition,

(c) quenching condition,

(d) ageing potential, and

(e) amount of previous ageing.

The effectiveness of LTMT is decided by the strengthening phase that precipitates on ageing. Usually, heating for ageing purpose after cold deformation is carried out to achieve only recovery and polygonization processes which diminish somewhat the hardening effect provided by LTMT (Novikov, 1978).

The formation of stable incoherent precipitates instead of semicoherent metastable precipitates during ageing of a strongly strain hardened solid solution can diminish the

hardening effect (Rabinovich, 1972). For this reason, the strength of aged alloy after a heavy deformation may turn to be lower than that of a less deformed alloy, notwithstanding, the strength level of the former before ageing.

Pre-ageing prior to plastic deformation accelerates micro structural changes as well as enhances the hardening effect in subsequent ageing process. One of the probable causes may be that plastic deformation of a preliminarily aged alloy forms a more favorable structure characterized by a high density of uniformly distributed dislocations. It is only reasonable that a time interval is allowed between quenching and cold deformation in LTMT of naturally ageing alloys. For instance, in LTMT of sheets and tubes of certain 6xxx alloy, this interval was observed to be at least 2 hours in order to obtain the maximum strengthening or hardening effect (Nes, 1995). Pre-ageing can be either natural or artificial.

Even though increased strength can also be obtained by using common cold deformation after ageing, LTMT ensures for same strength, higher ductility, lower residual stresses and a structure possessing a higher thermal stability. When resorting to LTMT, one should always consider the possible adverse effects, such as a reduced ductility, which is characteristic of most alloys, a lower creep resistance in some Aluminium alloys and anisotropy of properties.

In recent times, LTMT takes different forms, and is widely used in the manufacture of semiproducts and products from ageing copper, austenitic alloys, and some Aluminium alloys. Among the products produced in this way are sheets and tubes.

2.9.2 HIGH TEMPERATURE THERMOMECHANICAL TREATMENT (HTMT)

High temperature thermomechanical processing of alloys includes hot deformation, quenching from deformation temperature, and ageing.

Hot deformation increases the density of dislocation and produces hot strain hardening effect, which can be partially or fully removed owing to the development of dynamic polygonization and dynamic recrystallization.

The stress-strain curve of the process has an ascending section of creep stresses, which corresponds to the stage of hot strain-hardening and a descending stress section, which is due to the development first of polygonization and then of recrystallization. With dynamic polygonization, as is also common in static polygonization which is observed in heating after cold deformation, the formation and migration of low-angle boundaries are controlled by dislocation climb. In contrast to static polygonization however, dislocations are continuously "pumped" into the body of subgrains under the action of the stress applied in the course of hot straining. A similar difference exists between static recrystallization and dynamic recrystallization. In the course of hot deformation, the processes of hardening by increasing the dislocation density and softening due to decreasing number of dislocations in polygonization and recrystallization, alternate continuously. Gorelik (1981), affirmed that, depending on the nature of alloy, temperature, rate, degree and pattern of straining, the metal at the end of hot deformation may either strain-hardened or have a polygonized, recrystallized or mixed-type, partially polygonized and partially recrystallized, structure.

A fully recrystallized structure with the minimum dislocation density corresponds to the most stable state. If the structure has not been recrystallized, or has been recrystallized only partially at the end of hot deformation, there forms a stimulus to static recrystallization. Upon straining with a high degree of deformation, a very quick recystallization without any induction period may be observed, since the nuclei of recrystallized grains are formed in the course of hot deformation. According to Fridlander (1971), this process is called metadynamic recrystallization. In his words, the aim of HTMT in Aluminium alloys is to form a supersaturated solid solution with non-recrystallized structure upon hot deformation and quenching. In this respect, a structure having an increased density of imperfections (subgrain boundaries and free dislocations) results. An alloy of such a structure obtains better mechanical properties on subsequent ageing. In most cases, the polygonized matrix of the quenched alloy is the best choice. When using HTMT, at least three requirements must be fulfilled;

(a) a non-recrystallized structure must form at the end of hot deformation,

(b) probable recrystallization upon hot deformation must be prevented,

(c) the degree of supersaturation of the solid solution must be sufficient for subsequent ageing.

The use of HTMT is limited by a number of factors. An alloy may have a very narrow range of temperatures of heating for quenching so that it is practically impossible to maintain the temperature of hot plastic working in the same narrow range for instance within 15°C with Duralumin(Novikov,1978). The optimum temperature range of hot deformation may be substantially lower than the range of temperatures of heating for quenching. For instance, the rate of deformation in pressing of Aluminium alloys(without

the appearance of surface cracks), will be lower, the higher the temperature of deformation. If it is required to substantially increase the temperature level of heating for quenching, the rate of deformation must be inevitably reduced, which lowers the productivity. With an alloy having susceptibility to recrystallization, it may be difficult to form unrecrystallized structure towards the end of deformation and retain it in the period between the end of deformation and the moment when the temperature will drop down to the recrystallization temperature t_r^s, in cooling.

Omotoyinbo, et.al, (2006) reported that HTMT is used to improve the strength properties and ductility of steel compared with the properties they have in the recrystallized state. They established the fact that the coarser the grains, the better ductility because more extensive slippage can take place during plastic deformation before fracture.

Formation of fine and uniform precipitates from the solid solution with very fine grains structure, ensure high level of strength, and ductility upon HTMT. In contrast to LTMT, which noticeably lowers the ductility, the additional hardening effect produced by HTMT is obtained with the ductility being virtually unchanged. In Aluminium alloys, the ductility and impact toughness can even increase upon HTMT.

The hardening effect produced by HTMT can be retained at a higher temperatures than that obtained through LMTM. An increased heat resistance of alloys on HTMT may be attributed to the toothed shape of grain boundaries, which inhibit intergranular fracture and to the appearance of subgrain boundaries locked by precipitated particles, (Jensrud and Pedersen, 1998).

In particular, Al-Mg-Si alloys, being heat treatable are often subjected to HTMT, to explore the effect of such treatment on the quality of the alloys.

Aluminium may be characterized by high stacking fault energy, so that polygonization, can occur in it quite easily. Pressing usually forms a very stable polygonized structure in Aluminum alloys, so that special measures to form and retain this structure in HTMT are not usually needed, (Kevorkijan, 2002).

With ageing alloys, HTMT is used less frequently than LTMT in the industries, mainly because of the processing limitations and the lower hardening effect. A combination of HTMT and LTMT, called high-low temperature thermomechanical processing has been put to use in recent times. It comprises quenching from the deformation temperature, followed by cold deformation and ageing. The process gives a higher ultimate strength and a lower ductility than HTMT.

2.9.3 PRELIMINARY THERMOMECHANICAL TREATMENT (PTMT)

In preliminary thermomechanical treatment or processing (PTMT), the processes are such that a semiproduct, which has an unrecrystallized structure upon hot deformation, retains this structure during heating for quenching. PTMT differs from HTMT in that the operations of hot deformation and heating for quenching are performed separately (See Fig 2.5). According to Dobatkin (1965) and Nes, (1995), PTMT enhances structural strengthening in Aluminum, and the gain in the ultimate strength and yield strength in ageing Aluminium alloys is attributed to the retention of unrecrystallized structure which may be about 10-40 percent. Ageing of an uncrystallized alloy produces a higher hardening effect by increasing the difference between the properties of

recrystallized and unrecrystallized semi-products. The ductility is higher in alloys in recrystallized state.

Both in PTMT and HTMT, the formation of an unrecrystallized structure is favoured by higher temperature and lower rate deformation, a lower degree of deformation and by the pattern of deformation approaching uniform compression. It is worth noting that polygonization can develop intensively in Aluminium alloys and this produces a stable network of sub-boundaries, which can cause an unrecrystallized structure to be easily formed especially by pressing.

Structural strengthening of Aluminium alloys subjected to PTMT, has found a wide application in large-tonnage mass production of semi products and is an example of effective industrial use of thermomechanical processing.

2.10 PRECIPITATION STRENGTHENING OF Al-Mg-Si ALLOYS.

The strength and hardness of Al-Mg-Si alloys and some other metal alloys may be enhanced by the formation of extremely small uniformly dispersed particles of a second phase within the original phase matrix. The process by which this is accomplished is called precipitation strengthening or hardening. The small particles of the new phase (the second phase) are termed "precipitates". "Age hardening or strengthening" is also used to designate this process because the strength of the alloy develops with time or as the alloy ages.

The phenomenon of natural ageing was first discovered in Aluminium-Copper alloy, containing some amount of Magnesium, by Alfred Wilm, a German engineer, in 1906. He found that a quenched alloy of Aluminum with Copper and Magnesium (duralumin) increase its hardness when stored for a while at room temperature.

Heat treatable Al- Mg-Si alloys of the 6xxx series are known for their medium to high strength, excellent formability and good corrosion resistance (Murtha 1995; Kamat et al, 2002), making them more appropriate for certain applications than the stronger Al-Zn 7xxx series. Al -Mg-Si alloys can be strengthened through the precipitation of the metastable precursors of the equilibrium β(Mg_2Si) phase. A number of studies on the ageing behaviour of experimental Al-Mg-Si alloys (Murayama et. al., 1998, 2001; Murayama and Hono, 1991; Matsuda et. al., 1999; Takeda et. al., 1998) and commercial Al-Mg-Si, 6016 (Moons et. al., 1996; Gupta et. al., 2001), 6063 (Siddiqui et. al., 2000) are available.

In their attempt to study the ageing behaviour of the 6xxx series alloys, Miao and Laughlin (1999, 2000), suggested the following precipitation sequence in the Al-Mg-Si alloy, (e.g. 6022 alloy);

α(SSS) -→ GPzones → β"needles→β'rods + lath-like particles →β+

Si (various morphologies)

where α (SSS) is the supersaturated solid solution and GP zones are spherical clusters with unknown structure.

Precipitation strengthening involves two distinct stages. The first is the solution heat treating of the alloy and the second is the precipitation heat treating. Both are schematically represented in Fig.2.8.

Often it is more useful and convenient to present the data on the growth of the precipitate β particles in terms of the strengthening achieved with time. In this respect, the tensile strength, yield strength or hardness obtained at a temperature (T^0C) is plotted as a

function of the logarithm of ageing time. A typical characteristic curve of the ageing process for the Al-Mg-Si alloy is shown schematically in Fig 2.9. (After Callister Jnr., 1997)

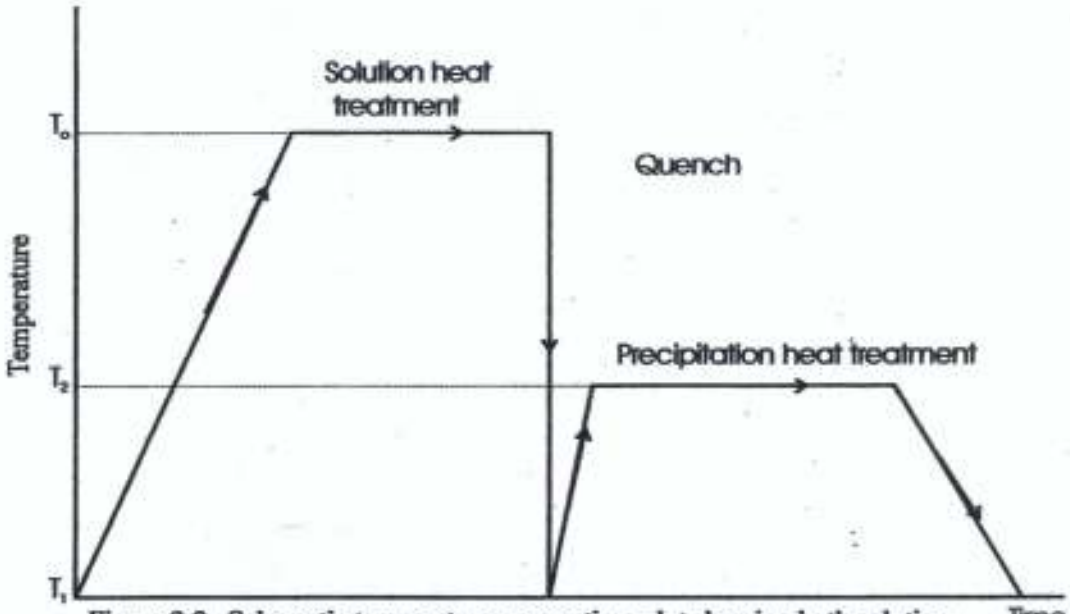

Figure 2.8 . Schematic temperature-versus-time plot showing both solution and precipitation heat treatments for precipitation strengthening

(After Callister Jnr., 1997)

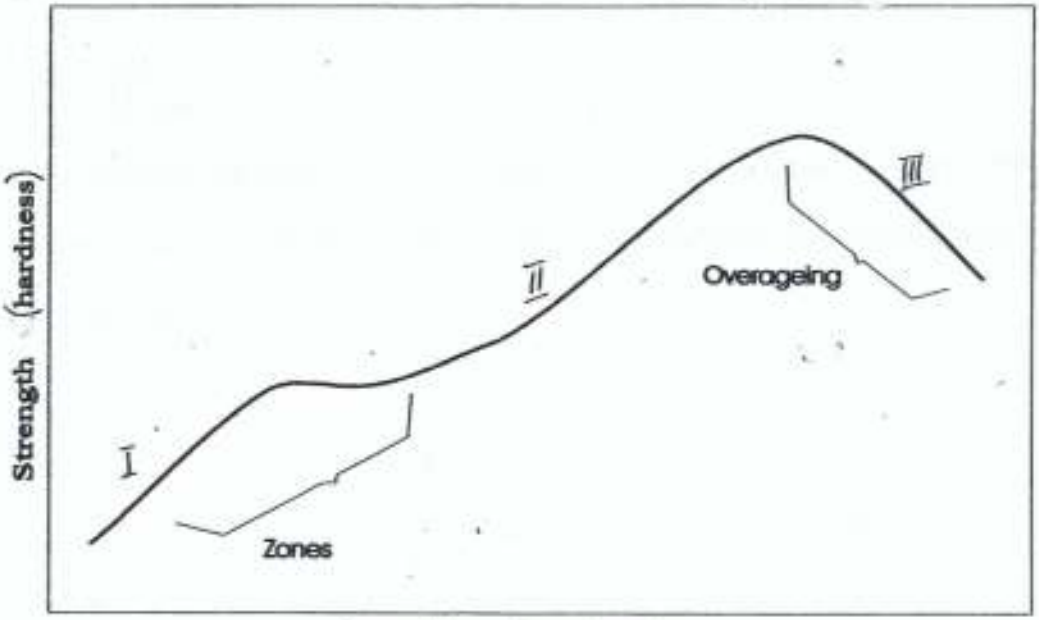

Figure 2.9 Schematic diagram showing strength and hardness as a function of the logarithm of ageing time at constant temperature during the precipitation heat treatment.

There are three principal zones.

Stage I- GP zone formation

Stage II- Formation of intermediate metastable phase

Stage III- Formation of intermediate stable phase

2.10.1. Kinetics and Sequence of Precipitation on Ageing.

Figure.2.10 shows the dependence of free energy on the composition of supersaturated α - solution which stratifies with the formation of G.P zones, metastable β' - phase and stable β – phase.

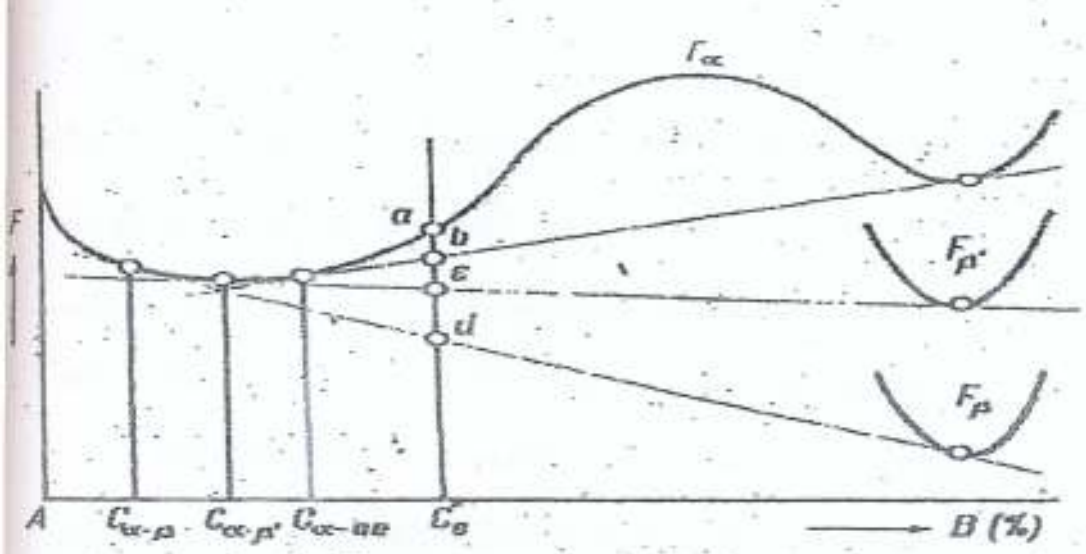

Figure 2.10 Dependence of free energy on composition of supersaturated α-Al solid solution which stratifies with the formation of G.P zones, metastable β'-phase and stable β-phase (After Novikov,1978)

The free energy in an alloy composition C_0 (of the Al- Mg-Si alloy) reduces more appreciably on the precipitation of the stable β-phase than on the formation of intermediate β'-phase and GP zones, i.e. ad> ac>ab as shown in the Figure 2.10. This,

however, by no means implies that the probability of formation of a stable phase in ageing is always greater. The ordinate axis in Fig 2.10, gives the values of the volume free energy. As has been established, the sequence of phase formation is controlled by the energy barrier on nucleation of a new phase, rather than by the attainable level of volume free energy.

The energy barrier of nucleation or the work of formation of a critical nucleus (ΔF_{cr}) without elastic component, is equal to one third of the surface energy as expressed below

$$\Delta F_{cr} = 1/3 S\gamma \qquad (10)$$

S is the surface area of the crystal and γ is the free energy per unit area.

The surface energy is at its minimum in G.P. zones and at its maximum with the incoherent precipitates of a stable phase. Therefore, $\Delta F_{cr}^{G.P} < \Delta F_{cr}^{\beta'} < \Delta F_{cr}^{\beta} < \Delta F_{cr}^{\beta}$. In ageing, the energy barrier to nucleation of precipitates is formed due to elastic deformation of the lattice, as well as to the formation of an interface.

The elastic deformation on nucleation of semi coherent precipitates of β' - phase is greater than that on nucleation of incoherent precipitates of β - phase.

Then, inequality $\Delta F_{cr}^{\beta'} < \Delta F_{cr}^{\beta}$ can only be satisfied if the gain in surface energy outweighs the possible loss in the elastic strain energy.

The rate of precipitates nucleation in an ageing alloy is determined by an expression such as

$$J = Ae^{\frac{-\Delta F_{cr}}{KT}} e^{\frac{-Q}{KT}} \quad (11)$$

Q is the activation energy of passage of an atom through an interface.

$e^{\frac{-\Delta F_{cr}}{KT}}$ is a factor, that determines the number of critical nuclei.

$e^{\frac{-Q}{KT}}$ is a factor, that determines the frequency with which atoms are attached to a nucleus.

It has been established that as the degree of undercooling increases, the number of critical nuclei formed in a unit volume per unit time owing to energy fluctuations also increases, and their number should be proportional to the factor, $e^{\frac{-\Delta F_{cr}}{KT}}$ (Edwards, et. al., 1998).

A critical nucleus becomes a center of crystallization only when it has attracted one or a few atoms of the mother phase. The frequency with which atoms are attached to a nucleus is proportional to the factor, $e^{\frac{-Q}{KT}}$, where Q is the activation energy of passage of an atom through an interface, or the activation energy of diffusion of the element having the lowest diffusion rate.

G.P. zones, intermediate metastable and stable phases can be characterized by their own C-curves (Fig.2.11). The upper branches of C-curves approach asymptotically the respective solvus temperatures $T_{G.P.}$, $T_{\beta'}$ and T_{β}.

Sections of the figure are the induction periods for each C-curve. An induction period is understood as the time before precipitation starts. With increasing temperature of ageing, the induction period first shortens owing to a higher diffusion mobility of atoms, and then increases due to lower supersaturation of the solid solution relative to a given phase.

Ageing at different temperatures results in transformation of α-matrix through one or more metastable intermediate phases before (if ever) reaching a stable intermediate phase β. In figure 2.11 for example, ageing at;

T_1 results in $\alpha \rightarrow$ G.P. $\rightarrow \beta' \rightarrow \beta$,

T_2 results in $\alpha \rightarrow \beta' \rightarrow \beta$, and

T_3 results in $\alpha \rightarrow \beta$.

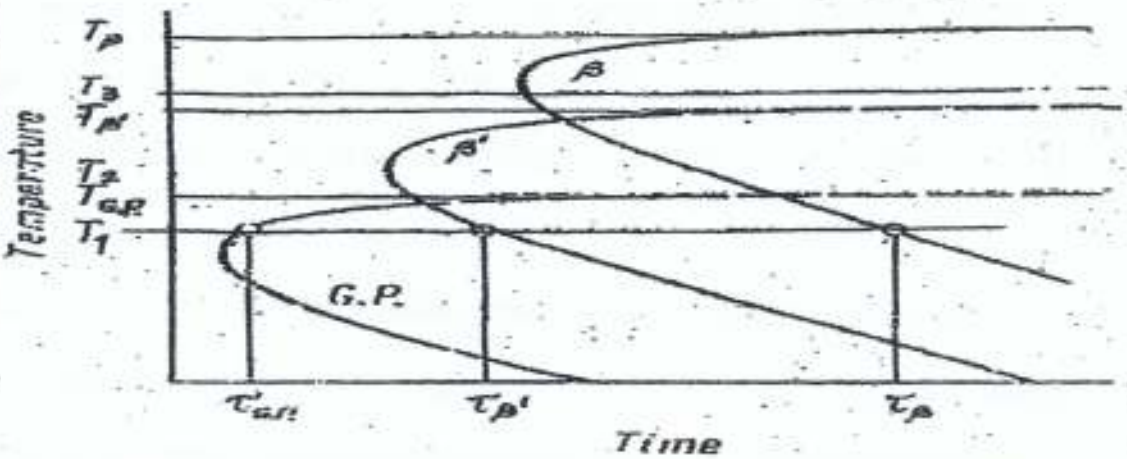

Fig.2.11 C-curve for formation of GP zones, intermediate β'-phase and stable β-phase on precipitation of supersaturated solution in an aged alloy (shematically) $T_{G.P.}$, $T_{\beta'}$, T_β-solvus temperatures of precipitates in Co alloy in figure 2.10. (After Novikov,1978)

It is even possible to have more C-curves for which the transformation of α-matrix could be of the type; $\alpha \rightarrow$ G.P. $\rightarrow \beta'' \rightarrow \beta' \rightarrow \beta$ or $\alpha \rightarrow$ G.P.1 $\rightarrow$ G.P.2 $\rightarrow \beta'' \rightarrow \beta' \rightarrow \beta$, depending on temperature.

The sequence of formation of precipitates is often written as $\alpha \rightarrow$ G.P. $\rightarrow \beta' \rightarrow \beta$, (or $\alpha \rightarrow$ G.P. $\rightarrow \beta'' \rightarrow \beta' \rightarrow \beta$). At ageing temperature T_2 which is higher than the solvus

temperature of G.P. zones, the β'-phase is first precipitated from the supersaturated solution followed by the precipitation of the β-phase, i.e. by the α→ β'→ β sequence of precipitates formation. At the temperature T_3, exceeding the solvus temperature of the β' - phase; only the stable β-phase can precipitate from the supersaturated solution. The above explains the general rule stating that, the lower the degree of supersaturation of the solid solution relative to a stable phase the smaller is the number of intermediate transformations (Frank, 2004)

The statement of the process of supersaturated solution precipitation α → G.P → β'→ β only indicates the time (at constant temperature) or temperature (at constant holding time) sequence of the appearance of various precipitates. This formula should not be understood as if G.P. zones always transform due to lattice rearrangement into β' - phase and latter, into β - phase.

Three possible ways for the formation of more stable precipitates are identified:

1. Direct transformation of less stable precipitates into stabler ones, i.e. a change in the types of lattice, allotropic transformation within the volume of a precipitate without the participation of the matrix. This method is only feasible at a low difference in the structures of precipitates, and is therefore used only rarely. G.P1--- >G.P2 (θ") e.g. in Al–Cu.
2. The nucleation of a β' - phase at G.P zones and the growth of β' - precipitates in the matrix and finally, the nucleation of β - phase at β' - precipitates and the growth of β - particles in the matrix.
3. An independent nucleation of a stabler phase in the matrix far from the precipitates of a less stable phase and far from G.P. zones.

2.10.2 Mechanism of Strengthening or Hardening.

Phase transformations in alloys can generate particles or precipitates of a second phase, which may differ from the matrix by their composition and structure, whether crystalline or amorphous. Important parameters of precipitation – hardening in alloys are the strength of the precipitate phase, its relative volume and volume fraction, and dispersion of the particles in the matrix, their mean sizes and the typical distance between them.

Two distinct or major mechanisms are recognized.

(a) *Interaction mechanisms between particles and dislocations.*

(b) *The Orowan mechanism*

(a) Interaction mechanisms between particles and dislocations. Precipitated particles can effectively obstruct the motion of dislocation in the matrix by one or more of the following mechanisms,

i) Parelastic interaction: The particles interact with dislocations via their stress field, generated by a volume contraction or expansion associated with phase transformation, or by coherency stresses between the particle and the matrix.

ii) Dielastic interaction: The particles alter the shear modulus G of the matrix. Since the energy,

$$E_L = \frac{Gb^2}{4\pi}\left(1+\frac{v}{1-v}\sin^2 Q\right)\ell n\left(\frac{R}{R_o}\right) \qquad (12)$$

of a dislocation per unit line length (Frank, 2004), is proportional to the shear modulus G, a local change of G implies an attractive or repulsive interaction between the

dislocation and the particle. R is the upper limit and R_o the lower limit of the radius within which Hooke's law is valid.

(iii) Particle intersection: If the particle is coherent with the matrix, thus if the glide planes of the matrix continue through the particle, a dislocation can intersect the particle, then glide through it. However, this will shear one half of the particle versus the other by b, the Burger's length. Since the particle shape is generally convex, in order to minimize the energy $\gamma_{\alpha\beta}$ (per unit area) associated with the particle – matrix interface, this process increases the interface areas and therefore requires additional interfacial energy. This implies a repulsive force (per unit length) of

$$F_{max} = \gamma_{\alpha\beta} \cdot r_p, \qquad (13)$$

where r_p, denotes the radius of the particle.

(b) The Orowan Mechanism.

The line energy of a dislocation implies a line tension – the dislocation tends to shorten itself, like a rubber band. Consider a dislocation segment between two dislocation – pinning precipitates separated by a distance *l*. Under a resolved shear stress τ, the dislocation segment bows out until the line tension balances the force generated on the dislocation segment by τ.

Consequently, the shape of the dislocation segment becomes a semi-circle with radius

$$r_c = \frac{E_L}{\pi b} \qquad (14)$$

However, if the distance l between the pining points is smaller than r_c, the dislocation becomes unstable and "swells" until the neighouring segments recombine behind the obstacles and leave behind a dislocation loop around it. Figure 2.12 illustrates the individual steps of this so-called "Orowan" mechanism.

Inserting $r_c=l$ in the equation above, and solving for τ yields the "Orowan stress" – the minimum stress required for the Orowan mechanism to operate

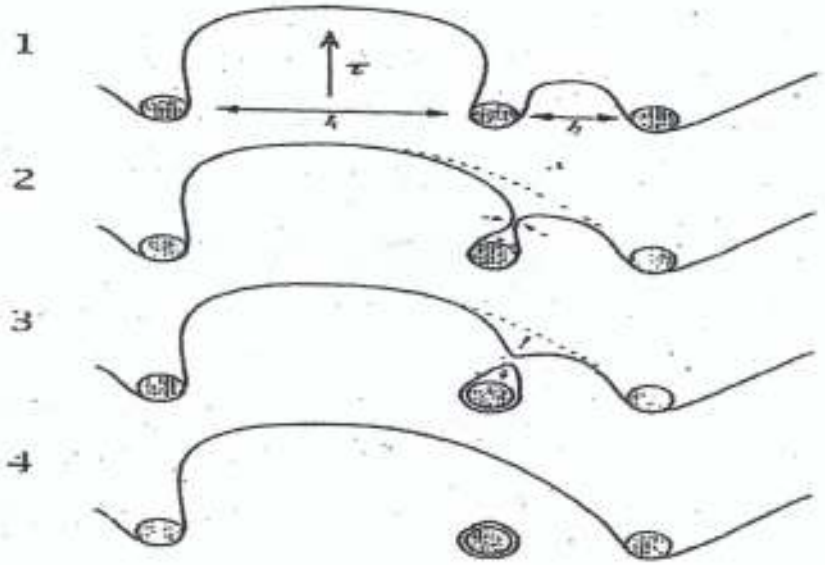

Figure. 2.12 Individual steps of the Orowan mechanism, by which a dislocation can overcome pinning obstacles like precipitates. (After Frank, 2004)

$$\tau_1 = \frac{2E_L}{b\ell} = \frac{\frac{2Gb^2}{4\pi}\left(1+\frac{\nu}{1-\nu}\right)\sin^2(Q)\ell n\left(\frac{R}{R_o}\right)}{b\ell} \approx \eta\frac{Gb}{\ell} \qquad (15)$$

where η is a scaling factor accounting for the interaction between the dislocation segment under consideration and neighbouring segments, and E_l has been approximated by $1/2Gb^2$.

2.10.3. Ageing and Overageing

It is a well established fact that, the hardening effect of precipitates depends on two parameters: the particles size (rp) and the particle spacing (l). In a model developed by Fleischer (1964), one considers the "Friedel length" l_f, the mean distance between the particles that a dislocation touches under a resolved shear stress τ. With increasing shear stress τ, the dislocation touches more particles, thus l_f decreases. For a maximum force, F_{max} between the dislocation and particles, mechanical equilibrium implies

$$\tau_{eq}.b.l_f = F_{max} \qquad (16)$$

Since the Friedel length l_f is related to the concentration Ca of particles in the glide plane (per unit area) by the expression, $\ell_f = \sqrt{\frac{6E_l}{\tau.b.Ca}}$ (17)

then the preceding expression implies

$$\tau_{eq} = \sqrt{\frac{F_{max}^3.Ca}{6E_l b^2}} \qquad (18)$$

For each kind of interaction, F_{max} can be replaced by a term $\gamma.r_p$ with an "effective" interface energy γ (for the parelastic interaction, $\gamma = Gb|\delta|$, where δ denotes the radial strain). This leads to $r_{eq} = \sqrt{\frac{\gamma^3 v_p r_p}{6E_l b^2}}$, (19)

where, Vp denotes the volume fraction of the particles.

Let us consider an alloy with a certain dispersion of precipitates, thus with a certain mean particle size and interparticle spacing. We assume that the volume fraction of the precipitated phase corresponds to the equilibrium volume fraction. On tempering the material, no further precipitation will occur. However, large particles will grow at the expense of small particles in order to reduce the total energy of the phase boundaries in the system – "Ostwald ripening". The question arises as to whether the strength of the material will increase or decrease. A fine dispersion of small particles, as it may exist at the beginning of the tempering process, will not effectively strengthen or harden the alloy because small particles are no strong obstacles for dislocations. A coarse dispersion of large particles, on the other hand, as it will form after prolonged annealing times, will not effectively strengthen or harden the alloy either.

While the particles are large and interact strongly with dislocations, their spacing is correspondingly large. Therefore, the dislocations can easily pass them via the Orowan mechanism.

Optimum strength or hardness, therefore, will result from dispersion between these two extremes. The particle radius r_p^* at which the hardness should reach its maximum for a given volume fraction Vp of precipitated phase is obtained from the following equation;

$$\eta\frac{Gb}{\ell}=\eta\frac{Gb}{r_p}\sqrt{V_p}=\sqrt{\frac{\gamma^3\gamma_p r_p}{6E_L b^2}}\approx\sqrt{\frac{\gamma^3\gamma_p r_p}{3Gb^4}} \qquad (20)$$

Again, the dislocation line energy has been approximated by $1/2Gb^2$

Solving the above equation for the particle diameter, yields the particle diameter required for maximum strengthening or hardening.

$$r_i^* = \frac{Gb^2}{\gamma}\left(3\eta^2\right)^{1/3} \qquad (21)$$

Generally, the strength of precipitation – hardened alloys increase with increasing particles size as long as dislocations can intersect the particles.

As so as it is more favourable that the dislocations pass the particles via the Orowan mechanism, increasing particle size decreases the strength. This behaviour is schematically illustrated in figure 2.13.

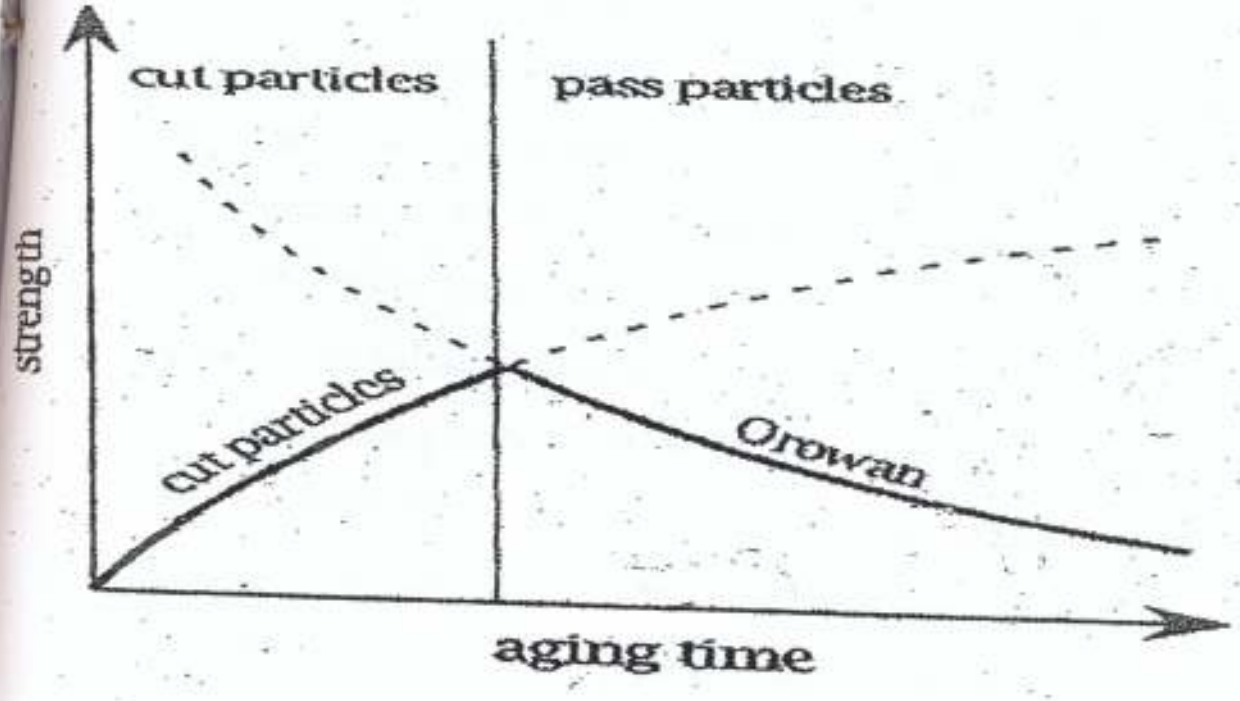

Figure 2.13 Effects of particle size on the stress required to make dislocations intersect or by pass particles (After Novikov,1978)

CHAPTER THREE
3.0 EXPERIMENTAL TECHNIQUES

3.1 MATERIALS AND PREPARATION

The 6063 aluminium alloy of commercial purity, used in this study, was obtained from the Nigerian Aluminium Extrusion (NIGALEX) Plc. Lagos. The material was produced as hot extruded, 16mm diameter rods of about 600mm length. The determination of the chemical composition of the alloy was carried out at the quality control laboratory of the same company using a computerized spark spectrometer. The results obtained are as presented in Table 4.1.

3.2 EQUIPMENT USED

The following major facilities which are situated in the laboratories and workshops of the School of Engineering and Engineering Technology, Federal University of Technology, Akure were used in this study; they are Carbolite heat treatment furnace, Monsato tensile testing, lathe, grinding, and polishing machines. Also used are impact and hardness testing machines that are located at the laboratory of the department of Material Science and Engineering, Obafemi Awolowo University, Ile-Ife. Others include laboratory rolling mill situated at the department of Mechanical Engineering University of Lagos, computerized spark spectrometer located in the quality control unit of the Nigerian Aluminium Extrusion (NIGALEX) also in Lagos, and optical metallurgical microscope situated at the Engineering Materials Development Institute, Akure. The transmission electron microscope at the department of Chemical and Materials Engineering, University of Manitoba, Canada was used for the TEM micrographs.

3.3 SOLUTION HEAT TREATMENT (SHT)

The as-received Al-Mg-Si(6063) alloy from NIGALEX was solution heat treated(SHT) by heating to 530^0C for 2hrs in a carbolite electric furnace situated at the laboratory of the Metallurgical and Materials Engineering Department, Federal University of Technology, Akure and finally water quenched to room temperature. This treatment is fundamental to all ageing processes on which the thermomechanical ageing operations depend. Consequently, all the samples were solution heat treated before subsequent ageing, thermoplastic working, and thermomechanical ageing.

From the solution heat treated samples, tensile and impact tests specimens were prepared using the lathe machine under liberal cooling to minimize heating and machining stresses. The specimens were tested accordingly and the results of the tests presented in Table 4.2 in appendix1.

3.4 THERMOPLASTIC PROCESSING OF SAMPLES (NO ARTIFICIAL AGEING)

Some as-received samples after solution heat treatment were subjected to varying degrees of deformation at 28^0C(room temperature),160^0C, 180^0C, 200^0C,220^0C and 240^0C warm temperatures by rolling ,a process hereby referred to as thermoplastic processing (TPP). Soaking time at each temperature was 45 minutes and the percentage deformation employed varied from 10% -50% at intervals of 10%.

The purpose of this treatment was to assess the effects of the temperature and degree of deformation, without ageing, on the tensile strength and plasticity indices of the alloy. For the purpose of this investigation and in accordance with

recent nomenclature of working temperature for alloys of this category (Goel and Singh, 1990), this temperature range (160^0C-240^0C) is considered "warm" temperatures. Below 150^0C constitute "cold" temperatures while those above 300^0C belong to "hot" temperatures (Gracio et.al. 2004).

The degree of plastic deformation is expressed in this experiment as percent warm work rather than as strain. Percent warm work (% WW) is defined as;

$$\% \text{ WW} = A_0 - A_d / A_0 \times 100,$$

where A_0 is the original area of the cross section that experiences deformation, and A_d is the cross sectional area after deformation at the chosen working temperature above 150^0C.

Tensile and impact tests specimens were machined from the thermoplastically worked samples and the mechanical properties of the worked alloy computed after the tests were carried out. The results are presented in Tables 4.3- 4.8.

3.5 AGEING OF SAMPLES (NO PLASTIC DEFORMATION)

The as-received 6063 alloy from NIGALEX was solution heat treated (SHT) by heating to 530^0C for 2hrs and water quenched to room temperature. Tensile and impact tests specimens were prepared from the solution heat treated alloy, and aged artificially at 160^0C, 180^0C,200^0C, and 220^0C for ageing times varying from 1hour to 20 hours at 2hours intervals, after which they were quenched in water. Thereafter the specimens were tested using standard procedures to determine the tensile and impact properties. The results of the tests are contained in Tables 4.9- 4.13 in appendix 1.

3.6 THERMOMECHANICAL AGEING

Thermomechanical ageing of the 6063 alloy was carried out according to the work schedules presented in Tables 3.1a, 3.1b, and 3.1c. The following operations were performed sequentially on the samples;

(a) solution heat treatment by heating the alloy to 530^{0}C for 2 hours and water quenched to room temperature,

(b) some samples of the alloy from (a) above were aged at 180^{0}C for 12hours and water quenched to room temperature after which the average hardness value was determined. The result obtained gave the peak hardness value for the alloy at 180^{0}C ageing temperature. The different degrees of preliminary ageing (pre-ageing) carried out on the alloy in the thermomechanical ageing (TMA) schedules I, II, and III are based on the time for peak ageing (12hrs) at the said temperature. For TMAI, pre-ageing time was 3hrs, referred to as 25% pre-ageing; for TMAII, the pre-ageing time was 6hrs (50% pre-ageing); for TMAIII, the pre-ageing time was 9hrs (75% pre-ageing),

(c) warm rolling at 180^{0}C with degree of deformation that varied from 10% to 50%, at 10% intervals,

(d) final ageing at 180^{0}C for ageing time varying from 1hour to 20 hours at 2hours intervals, and

(e) water quenching to room temperature.

Table 3.1a: Details of the TMA treatments at 180°C for specimens which were preaged for 3hours before warm rolling (TMA1).

TMA IA-IE

Treatment designation	Schematic Representation	Details of treatment
As Quenched (AQ)		(a) Solution heat treatment (SHT) at 530°C for 2hrs. (b) Water-quenched to room temperature.
Peak aged (PA)	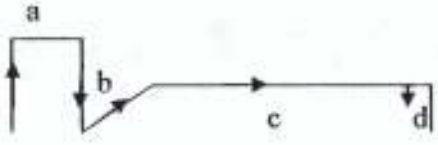	(a) SHT (b) Water-quenched (c) Aged at 180°C for 2hrs (d) Water quenched to room temperature.
TMA IA		(a) SHT (b) Water-Quenched (c) Pre-ageing at 180°C for 3hrs (d) 10% warm rolling at 180°C (e) Final ageing at 180°C. (f) Water quenched to room temperature.
TMA IB	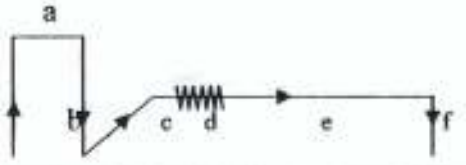	(a) SHT (b) Water-Quenched (c) Pre-ageing at 180°C for 3hrs (d) 20% warm rolling at 180°C (e) Final ageing at 180°C. (f) Water quenched to room temperature
TMA IC	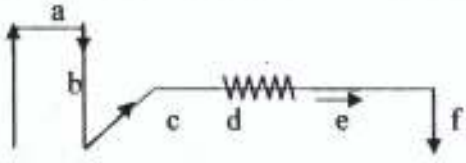	(a) SHT (b) Water-Quenched (c) Pre-ageing at 180°C for 3hrs (d) 30% warm rolling at 180°C (e) Final ageing at 180°C. (f) Water quenched to room temperature
TMA ID	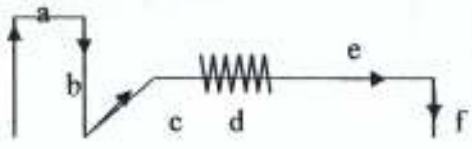	(a) SHT (b) Water-Quenched (c) Pre-ageing at 180°C for 3hrs (d) 40% warm rolling at 180°C (e) Final ageing at 180°C. (f) Water quenched to room temperature
TMA IE	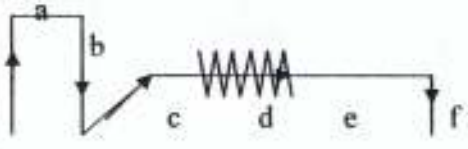	(a) SHT (b) Water-Quenched (c) Pre-ageing at 180°C (d) 50% warm rolling at 180°C (e) Final ageing at 180°C. (f) Water quenched to room temperature

Table 3.1b: Details of the TMA treatments at 180°C for specimens which were preaged for 6hours before warm rolling (TMAII).

Treatment Designation	Schematic Representation	Details of Treatment.
TMA IIA	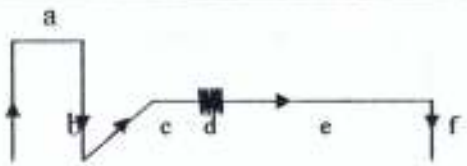	(a) SHT (b) Water-Quenched (c) Pre-ageing at 180°C for 6hrs (d) 10% warm rolling at 180°C (e) Final ageing at 180°C. (f) Water quenched to room temperature.
TMA IIB	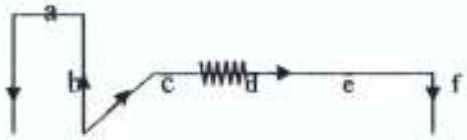	(a) SHT (b) Water-Quenched (c) Pre-ageing at 180°C for 6hrs (d) 20% warm rolling at 180°C (e) Final ageing at 180°C. (f) Water quenched to room temperature.
TMA IIC	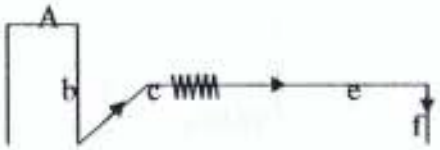	(a) SHT (b) Water-Quenched (c) Pre-ageing at 180°C (d) 30% warm rolling at 180°C (e) Final ageing at 180°C. (f) Water quenched to room temperature.
TMA IID	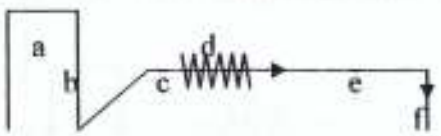	(a) SHT (b) Water-Quenched (c) Pre-ageing at 180°C for 6hrs (d) 40% warm rolling at 180°C (e) Final ageing at 180°C. (f) Water quenched to room temperature.
TMA IIE	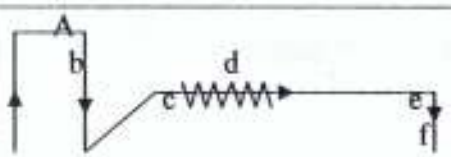	(a) SHT (b) Water-Quenched (c) Pre-ageing at 180°C for 6hrs (d) 50% warm rolling at 180°C (e) Final ageing at 180°C. (f) Water quenched to room temperature

Table 3.1c Details of the TMA treatments at 180°C for specimens which were preaged for 9hours before warm rolling (TMAIII).

Treatment designation	Schematic Representation	Details of Treatment
TMA IIIA	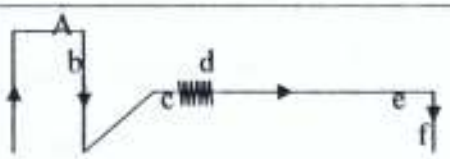	(a) SHT (b) Water-Quenched (c) Pre-ageing at 180°C for 9hrs (d) Warm rolling at 180°C (e) Final ageing at 180°C. (f) Water quenched to room temperature
TMA IIIB	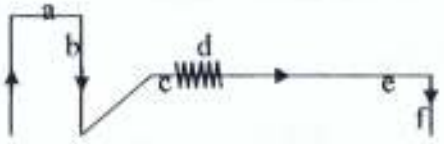	(a) SHT (b) Water-Quenched (c) Pre-ageing at 180°C for 9hrs (d) 20% warm rolling at 180°C (e) Final ageing at 180°C. (f) Water quenched to room temperature
TMA IIIC	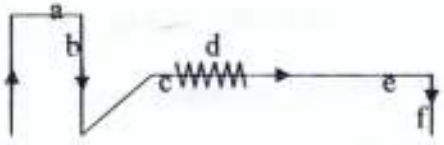	(a) SHT (b) Water-Quenched (c) Pre-ageing at 180°C for 9hrs (d) 30% warm rolling at 180°C (e) Final ageing at 180°C. (f) Water quenched to room temperature
TMA IIID	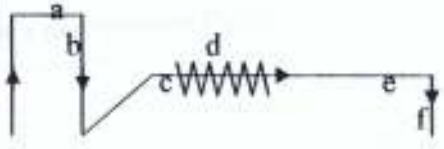	(a) SHT (b) Water-Quenched (c) Pre-ageing at 180°C for 9hrs (d) 40% warm rolling at 180°C (e) Final ageing at 180°C. (f) Water quenched to room temperature
TMA IIIE	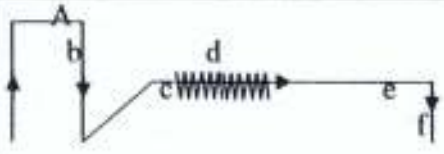	(a) SHT (b) Water-Quenched (c) Pre-ageing at 180°C for 9hrs (d) 50% warm rolling at 180°C (e) Final ageing at 180°C. (f) Water quenched to room temperature

Peak ageing to peak hardness level of 93HB, done for 12hrs.
75% pre-ageing = holding up to 9hours ageing time.
50% pre-ageing = holding up to 6hours ageing time.
25% pre-ageing = holding up to 3hours ageing time.

Tensile and impact tests specimens were machined from the thermomechanically aged rods and the tests for mechanical properties carried out at room temperature. Multiple tests were performed in each case and the average values for tensile strengths and plasticity indices computed. The results are contained in Tables 4.14- 4.28 in appendix 1

3.7 DETERMINATION OF MECHANICAL PROPERTIES

Tensile and impact test specimens were prepared for the determination of mechanical properties of the Al-Mg-Si alloy in various processed conditions. All machining operations for the production of test pieces were carefully done on the lathe machine under liberal cooling to prevent excessive heat or deformation capable of altering the structure and properties of the alloy.

3.7.1 Tensile Properties Measurement

Tensile test specimens conforming to standard dimensions such as laid down by the British standard BS131 were prepared and used for the measurement. The dimensions of the test specimens are as shown in Figure 3.1

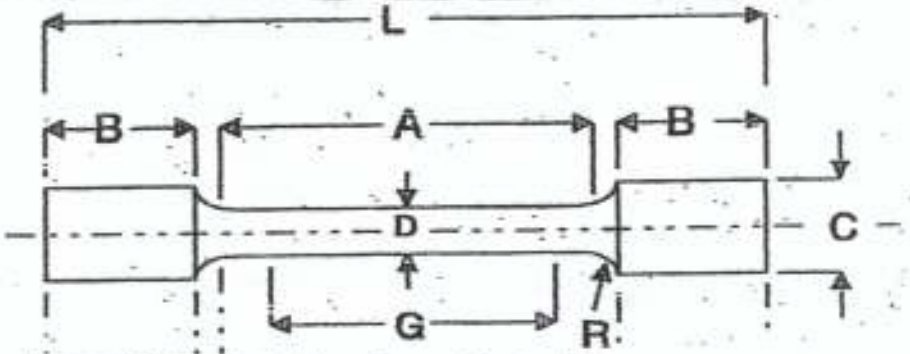

Figure 3.1 Tensile test specimen Standard Design

L =47.5, G=25, B =6 , A=35, C=12.5, D=6.25 ,R= 5

Dimensions in mm

Test specimens were subjected to tensile loads using the Monsanto tensometer. The loads were measured as the specimens stretched gradually to their breaking points. From the tensile test results, properties such as ultimate tensile strength, yield strength, and ductility were determined using the expressions;

$$\text{Ultimate tensile strength } (\sigma_{uts}) = \frac{\text{Maximum load}}{\text{Original cross sectional area of the specimen}}$$

The yield strength σ_y is determined using the 0.002 strain offset method. This is shown graphically in Figure 3.2

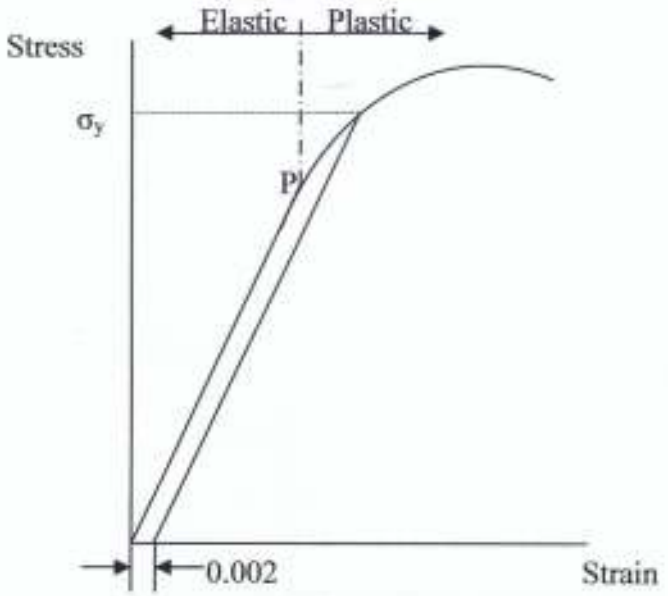

Figure 3.2 Stress-Strain curve for 6063 Aluminium alloy for the determination of yield strength using the 0.002 strain offset method.

The 0.002 strain offset method gives us the 0.2% proof stress which is taken as the yield strength of the alloy.

We assessed ductility from the percentage elongation of the test piece using the relationship;

$$\text{Percentage elongation (\% E)} = \frac{\text{Change in length}}{\text{Original gauge length of test piece}} \times 100$$

Impact Energy Measurement

The Izod impact test method was used in this study. In the Izod test (the specimen machined according to the British standard BS131), the specimens are 55mm long by 10mmx10mm. They have a 45^0 angle notch with root radius 0.25mm cut across one face to a depth of 2mm. Details of other specifications are contained in Fig.3.3.

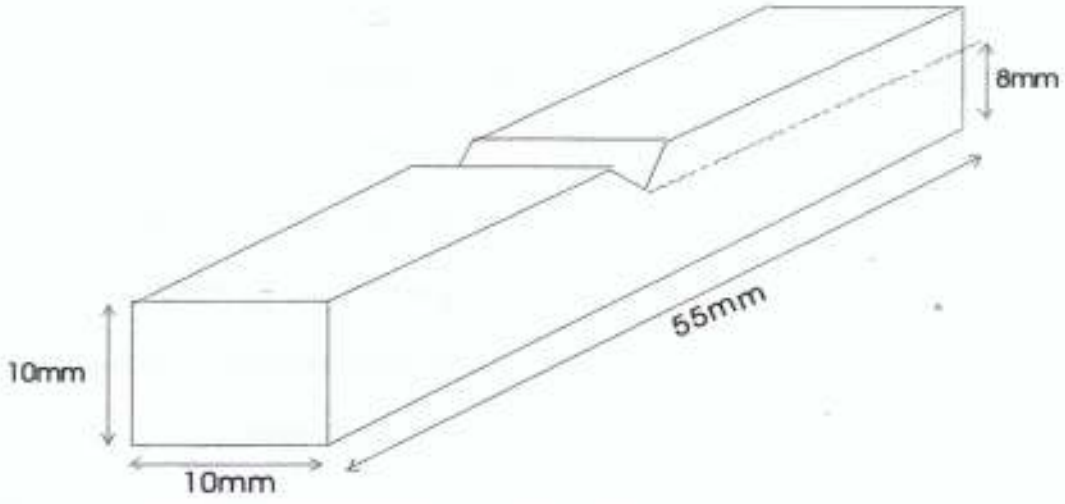

Figure 3.3 Impact Specimen Standard Design

The test specimens were produced from the solution heat-treated, aged, thermoplastically worked, and thermomechanically aged samples, using the lathe machine.

During testing, the specimen is supported in a vice and the energy of a swinging pendulum with a 27.2 kg hammer, is transferred to the specimen. The energy (in joules) absorbed by fracturing the specimen, or bending it to allow free passage, of the pendulum is obtained from the decrease in amplitude of the pendulum.

3.7.3 Metallographic Examination

Specimens were obtained from the different samples of Al-Mg-Si alloy that have been subjected to some kind of heat treatment and thermomechanical processing. In this respect, specimens were prepared for optical and transmission electron microscopy.

All specimens for optical microscopy were cut under liberal cooling. This is to minimize heating associated with cutting operations. The specimens were subjected to normal processes of grinding, polishing, and etching in the Metallurgical and Materials Engineering laboratory, Federal University of Technology, Akure.

Polishing of the samples was carried out gradually using different grades of emery papers in succeeding order of fineness starting from the coarsest. Samples were rotated by 90^0 at the turn of each grade of emery paper in order to remove or lessen the amount of surface scratches.

Also prior washing in water was done before polishing on different grades of emery papers. The grades used are 20, 320, 400, 600, and 800 grits. At the completion of polishing on the last finest emery paper, the samples were washed and dried. Final polishing was carried out using 6 micron and 1-micron emery cloth with diamond paste. The samples were subsequently washed with alcohol and dried. Etching was done using a

freshly prepared etchant containing hydrochloric acid, nitric acid, hydrofluoric acid and water. The etching time was not more than 15-30 seconds. Microstructural examinations of the etched specimens were conducted on a high-resolution power metallurgical microscope, available at the Engineering Materials Development Institute (EMDI), Akure. The images were downloaded on a computer and printed out.

Samples for transmission electron microscopy (TEM) were sent to the Department of Mechanical and Materials Engineering, University of Manitoba, Canada, courtesy of Dr. A.G. Odeshi, where all specimen preparations and TEM micrographic works were done.

3.8 DEVELOPMENT OF MATHEMATICAL MODELS

3.8.1 Introduction

Mathematical models for relating the major thermomechanical processing parameters to evolving mechanical properties of the alloy were developed. The processing parameters are treated as the independent variables while the evolving mechanical properties are the dependent variables. Thermomechanical processing is a dynamic system in which there is a possibility of the growth or improvement of mechanical properties of alloys by virtue of imposed thermal and mechanical loads. Data in Tables 4.3-4.8 in Appendix 1 for thermoplastically worked alloy was used to generate a relationship as contained in Table 3.1

3.8.2 MATHEMATICAL MODELS FOR THERMOMECHANICAL PROPERTIES OF 6063 ALUMINUM ALLOY

Some mechanical properties of 6063 Aluminium alloy such as the ultimate tensile strength, the yield strength and impact energy were investigated and for these, pertinent

geometric and mechanical characteristics were identified. Invoking the mathematical concept of non-dimensionalization and defining appropriate logarithmic variables, an interim implicit model was obtained. Using a submodel constructed from a subexperiment on elongation against deformation temperatures for thermoplastically worked alloy, we upgrade this to a full model (i.e. an explicit model). Values of the obtained thermomechanical properties from this model and from experiments are displayed in tables 4.1a - 4.1c.

Table 3.1 Variation of percentage elongation with deformation temperature at 10% degree of deformation

Temperature of Deformation	Percentage elongation
28°C	20%
160°C	14.71%
180°C	15.38%
200°C	16.26%
220°C	15.98%
240°C	16.98%

Suitable indices amounting to nondimensionalization procedure for the parameters of the processes under consideration are given as follows:

$$i_D = \frac{D(T)}{D(O)};\quad i_E = \frac{E(T)}{E(O)}\ i_A = \frac{A(T)}{A(O)},\ D(O) \neq 0,\ E(O) \neq 0,\ A(O) \neq 0, \quad \ldots (21)$$

where,

D(T) is the amount of deformation at temperature T.

E(T) is the amount of percentage elongation at temperature T.

A(T) is the amount of evolving mechanical properties at temperature T.

This need for nondimensionalization procedure cannot be overemphasized for any physical process, since this is what will enable us, design engineers, extend any result/denudation obtained from models to prototypes and vice versa.

Now, if we know the slope and a point through which a line passes, we can plot the graph of that line. Logarithmic relation provides this opportunity, as it naturally endows a line through the origin and of a given slope.

For this, we define (involve) the two new variables ξ (T) and ψ(T) from the earlier defined three indices, so that we have,

$$\xi(T) = \ell n\left(\frac{i_E}{i_D}\right), \quad \Psi(T) = \ell n\left(\frac{i_A}{i_D}\right) \tag{22}$$

Now, we plot ξ(T) against ψ(T) and obtain a slope γ. From logarithmic properties we obtain the model;

$$i_{A(T)} = (i_{E(T)})^{\gamma} (i_{D(T)})^{1-\gamma} \tag{23}$$

Consequently, putting (21) in (23) we obtain the thermomechanical property (dependent variable) A(T) in terms of the geometric parameters (processing parameters or the independent variables) E(T) and D(T):

$$A(T) = CE(T)^{\gamma} D(T)^{1-\gamma}, \tag{24}$$

$$\text{where } C = \frac{A(T)}{E(T)^{\gamma}D(T)^{1-\gamma}} \tag{25}$$

Now, (24) is an expression relating one dependent variable to two independent variables. We say this is an under-determined system (or non-explicit or implicit or open system). To make it closed we carry out sub-experiment or invoke sub-model (or

intermediary model.). For this, we consider the model (sub-model), arising from experiment on elongation against temperature.

$$E_{(T)} = \frac{KE(o)}{K + \ell n\alpha\left(\frac{2T - To}{To}\right)}; \qquad k=10,\ \alpha=0.75;\ K.E_{(o)} = 2. \qquad (26)$$

The plot of $\xi(T)$ against $\psi(T)$ has a slope of, i.e. $\gamma = 0.23$ and $1-\gamma = 0.77$, for $A(T)=\sigma_{ult.}$ where $\sigma_{ult.}$, is the ultimate tensile strength.

Reflecting (26) in (24) now makes (24) explicit and gives the desired model.

$$A(T) = C\left(\frac{KE(O)}{K + \ell n\alpha\left(\frac{2T - To}{To}\right)}\right)^{\gamma} D(T)^{1-\gamma} \qquad (27)$$

Using this model we establish in turn the values when the interested dependent variable (the mechanical parameter) A(T), is the ultimate tensile strength $\sigma_{ult.}$, yield strength σ_y and impact energy $\omega_{imp.}$ For the ultimate tensile strength, yield strength and impact energy the models are of the form $\sigma_{ult.} = C_u E(T)^{0.23} D(T)^{0.77}$, $\sigma_y = C_y E(T)^{0.28} D(T)^{0.72}$ and $\omega_{imp} = C_\omega E(T)^{0.80} D(T)^{0.20}$ respectively; C_u=2071, C_y = 1545, and C_ω = 373.

Similarly, the concept of non-dimensionalization was used for developing models for the artificially aged and thermomechanically aged 6063 Aluminium alloy.

Tables 4.9-4.13 in Appendix 1, for artificially aged 6063 alloy were summarized by plotting the mechanical properties against ageing time at different temperatures on the same graph. The peaks of the different mechanical properties were then taken as recorded in Table 3.2. The table is then used for modeling.

Table 3.2 Peaks of mechanical properties in artificially aged 6063 alloy.

T°C	Ageing time hrs	%E	σ_{ULT} N/mm^2 expt.	σ_y N/mm^2 expt.	ω_{imp}(J) expt.
28	20	16.4	313.81	233.46	30.05
160	16	13.0	337.85	272.05	35.54
180	12	12.6	343.38	279.01	30.02
200	8	13.01	354.30	297.43	30.00
220	6	12.00	360.62	303.68	25.33

T (T) - amount of holding time t, where t is measured in hours.

A (T) - amount of evolving property in time t.

E (T) - amount of strain or ductility inherently posed in time t.

The indices are;

$$it_{(T)} = \frac{t(T)}{t(0)}; \qquad i_{E(T)} = \frac{E(T)}{E(0)}; \qquad i_A = \frac{A(T)}{A(0)}$$

$$\xi(T) \equiv \ell n\left(\frac{i_E}{i_t}\right); \qquad \Psi(T) \equiv \ell n\left(\frac{i_E}{i_t}\right);$$

$$i_{A(T)} = \{i_{E(T)}\}^{\gamma} \{i_{(T)}\}^{1-\gamma} \quad \text{.....(30)}$$

$$i_{A(T)} = \{i_E(T)\}^{1/\beta} \{i_t(T)\}^{\frac{\beta-1}{\beta}} \quad \text{.....(31)}$$

$$A(T) = KE_{(T)}^{1/\beta} t_{(T)}^{\beta-1}; \qquad K = A_{(0)} E_{(0)}^{-1/\beta} t_{(0)}^{\frac{1-\beta}{\beta}}$$

For σ_{ult}; $\beta = 2/3$:

$$\sigma_{ult} = kE_{(T)}^{3/2} t_{(T)}^{-1/2}; \quad \text{.....(32)}$$

$$K = 313.8(16.4)^{-3/2}(20)^{1/2} = \frac{313.8(20)^{1/2}}{(16.4)^{3/2}} = 21.13$$

For σy, $\beta = 3/5$. $\sigma y = k_2 E(T)^{5/3} t(T)^{-2/3}$

For ω, β=3/4. $\omega = k_3 E(T)^{4/3} t(T)^{-1/3}$

Therefore $\sigma_{ult} = K_2 E_{(T)}^{3/2} t_{(T)}^{-1/2}$

$$\sigma y = k_2 E_{(T)}^{\frac{5}{3}} t_{(T)}^{\frac{-2}{3}} \quad \text{..... (33)}$$

$$\omega = K_3 E_{(T)}^{4/3} t_{(T)}^{-1/3} \quad \text{..... (34)}$$

The concept of non-dimensionalization put eminence on how properties are changing rather than how big or small they are. The trend of change of parameters is profoundly important.

The data in tables 4.14 - 4.18 are summarized in the plots of property changes against ageing time presented in figures 4.9- 4.12 and are used in developing the models.

Again we define the parametric indices as, deformation index $i_{D(tA)}$= D(tA)/D(0); property index $i_{P(tA)}$=P(tA)/P(0); process enhancement index $i_{E(tA)}$= E(tA)/E(0), tA denotes final ageing time in thermomechanical ageing processing.

The process enhancement index is a function of both the ductile nature of the material and the ageing time.

We define the usual corresponding logarithmic variables as $\xi(tA) = \ln i_{E(tA)}/ i_{D(tA)}$ and $\psi(tA) = \ln i_{P(tA)}/ i_{D(tA)}$. In the case of thermomechanical ageing schedules employed in this investigation, a number of factors come into play in determining the property changes. These factors are:

1) the degree of preageing which directly affects the solute concentration,

2) the degree of warm deformation which influences the number of precipitation sites,

3) the final ageing time which controls the size and distribution of the precipitated particles.

The initial ductility of the alloy is considered an important enhancement factor since inherently brittle alloys cannot be worked. We take the percentage elongation of the alloy at the minimum ageing time

employed as the initial enhancement factor E(0). The subsequent values of this factor are derived using the expression, $E_{(tA)} = \frac{KE(o)}{K + \ell n\alpha\left(\frac{2tA - tAo}{tAo}\right)}$ for different chosen ageing times.

The models obtained for thermomechanical ageing processing are;

$P_{(tf)} = \frac{C_1 E^{\gamma}_{(tA)} D^{1-\gamma}_{(tA)}}{0.25\mu i}$ for TMAI, where γ = -0.58 for σ_{ult}, C_1 = 1048.40

$P_{(tf)} = \frac{C_2 E^{\gamma}_{(tA)} D^{1-\gamma}_{(tA)}}{0.50\mu i}$ for TMAII γ

$P_{(tf)} = \frac{C_3 E^{\gamma}_{(tA)} D^{1-\gamma}_{(tA)}}{0.75\mu i}$ for TMAIII;

where μi accounts for the nature of precipitated phase. For β'', μ_1 is 4.02, for β' μ_2 is 3.67 and for β, μ_3 is 4.03.

CHAPTER FOUR

RESULTS AND DISCUSSION

Chemical Composition.

Results of chemical analysis are shown in Table 4.1.

Table 4.1.The chemical composition in weight percentage of the 6063 Aluminium alloy

Element	% composition
Si	0.4430
Fe	0.1638
Cu	0.0041
Mn	0.0132
Mg	0.5835
Zn	0.0005
Cr	0.0024
Ti	0.0078
Ca	0.0003
Sr	0.0002
Al	Balance

From this table, the main effective alloying elements are 0.443%Si and 0.583%Mg. The other element, which is 0.1638% Fe, exists as deleterious element within the acceptable limit. This Al-Mg-Si alloy has compositions, which offer good age-hardening potential especially for both artificial and forced ageing.

4.1.1 Tensile Strength and Plasticity Indices of Solution Heat Treated 6063 Aluminium Alloy

The average tensile strength and plasticity indices of solution heat treated Al-Mg-Si alloy are shown in Table 4.2 in appendix 1.

4.1.2 Deformation strengthening or Work hardening Potential of 6063 Aluminium alloy

The effects of thermoplastic processing on the tensile and plasticity properties of the

Al-Mg-Si alloy at different working temperatures are shown in Tables 4.3- 4.8 in appendix 1, and the corresponding graphs are presented in Figures 4.1-4.4.

4.1.3 Ageing Characteristics of Al-Mg-Si alloy

Results of the tensile and plasticity properties of aged samples are contained in Tables 4.9-4.13 in appendix 1. The ultimate tensile strength, yield strength, percentage elongation and impact energy varied substantially with ageing parameters as shown in Figures 4.5-4.8

4.1.4 Thermomechanical Ageing Characteristics

Results of the tests carried out on the thermomechanically aged samples are contained in Tables 4.14-4.28 in appendix 1, and the graphs are presented in Figures 4.9- 4.20.

4.1.5 Evaluated Models

1. for the ultimate tensile strength σ_{ult}, the model is obtained in the form

$$\sigma_{ult} = CE_{(T)}^{0.23} D_{(T)}^{0.77} \quad (28)$$

By appropriate estimation C=2071, therefore $\sigma_{ult} = 2071\, CE_{(T)}^{0.23} D_{(T)}^{0.77}$, which yielded the result in the Table 4.1a.

Table 4.1a Evaluated ultimate tensile strength values from model and experiments in TPP

T°C	$E_{(T)}$	$D_{(T)}$	σ_{ult} N/mm^2 by model	σ_{ult} N/mm^2 Experiment
28	0.20	0.1	244.52	241
160	0.16588	0.1	232.64	230
180	0.16413	0.1	232.09	238
200	0.16261	0.1	231.60	239
220	0.16127	0.1	231.17	231
240	0.16008	0.1	230.70	230

For impact energy, C=373.06; γ=0.80 1-γ=0.20

Impact Energy, $W(T) = CE_{(T)}^{\gamma} D_{(T)}^{1-\gamma}$ .....(29)

$$W(T) = 373.06\ E_{(T)}^{0.80} D_{(T)}^{0.20}$$

Table 4.1b Evaluated impact strength values from model and experiments inTPP

T°C	$E_{(T)}$	$D_{(T)}$	W(T) (J) by model	W(T) (J) Experiment
28	0.20	0.1	65.49	46.27
160	0.16588	0.1	55.93	42.66
180	0.16413	0.1	55.45	56.65
200	0.16261	0.1	55.04	58.29
220	0.16127	0.1	54.68	64.56
240	0.16008	0.1	54.36	64.01

Tables 4.9-4.13 in Appendix 1, for artificially aged 6063 alloy were summarized by plotting the mechanical properties against ageing time at different temperatures on the same graph. The peaks of the different mechanical properties were then taken as recorded in Table 4.1c. The table is then used for modeling.

Table 4.1c Evaluated mechanical properties values from models and experiments in AAT

T°C	Ageing time hrs	%E	σ_{ULT} N/mm^2	σ_y N/mm^2	ω_{imp} Impact E (J)	σ_{UTS} model	σ_y model	Impact model
28	20	16.4	313.81	233.46	30.05	313.79	233.46	30.05
160	16	13.0	337.85	272.05	35.54	247.60	183.52	23.79
180	12	12.6	343.38	279.01	30.02	273.14	210.60	25.09
200	8	13.01	354.30	297.43	30.00	350.37	290.34	29.94
220	6	12.00	360.62	303.68	25.33	358.51	306.73	29.56

4.2 DISCUSSION OF RESULTS

4.2.1 Effects of Solution Heat Treatment on the Tensile Strength and Plasticity Indices of 6063 Aluminium Alloy.

The solution heat treated (SHT) 6063 Aluminium alloy, which is coined as the as-received alloy had on the average an ultimate tensile strength of 297.36 N/mm^2, yield strength of 227.76N/mm^2, 18.96% elongation, and 40.49 joules impact energy when tested severally within 1hour to 20hours at room temperature. The solution heat treated condition is essentially retained during quenching to room temperature. Because the alloying elements are greatly supersaturated at lower temperatures, precipitation occurs at room temperature over a period of days or weeks and the property of the alloy changes accordingly.

4.2.2 Effects of the Variation of Percentage Deformation and Working Temperature on the Tensile Strength and Plasticity Indices of Thermoplastically Processed 6063 Aluminium Alloy.

Plastic deformation produces deformation strengthening in Al-Mg-Si alloys at low working temperatures and the strengthening increases with increasing percentage deformation (Figs.4.1and 4.2).

However, deforming at elevated temperatures caused reduced strain hardening or strengthening which decreases further with increasing temperature. In fact, for temperatures greater than 180^0C there was drastic drop in ultimate tensile strength and yield strength for percentage deformation greater than 20%. This shows that a combination of high working temperature and high degree of deformation caused rapid

precipitation of the stable β-phase (Plates 7,8,10 and 3TPP) which resulted in very low ultimate tensile strength and yield strength. There was a corresponding reduction in ductility and toughness for deforming at temperatures less than 180^{0}C as shown in Figures 4.3 and 4.4, for reason of increased strain hardening.

Deformation at temperatures greater than 180^{0}C caused a rise in ductility and toughness of the Al-Mg-Si alloy. This is because of working above the recrystallization temperature. The observed behaviours of the alloy due to thermoplastic working, in the absence of imposed ageing, conformed with those reported in similar works conducted by El-Baradie and El-Sayed (1996), Dutkiewicz and Litynska(2002), as well as Wang and Pragnell(2002).

The changes in microstructural features, in particular increasing density of structural imperfections and their interactions, account for the property variations observed.

Grigoriev and Kojaspirov (1981), and Cimenoglu et. al.(1999), remarked that the basic factors that cause increased strength during thermoplastic working are increased dislocation density, and their more uniformly distributed pattern within the metal volume. Other factors include the creation of dislocation barriers in the forms of grain boundaries and subgrains, twin boundaries, dispersed secondary phases, and dislocation forests.

It was also affirmed that decreased grain size, and the formation of substructures that are bounded by dislocational barriers, as well as increased degree of dispersion of secondary phases contributed largely to the strengthening of worked alloys. Substructures such as

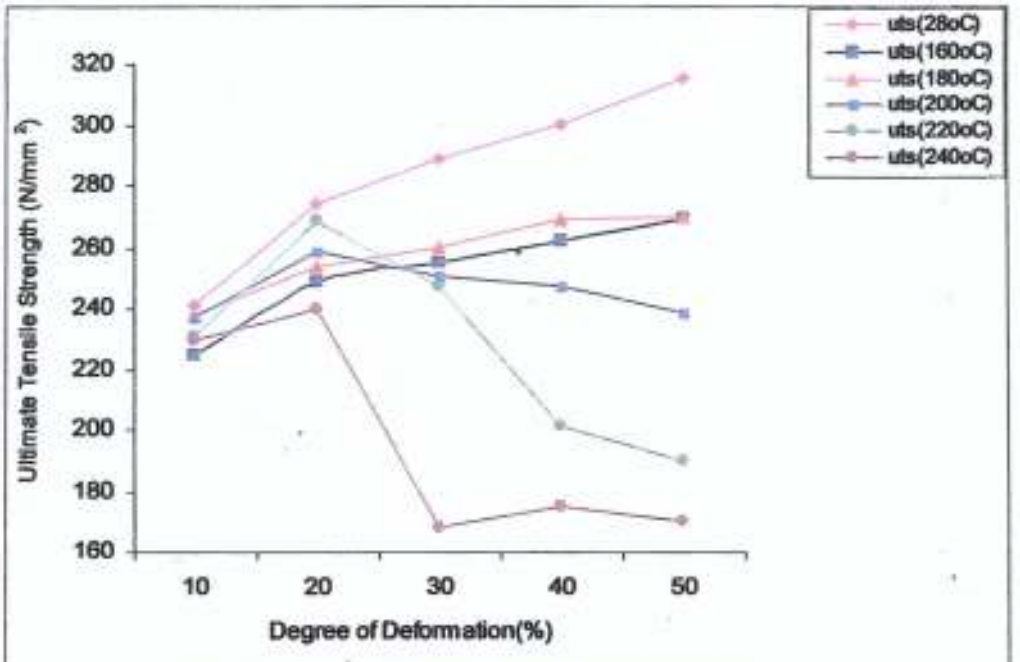

Fig.4.1 Variation of Ultimate Tensile Strength(UTS) with Degree of Deformation at different working temperatures.

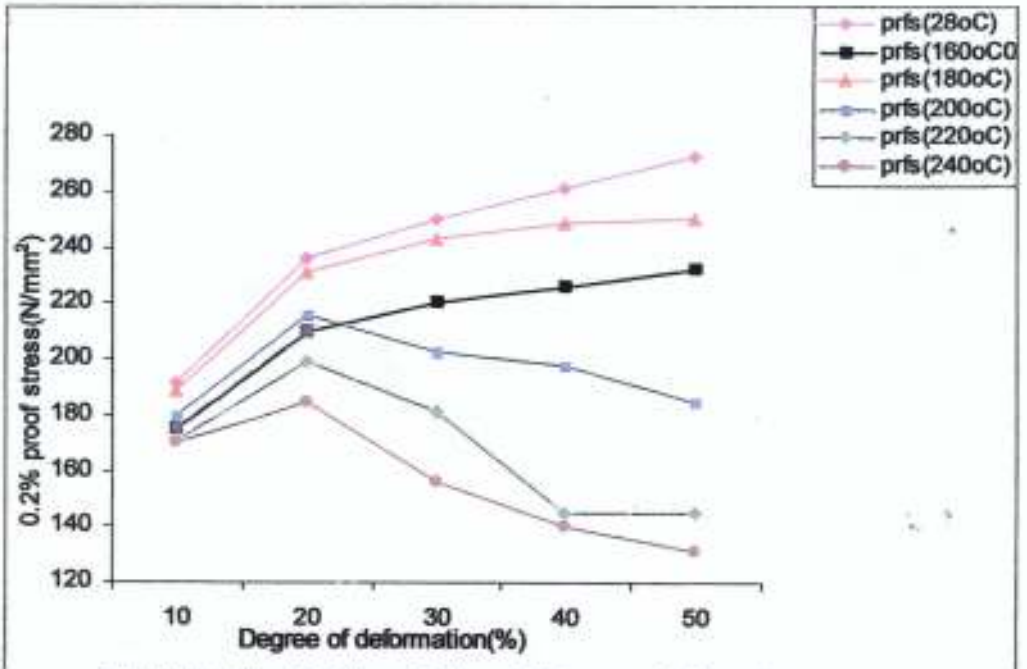

Fig.4.2 Variation of 0.2% proof stress with degree of deformation at different working temperatures.

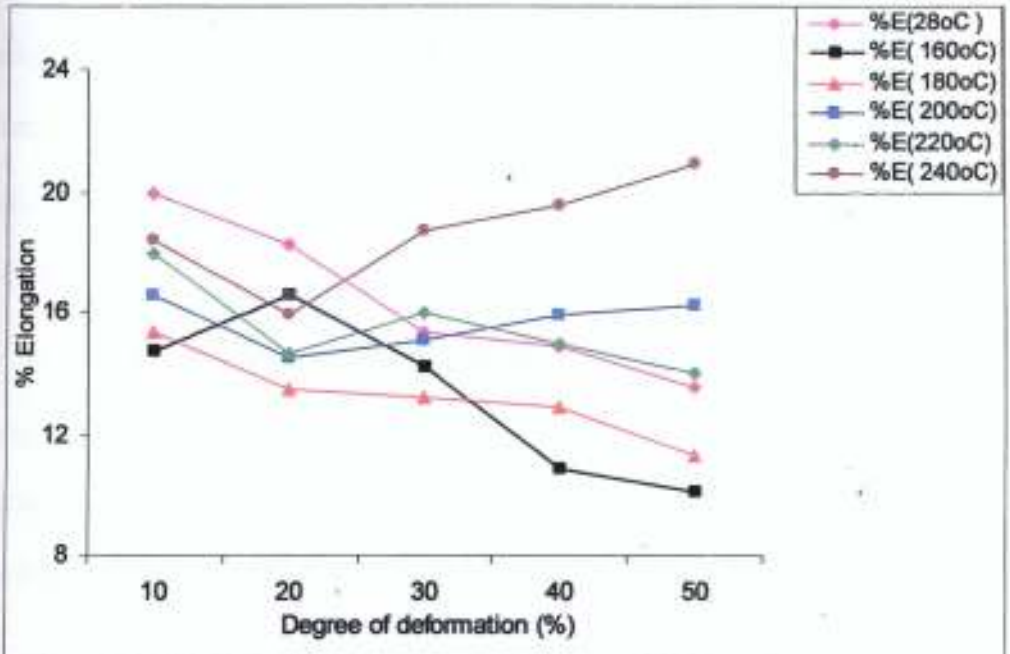

Fig.4.3 Variation of %Elongation with Degree of deformation at different working temperature

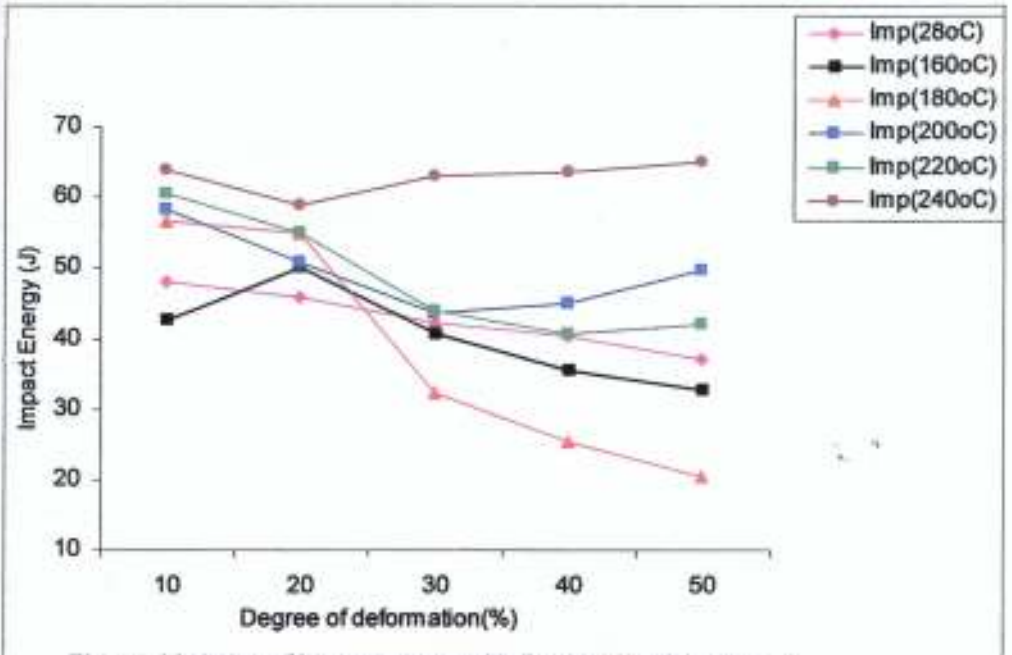

Fig.4.4 Variation of Impact energy with Degree of deformation at different working temperatures

grain boundaries and twin boundaries among others, act as barriers to dislocation motion, thereby restricting the motion of these dislocations. In order to move these dislocations, higher deformation forces are required, which culminates in increased strength of the metal. Therefore, higher strength is an indication of increased barrier to dislocation motion.

At 10% deformation, for each working temperature the value of ultimate tensile strength, and yield strength are much lower than at 50% deformation, but the ductility and impact energy values are higher at 10% deformation. This is in agreement with the fact that ductility is usually sacrificed for increased strength of an alloy.

The micrographs differ in details culminating into different values of tensile strengths and plasticity indices. At higher deformation temperatures and percentage deformations, the secondary phases are more in number and varied considerably in size compared to the room temperature situations (Plates 8, 10).

The decrease in strength and the increase in plasticity indices as the processing or working temperature is increased are as a result of increased mobility of the dislocations. Increased temperature assisted the dislocations to overcome the energy barriers to their motion, hence less force is required to cause them to move, culminating in decreased strength (Dutkiewicz and Litynska 2002).

Furthermore, deformation increases the density of dislocations and causes them to interact in such a manner that their further motion is impeded. If deformation is performed at elevated temperature, thermal activation eliminates or overcomes most of these impediments to the dislocation motion, and thus the rate of strain hardening is much reduced, amounting to reduced strength.

From the results of this preliminary investigation, it could be concluded that thermoplastic working of 6063 Aluminium alloy at a working temperature not greater than 180^0C improves the tensile strengths as the percentage deformation increases, at least within the deformation limit employed in this study. The plasticity indices however, reduced with increasing percentage deformation, though the decrease was not drastic.

On the other hand, increasing working temperature resulted in decreased strength and improved plasticity for the reasons highlighted above.

Effects of the Variation of Ageing Temperature and Time on the Tensile Strengths and Plasticity Indices of Artificially Aged 6063 Aluminium Alloy.

Figures 4.5-4.8 show that the Al-Mg-Si alloy under study responds very well to precipitation strengthening or age-hardening process, both at room and elevated temperatures.

It is clear that maximum ultimate tensile strength and yield strength (Figs.4.5 and 4.6) were not obtained after ageing at room temperature for 20 hours. On the other hand, percentage elongation and toughness progressively reduced (Figs.4.7-4.8). Within the time frame of 20 hours, there was an increase of 49.35N/mm^2 (ageing at 28^0C) for ultimate tensile strength and 34.80N/mm^2 for yield strength, (Figs.4.5 and 4.6).

Ageing at elevated temperatures of between 160^0C and 220^0C caused peak values to occur at short ageing times. This is in respect of ultimate tensile strength and yield strength. Such peak values are indicative of structural changes, precisely the formation of metastable β" and β' phases and the more stable β-phase from the solid solution matrix.

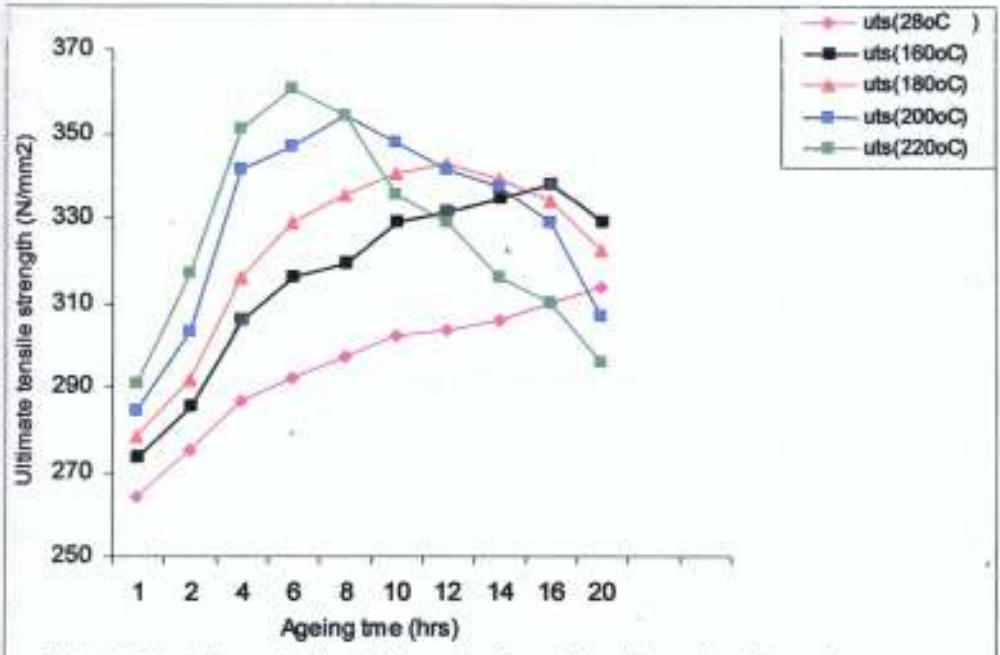

Fig.4.5 Variation of ultimate tensile strength with ageing time at different ageing temperatures

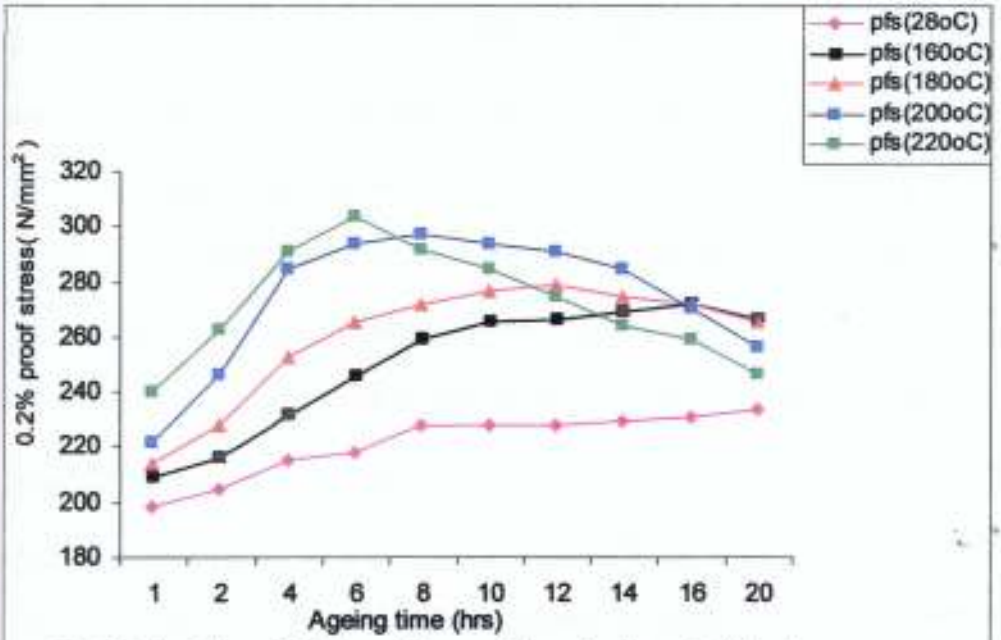

Fig.4.6 Variation of 0.2% proof stress with ageing time at different ageing temperatures

It is clear from Figures 4.5 and 4.6 that the higher the ageing temperature, the higher the peak values of ultimate tensile strength and yield strength, and are obtained at shorter ageing periods. These observations are in agreement with the findings of Moon et.al.(1996), and Cai et.al.(2004) but slightly deviated from the findings of Gracio et.al.(2004) and Siddique et. al. (2000). According to Pavlov (1983), such deviations bordered on the fact that evolution of properties consequent upon processing parameters are often stochastic, since some of the material properties are independent on the metallurgical conditions.

Another observation reflected from the isothermal ageing curves in Figures 4.5- 4.8 is the fact that the form of the curves is independent of the treatment temperature. In each case, there is an initial increase in tensile strengths (underage condition) until the peak- aged condition, and, finally a decrease in tensile strengths as the specimens become over-aged. A reverse trend is observed for percentage elongation and toughness (plasticity indices), where progressive decrease in values are obtained at shorter ageing times before a rise at a much longer ageing times. This means, at the early stage of ageing, embrittlement occurs which reverts to toughening at a later stage. There is therefore the need to conduct ageing at a convenient temperature for optimum properties. For this work, ageing at 180^0C was found to be appropriate and was chosen for further work

The curves in Figures 4.5-4.8 also demonstrate that each ageing condition imparts certain specific mechanical behaviour to the alloy.

Optical micrographs in Plates 11-20, and the TEM micrographs in Plates 6AA-10AA, show that the ageing products increase with increasing ageing time and temperatures.

A comparison of Plates 15, 16, 17, 18 and 22 also gave credence to the fact that ageing products increased with increasing ageing temperature.

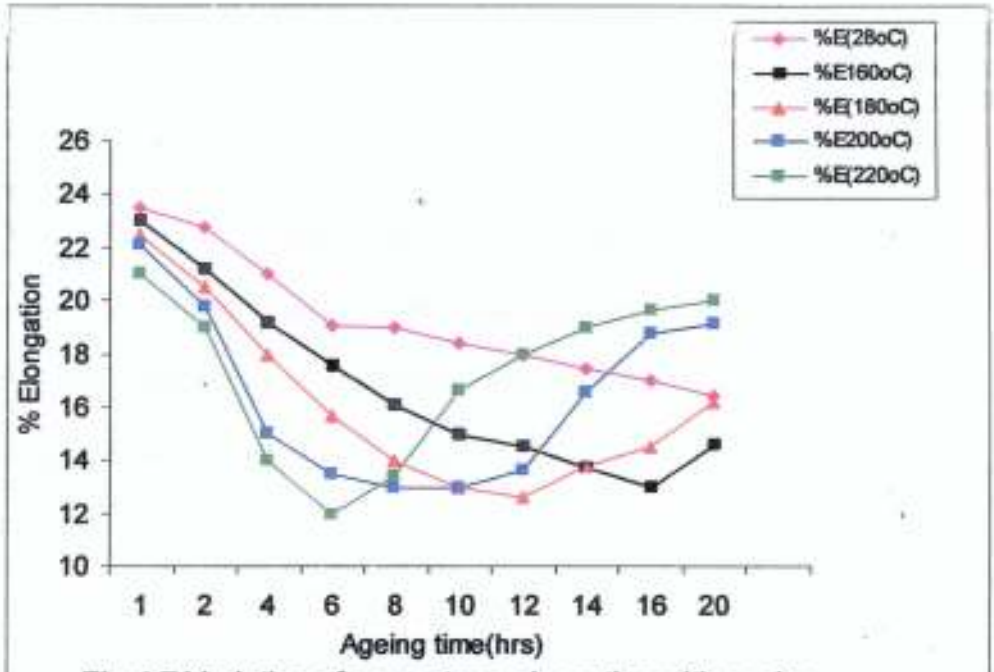

Fig.4.7 Variation of percentage elongation with ageing time at different ageing temperatures

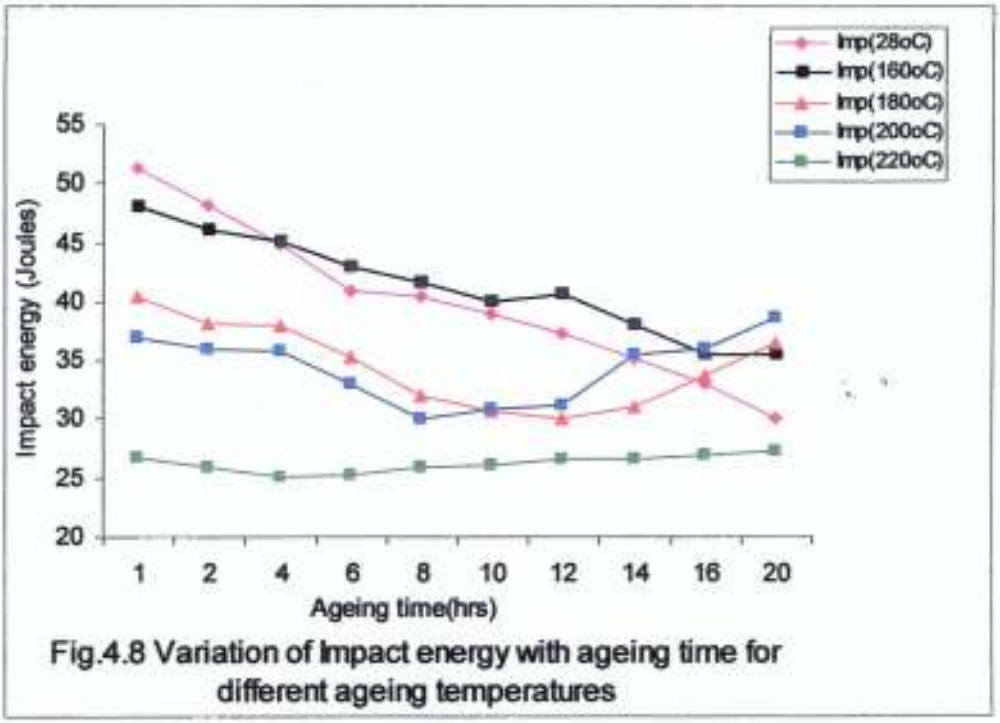

Fig.4.8 Variation of Impact energy with ageing time for different ageing temperatures

Plates 6AA-10AA are typical TEM micrographs showing the strengthening particles and some other integral features of the underage, peakage, overage and strongly overage conditions

Consideration of the individual ageing temperatures, reveal the gains and loses in tensile strength and plasticity indices with respect to each processing condition.

At 160^0C ageing temperature and 16 hours ageing time, the ultimate tensile strength and yield strength reached an average maximum value of 337.85N/mm^2 and 272.05N/mm^2 respectively, compared to 297.36N/mm^2 and 227.76N/mm^2 respectively for the as-received sample (Figs. 4.5 and 4.6). However, a percentage elongation of 13% and impact energy of 35.54joules were recorded against a percentage elongation of 18.96% and impact energy of 40.49 joules for the as-received alloy (Figs.4.7 and 4.8).

In other words, at the point when the tensile strengths assumed the highest values, the plasticity indices assumed the minimal values.

At 180^0C ageing temperature, the behaviour of the alloy do not depart appreciably from that observed at 160^0C, except that the time taken to reach the maximum values of ultimate tensile strength and yield strength was shorter than that of 160^0C (Figs.4.5 and 4.6). In this case, at 12 hours aging time, ultimate tensile strength and yield strength values of 343N/mm^2 and 279N/mm^2 respectively were recorded, as well as corresponding values of 12.6% elongation, and 30 joules impact energy. Similarly, at 200^0C, it took only 8 hours for the alloy to reach a peak value of 354N/mm^2 ultimate tensile strength and 297N/mm^2 yield strength, with 13% elongation and 30 joules impact energy. The peak values obtained at 220^0C ageing temperature for the ultimate tensile strength and

yield strength were 361N/mm^2 and 304N/mm^2 respectively, recorded at 6 hours ageing time. Correspondingly, 12% elongation and 25 joules impact energy values were recorded at this ageing time and temperature for the alloy.

Obviously, a general trend of increasing peak of ultimate tensile strength and yield strength with increasing magnitude of ageing temperature was observed within the chosen range of temperature. Similarly, the peak of the plasticity indices decrease, improves with increasing ageing temperature within the same processing window.

The initial increase in strength, in each case, corresponds to certain structural changes in the alloy. The solution treated alloy, which is a supersaturated solution, is thought to be precipitating the excess solute dissolved at the much higher solution treatment temperature. The precipitation that takes place in stages is characterized by a mechanism as reported by Siddiqui et.al, (2000), Urreta et.al. (2001), Cai et.al. (2004), and Garrett et.al. (2005).

As earlier remarked, the form of the curves (Figs. 4.5-4.8) is independent of the treatment temperature: An initial increase in strengths (or decrease in plasticity indices) after 1 hour ageing time, until the peak –aged stage is attained and finally, a decrease in strengths (or increase in plasticity indices) as the alloy becomes over-aged. However, a cursory look at the curves, reveal that the peak-aged condition itself depends strongly on the treatment temperature; that is, the higher the ageing temperature, the faster the response. This is in accordance with literature (Hatch, 1984; Takeda et.al., (1998).

From an industrial point of view, it is interesting to note that at high temperatures the artificial ageing response is quite rapid. In this case, after a limited time interval of 5 hours, at 220^{0}C (Fig. 4.5), the ultimate tensile strength increases from 291N/mm^2 (1 hour

ageing time) to 361N/mm^2 (6 hours ageing time), while the yield strength increases correspondingly from 240N/mm^2 to 304N/mm^2. The ductility decreases from 21% to 12%, while the impact energy shows a little decrease from 27 joules to 25 joules.

The mechanism of precipitation of secondary phases in Al-Mg-Si (6063) alloy, during ageing is well documented in literature (Gupta and Lloyd, 1992; Edwards et.al.1998; Siddiqui et.al., 2000; Murayama et.al., 1998, 2001), and the sequence of formation of precipitates is often written as:

α (sss) ----> GP Zones ----> β"needles---->β'rods + lath-like particles----> β.

Clusters or aggregates of alloying elements which form in the supersaturated solid solution (α -sss) at the onset of ageing, and which are detectable by structural methods are called the Guinier –Preston zones (GP-Zones), (Plate 6AA). They have the same crystal lattice as the α-solid solution matrix, but are very fine particles that are coherent with the matrix solid solution. They are acicular in shape. The β"and β' particles are precipitated at an ageing temperature or heat content, higher than the solvus temperature of the GP Zones. These are fine, metastable secondary phase particles (Plate 6AA), which eventually impart strength to the alloy when they are trapped in the metal under specific production conditions. The increasing strength displayed by the alloy during the early moments of ageing (under-ageing) is in part due to the particle size of the GP, β", and β' precipitates as revealed by the TEM micrographs. The peak strength (peak ageing) is accounted for largely by the particle size of the β'-phase, interaction of dislocations, and the onset of the stable β-phase precipitation.

The reduced strength of the alloy, which is observed after the peak strength, is because of the presence of large numbers of stable β-phase precipitates, arising from over-ageing.

The contributions of particles, grain size, and dislocations to the overall strength of the alloy can be combined in an additive form as suggested by Cai (2003), in equation 35;

$\sigma_y = \sigma_o + k_1\mu b/r + k_2 d^{-\alpha} + k_3\mu b\sqrt{\rho}$ ---------- (35)

where σ_y is the yield strength of the aged alloy. σ_o is the yield strength of the matrix, b is the Burger's vector, μ is the shear modulus, r is the mean radius of the precipitate, d is the mean grain/ subgrain diameter, α is the stress/ microstructure-dependent parameter, ρ is the density of dislocations and k_i (i= 1, 2, 3) are the constants.

The differences in precipitate size, dislocation density, and grain structure determine the mechanical properties of the aged 6063 Aluminium alloy.

4 Effect of the variation of processing parameters on the tensile strengths and plasticity indices of thermomechanically aged 6063 Aluminium alloy.

Figures 4.9-4.20 show the effect of thermomechanical ageing on the tensile strength and plasticity of 6063 Aluminium alloy. The alloy was preliminarily aged (pre-ageing) at 180^{0}C in batches for 3hours, 6hours, and 9hours corresponding to 25%, 50%, and 75% degree of pre-ageing respectively. This treatment was succeeded by 10% to 50% degrees of deformation of the alloy at 180^{0}C, which in turn was followed by final ageing at the same temperature for ageing time ranging from 1hour to 20 hours.

The characteristic curves for each thermomechanical ageing route in the Figures 4.9 - 4.20, show initial increasing values for the ultimate tensile and yield strengths, leading to a maximum value in each case before dropping off. All ultimate tensile strength curves obtained in the thermomechanical ageing routes with 25% preageing, are significantly lower than that of the ultimate tensile strength curve obtained from the solution heat-treated alloy (Fig.4.9).

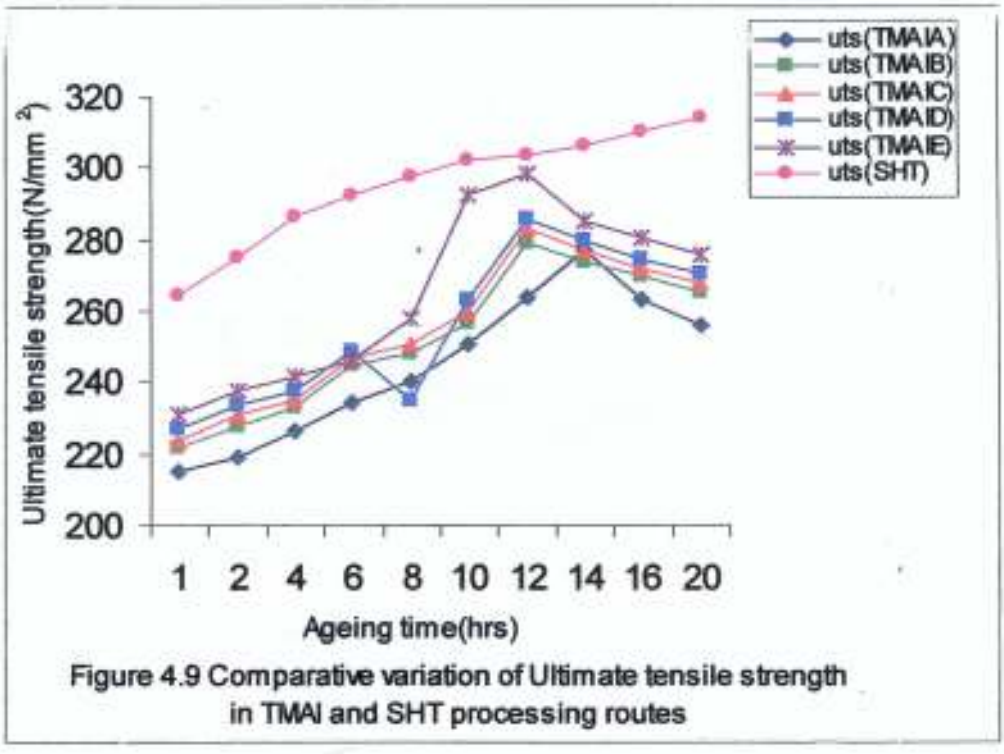

Figure 4.9 Comparative variation of Ultimate tensile strength in TMAI and SHT processing routes

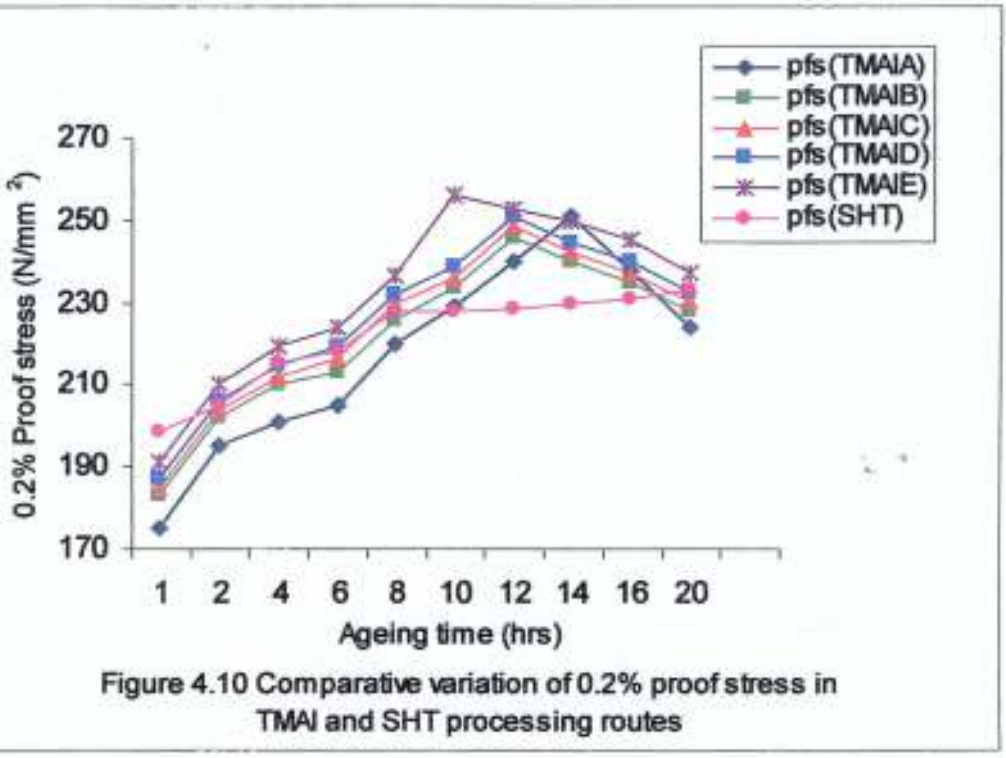

Figure 4.10 Comparative variation of 0.2% proof stress in TMAI and SHT processing routes

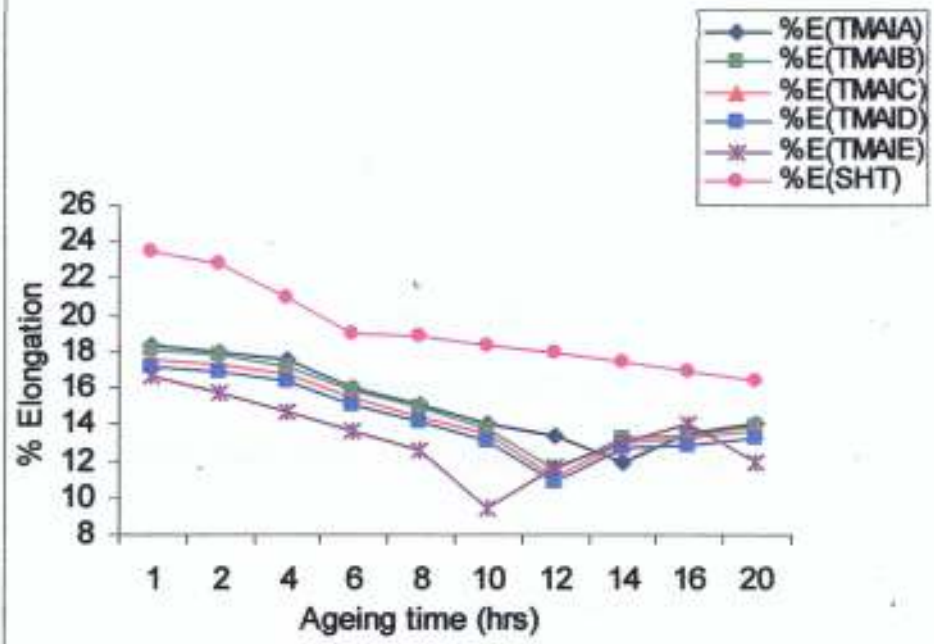

Figure 4.11 Comparative variation of Percentage elongation in TMAI and SHT processing routes

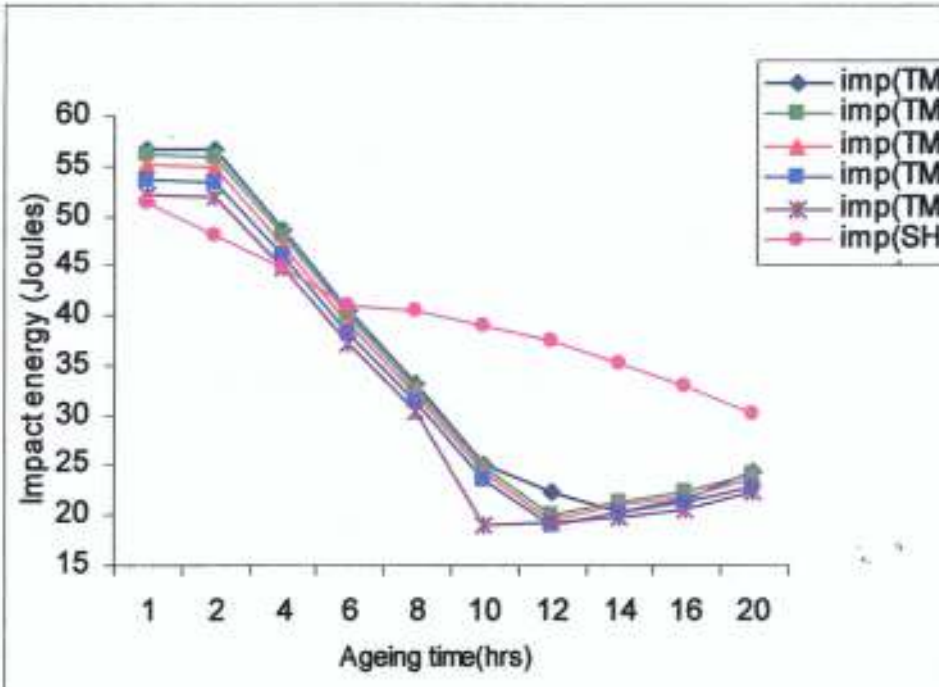

Figure4.12 Comparative variation of Impact energy in TMAI and SHT processing routes

As expected, the ultimate tensile and yield strengths were raised with increasing degree of deformation and this is particularly glaring in figures 4.17 and 4.18.

The significantly higher values of the ultimate tensile and yield strengths in these figures show that the stage at which plastic deformation is carried out in the thermomechanical ageing route is important. Early application of plastic deformation (shorter preageing time) produces reduction in ultimate tensile and yield strengths, while optimum values were obtained in the much longer time of preageing due to the quantity and morphology of the precipitates.

Peak values occur for ultimate tensile and yield strengths between 8-12hours of final ageing time, after the imposed plastic deformation, for all thermomechanical ageing routes.

Thermomechanical ageing only caused some increase in the yield strength (Fig.4.10).This is seen from the position of the curve for the solution heat-treated Al-Mg-Si alloy. There were high increases in yield strength with increased degree of preageing (Fig.4.14), and a much significant increase is obtained with further increase in the degree of preageing (Fig.4.18).

Percentage elongation reduces gradually with increasing ageing time before reaching a minimum at 10-12hours ageing time (Figs. 4.11 and 4.19) and at 8-10hours ageing time (Fig.4.15).In general minimal values of yield strength are obtained between 8-12 hours ageing time after which, there is a gradual increase in the values of yield strength.

In figures, 4.11 and 4.15 thermomechanical ageing treatments generally reduced ductility when compared with that of the solution heat-treated alloy. However, figure 4.19 shows that an averagely moderate degree of deformation at 180^0C appeared to increase the

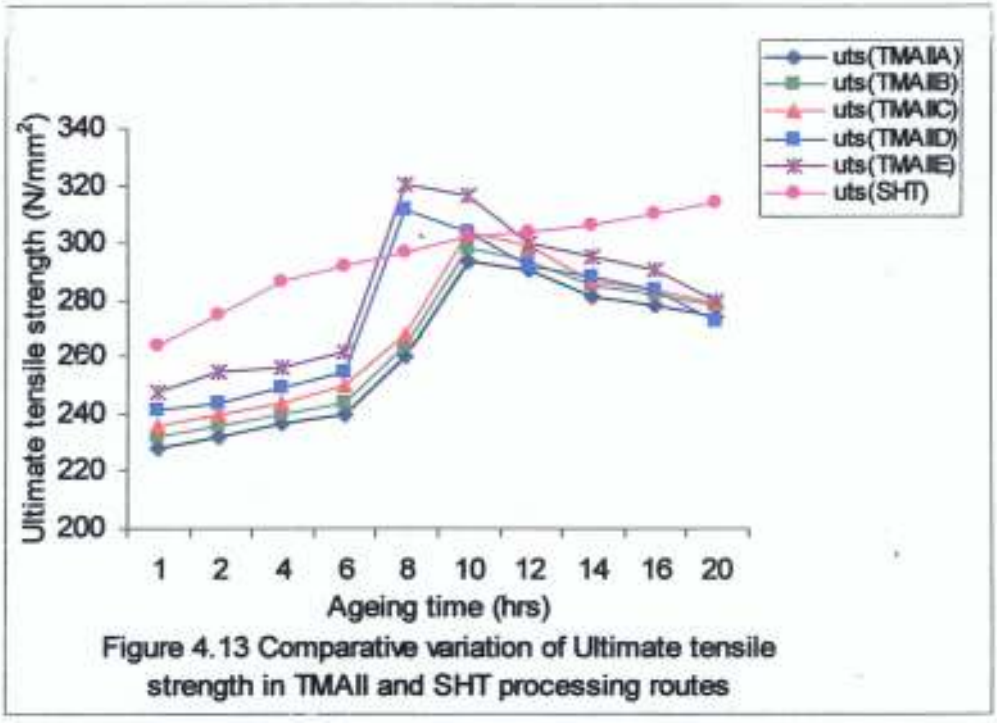

Figure 4.13 Comparative variation of Ultimate tensile strength in TMAII and SHT processing routes

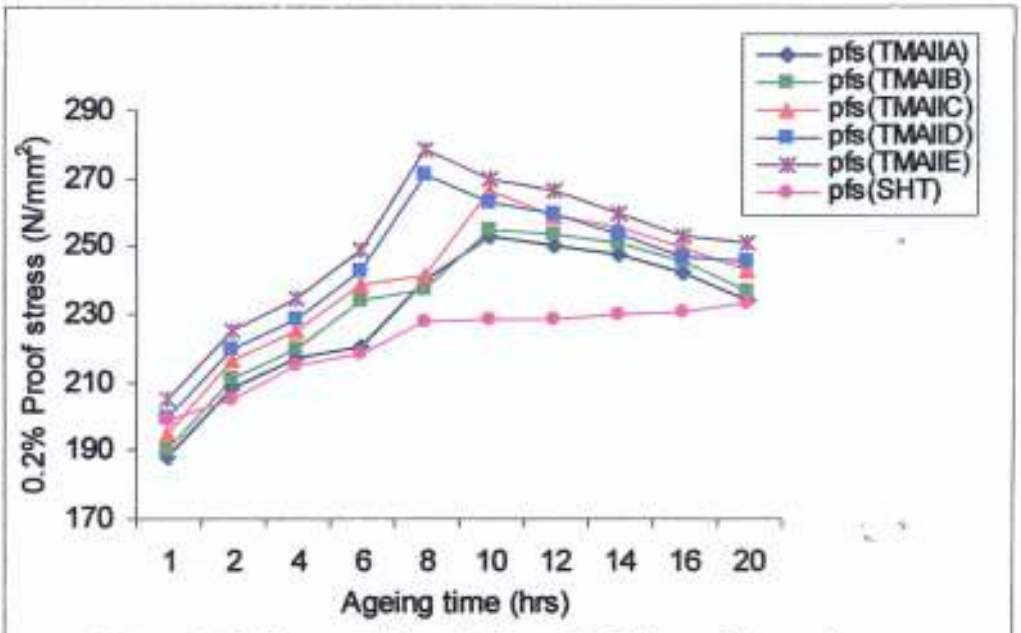

Figure 4.14 Comparative variation of 0.2% proof stress in TMAII and SHT processing routes

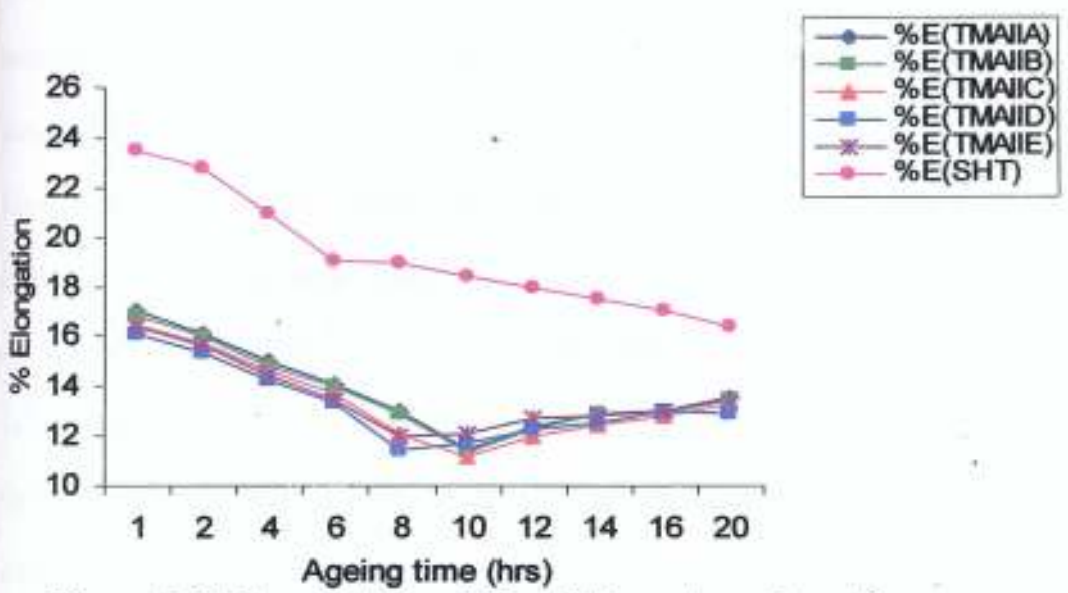

Figure 4.15 Comparative variation of Percentage elongation in TMAII and SHT processing routes

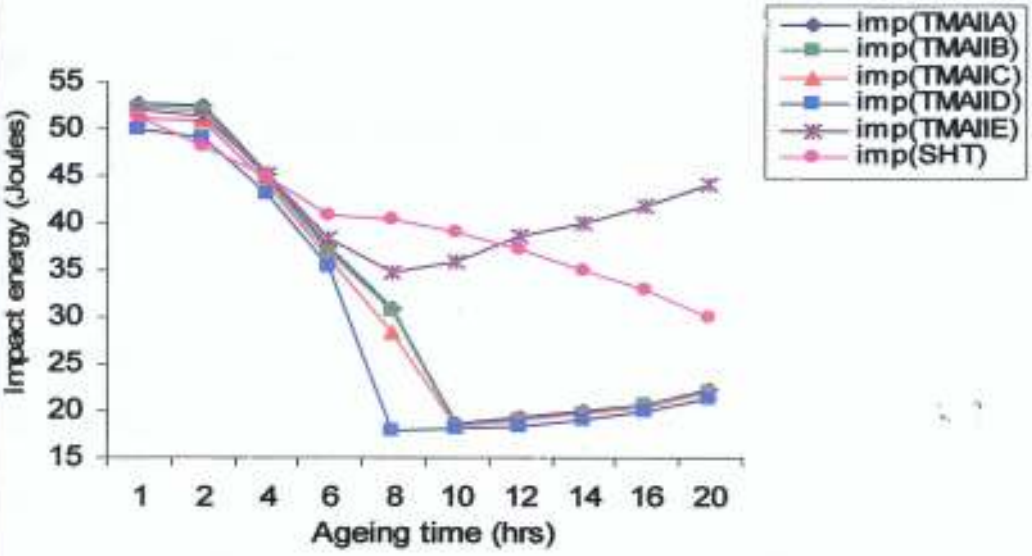

Figure 4.16 Comparative variation of Impact energy in TMAII and SHT processing routes

ductility in thermomechanically aged Al-Mg-Si alloy. This is obvious in TMAIIIC processing route, which utilized 30% degree of deformation.

The increase in ductility reflects on the nature of precipitates formed and their interactions with dislocations formation, mobility, and annihilation (Plates 11TMA and 13TMA). These have affected the final state of the alloy.

Impact energy curves presented in Figures 4.12 and 4.16, show a sharp drop in toughness after ageing for more than 2hours, and practically leveling out after about 8-12 hours of ageing. Figure 4.20 shows a progressive reduction in impact energy, reaching a minimum value after 8-10 hours of ageing time before increasing.

Generally, toughness reduced with thermomechanical ageing of the alloy (Fig.4.20) when compared to that of the solution heat-treated alloy. However, in figure 4.16 it is clearly shown that the toughness of the thermomechanically aged 6063 alloy increased substantially after 8hours of final ageing time, obviously due to 50% preageing, and 50% post preageing degree of plastic deformation.

In Figures 4.9, 4.11, and 4.12, it is clearly reflected that the solution heat-treated 6063 alloy had high ultimate tensile strength, ductility, and toughness compared to when it is thermomechanically aged especially at higher final ageing time of the TMA processing route.

Microstructural examinations of the thermomechanically aged samples show that TMA clearly affects the structure-property relationship of the alloy. Typical optical micrographs of the TMA processed alloy are shown in Plates 23 to 65, while Plates 9TMA-14TMA are representative TEM micrographs showing the type and distribution of the strengthening precipitates, and other striking features.

Accordingly, the property changes obtained in the 6063 Aluminium alloy subjected to TMA processing are explained in terms of size, shape and distribution of precipitates and their interaction with dislocations. These microstructural features are affected by;

(i) degree of pre-ageing, which affects the solute concentration;

(ii) degree of deformation, which affects the potential sites for the

(iii) precipitation of intermediate phases and enhances the diffusion rates; and

(iv) final ageing treatment, which governs subsequent ageing steps and interaction of precipitates with dislocations (Petersen et.al.1998; Martin 1998; Celentano, 2002; Engler and Hirsch, 2002; Garrett et.al.2005).

The strengthening effects in the studied 6063 Aluminium alloy after various TMA treatments may be considered to be due to (i) coherent precipitates $\beta^{"}$, (ii) partially coherent $\beta^{'}$ precipitates and (iii) dislocation substructures,(Plates 9TMA-14TMA). According to Miao and Laughlin,(1999, 2000), Urreta et.al.,(2001), the following precipitation sequence for the studied Al-Mg-Si alloy may be suggested based on the microstructure obtained;

α(sss)---->GP-Zones---->$\beta^{"}$needles---->$\beta^{'}$rods +lath-like particles---->β

The degree of strengthening arising from the GP-zones, $\beta^{"}$, and $\beta^{'}$ precipitates is a function of their size, mean interparticle spacing, volume fraction and their distribution in the matrix (Myhr et.al, 2004 and Cai et.al, 2004). All these factors are interrelated. The GP-zones, $\beta^{"}$, and $\beta^{'}$, particles may be cut by the dislocations ("chemical" hardening) at stress levels much above those required to move dislocations through the matrix. On the other hand, the GP-zones, $\beta^{"}$, and $\beta^{'}$, particles, may also resist cutting and the dislocations may be forced to take a path around the obstacles, that is, they can act as strong

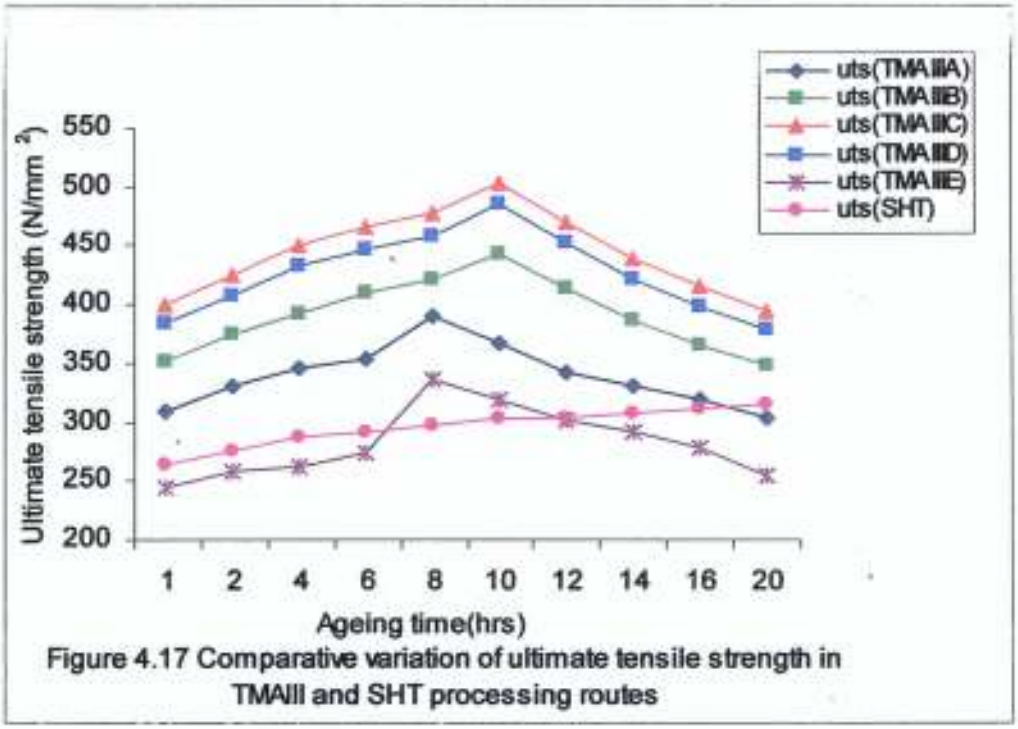

Figure 4.17 Comparative variation of ultimate tensile strength in TMAIII and SHT processing routes

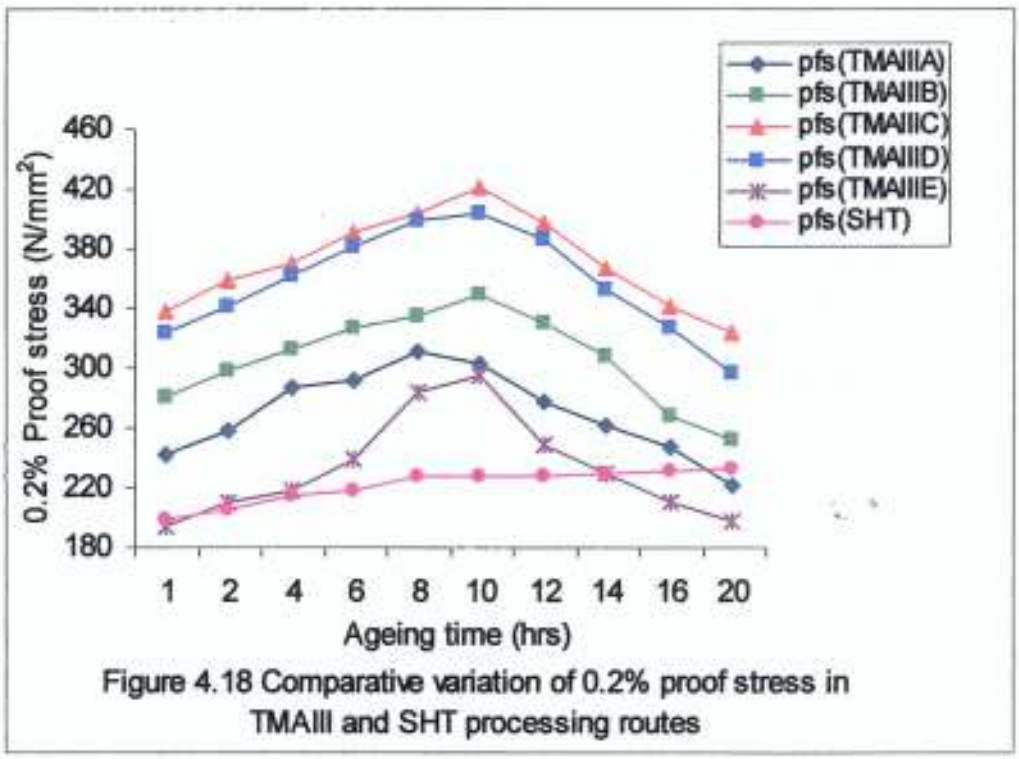

Figure 4.18 Comparative variation of 0.2% proof stress in TMAIII and SHT processing routes

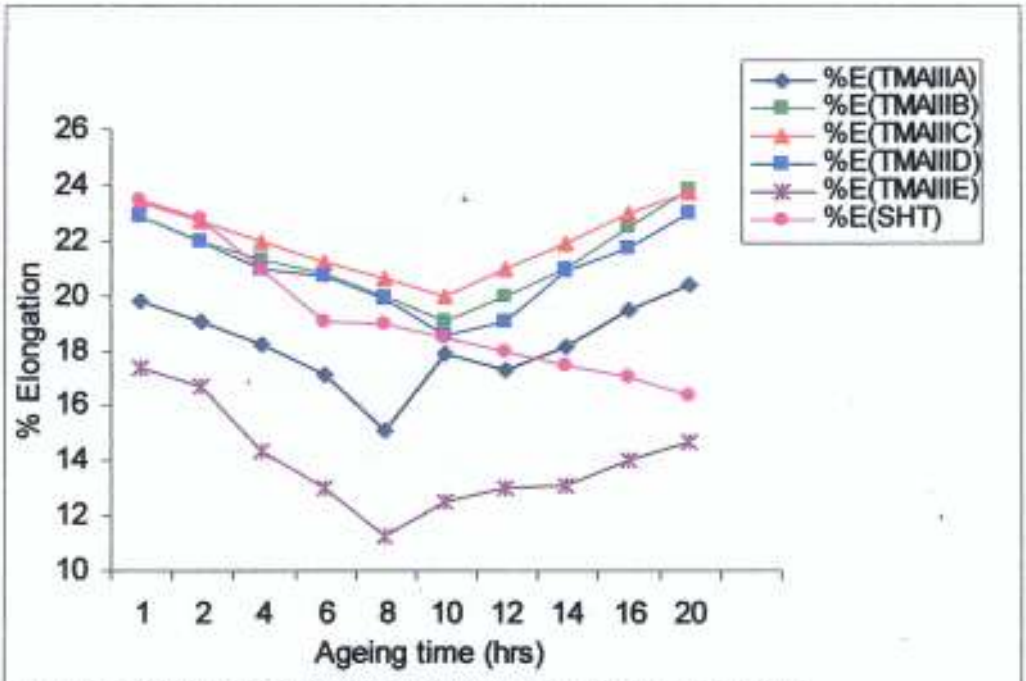

Figure 4.19 Comparative variation of Percentage elongation in TMAIII and SHT processing routes

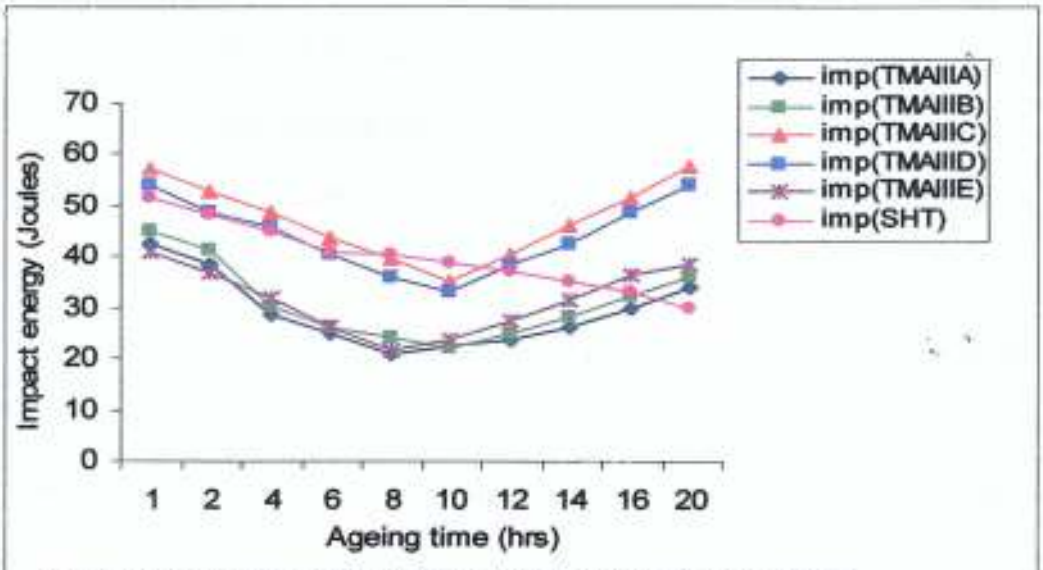

Figure 4.20 Comparative variation of Impact energy in TMAIII and SHT processing routes

impenetrable particles through which dislocations can move only by sharp changes in curvature of the dislocations (Orowan mechanism). It is believed that the first mechanism is operative only in the presence of GP-zone and β", while in the presence of semi-coherent β' particles the second mechanism appears to be operative. A dislocation may in passing through the matrix, be arrested by the dispersion of β' particles (Jensrud, 1997).

The pattern of the variation of tensile strength and plasticity indices in TMAI,TMAII, and TMAIII tally with the above reasoning.

However, the stress required to bulge round the particles according to Sheljaskov (1994), is given by

$$\tau = 2Gb/\lambda \qquad \text{---------- (36)}$$

where, G is the shear modulus, b the Burger's vector and λ is interparticle spacing.

This relation clearly shows that for a given volume fraction of GP-zone, β" and β', a higher stress τ, is required for a finer size of precipitate particles because this would result in a smaller interparticle spacing λ.

After bulging through between the particles, the dislocation line reforms, leaving a dislocation loop around the particles, effectively increasing its size and decreasing the spacing between nearby particles, so that an ever increasing stress is required to push successive dislocations through. This culminates in an increased tensile strength.

Besides the contribution of GP-zones, β" and β' particles, the dislocation substructure produced in the TMA treatments also plays a vital role in overall strengthening mechanism. The dislocation substructure produced in TMA treatments consists of tangles of dislocations and dislocation cells (Urreta et.al.2001). The strengthening is caused by

work hardening effects produced between moving dislocations and the dislocation substructure.

According to Thompson and Kramer, (1994) the flow stress is also related to the dislocation cell size in the form,

$$\tau = \alpha k G b d \quad \text{---------- (37)}$$

α is a constant of the order 0.5, G is shear modulus, b is Burger's vector , d is the dislocation cell diameter, and k is a constant for a given material. Higher flow stresses have been observed in smaller cells in accordance with this equation.

The existence of Fe_3SiAl_{12} dispersoid contributes to the strengthening of the alloy only weakly and in contrast to the contributions of GP-zone, β'', β' and dislocation substructure, their effects on overall strengthening may be neglected.

These dispersoids are very coarse in size, and can be seen easily under an optical microscope at low magnifications (Plates 23-65).They are also mechanically weak particles and are observed to break at low stresses (Hasegawa and Yakou, 1980).
Because the nucleation of β'' and β' is enhanced by the presence of dislocations (produced in large numbers through plastic deformation), the strength will be high when fine β'' and β' particles are formed in a dense dislocation cell substructure.

The strength in the peak-aged condition is therefore proposed to be associated with the presence of β'' and β'. However, in all the thermomechanically aged samples, the peak strength is found to be associated with β' only, as no evidence of β'' is seen in the peak-aged samples,(plates 12TMA-13TMA).

A cursory look at the results obtained from the TMA treatments revealed the fact that maximum increase in ultimate tensile strength and yield strength was obtained in

TMAIIIC treatment. In this study, the TMAIIIC treatment provided enhanced yield strength of the alloy from 227.76N/mm^2 (achieved in SHT condition) to 420N/mm^2 and ultimate tensile strength from 297.36N/mm^2 to 504N/mm^2; percentage elongation from 19% to 21% ; a steadfast hold on impact energy at 40joules.

These results represent the optimum values obtained in the TMA treatments and show that thermomechanical ageing is capable of providing improvement in the strength and plasticity of the Al-Mg-Si alloy if appropriately utilized. Precisely, Grigoriev and Kojaspirov (1981), obtained improved strength and plasticity of stainless steel concurrently through thermomechanical ageing processing of the alloy, while Singh and Goel,(1990), also obtained similar results for Al-Cu (2014) alloy through thermomechanical ageing, even though for Al-Cu, the gain in plasticity indices was not quite substantial.

In the case of 2014 Aluminum alloy worked upon by Singh and Goel (1990), the stabilization of ultimate tensile strength and yield strength values is directly linked to the dislocation density in the dislocation substructures produced by different TMA treatments. Furthermore, it was popularly remarked in literature that most Aluminum alloys will stabilize by the same mechanism since the α-matrix material is the f.c.c. crystal lattice.

Consequently, maximum stabilization in ultimate tensile strength and yield strength at elevated temperature is expected in the alloy after TMAIIIC treatment which is presumed to produce the densest dislocation - particle tangles (Urreta et.al.2001). However, plasticity indices are expected to rise steeply in response to small drops in tensile properties after prolonged exposure to elevated temperature.

The stabilization of strength properties at elevated temperature is considered to be specifically due to the presence of fine β' particles in the deformed structure, which inhibit recrystallization (Takeda et.al, 1998).

The discussions that follow look at the specifics in each of the TMAI, TMAII, and TMAIII processing schedules.

Influence of TMAI treatment on the Tensile Strength and Plasticity of 6063 Aluminium alloy

Figures 4.9 to 4.12 show the plots of tensile strength and plasticity indices obtained in TMAI, against ageing temperature. It is seen that in all cases of TMAI, the strength rises to higher values, with increasing ageing time up to a maximum, and thereafter start to decrease with further increase in ageing time. In contrast, the solution heat treated (SHT) alloy show no remarkable decline in tensile strength properties (Figs.4.9 and 4.10).

A close look at the results obtained from the TMA I, A-E treatments, show that TMAIE gave the best indices in terms of strength, where a peak ultimate tensile strength of 292N/mm^2 and yield strength of 256N/mm^2 were recorded after about 11 hours of ageing time at 180^{0}C. However, the plasticity indices are very low, 10% elongation and 19 joules impact energy, which are considered not good enough for heavy structural works.

The plasticity indices recorded for TMAIC at 12 hours ageing time, show better values, which are 13% elongation, and 21 joules impact energy. Notwithstanding, the peak ultimate tensile strength and yield strength were 277N/mm^2 and 242N/mm^2 respectively. These values are a little lower than that of TMAI

Influence of TMAII treatment on the Tensile Strength and Plasticity of 6063 Aluminium alloy.

Figures 4.13 to 4.16 graphically represent the variations in tensile and plasticity indices with ageing time obtained for the alloy by virtue of TMAII treatments. Again the tensile strengths (ultimate and yield) increase to higher values with increasing ageing time and reach a peak , and thereafter decrease with further increase in ageing time. Simultaneously, the plasticity indices decrease to lower values as the ageing time progressed, reaching a minimum value after which the parameters show increase with further increase in ageing time. In fact this is the observed behaviour for all the TMA treatments. Gracio et.al, (2004), remarked that the higher the ageing temperature and/or degree of deformation, the faster the response.

In a similar manner to what obtained in TMAIE, the peak values of ultimate tensile strength and yield strength are highest in TMAIIE, (321N/mm^2 and 279N/mm^2 respectively), while plasticity parameters (percentage elongation and impact energy) are 12% and 32 joules respectively. TMAIIE is the best of all the TMAII treatments. Here the tensile strengths and the plasticity indices are comparatively superior.

Furthermore, these values were obtained at about 8 hours ageing time, faster than the rest even though all were subjected to the same ageing temperature of 180^{0}C and preageing time, however, the percentage deformation here (50%) surpasses the others. This suggests that the extent of plastic deformation has a vital role to play in the improvement of the quality of deformed alloys.

4.7 Influence of TMAIII treatment on the Tensile Strength and Plasticity of 6063 Aluminium alloy.

Figures 4.17 to 4.20 show the variations of tensile strength and plasticity with ageing time for the TMAIII processing routes. Unlike the previous TMAIE and TMAIIE treatments whereby the strength (ultimate and yield) were higher in comparison with any other within the respective schedules, the strengths (ultimate and yield) in TMAIIIE, are lower than any other one within the TMAIII,A-E options. Same is true of the plasticity indices. This appears to be a strange development despite the fact that the percentage deformation is 50%. One tend to suggest that, there is a likelihood of very intensive strain hardening beyond 30% deformation, which might have generated some local cracks or dimples within the alloy matrix, and this situation in conjunction with possible annihilation of dislocations as the ageing time is prolonged may have subsequently lowered the resistance of the alloy to deformation. Evidence of such possibilities abound in plates 36 and 3TPP.

TMAIIIC processing route imparts a peak ultimate tensile strength of 504N/mm^2, yield strength of 420N/mm^2, minimum of 21% elongation, and 40 joules impact energy to the alloy. These figures when compared to all others reflect the highest quality of the alloy as obtained in this study. Surprisingly this is happening at 30% deformation. TMAIIID also produced a product whose strength and plasticity indices are high when compared to those of TMAI and TMAII.

Above all, it appears that TMAIII schedules gave better improvement on the strength and plasticity indices of the alloy with the exception of TMAIIIE. The much-

improved properties witnessed in TMAIII treatments may be accounted for in part, possibly by the degree of pre-ageing (75%), the highest in this study

Comparison of TMAI, TMAII and TMAIII.

The comparisons were made at 8 hours ageing time, by virtue of its relevance to industrial setting, but the comparison could also be made at any chosen ageing time.

In fig.4.21, we observed the changes in properties with increasing degree of deformation for TMAI schedule. The tensile properties are enhanced as the degree of deformation increases with TMAIE showing the highest value of ultimate tensile strength and yield strength. However, the plasticity parameters decreased from TMAIA to TMAIE.

At this ageing time (8 hours) and temperature (180^0C), there is no pronounced advantage of any TMAI processing route over the other.

In fig. 4.22, the TMAII processing routes are compared also at 8 hours ageing time. It is observed here that the processing routes TMAIID and TMAIIE have pronounced advantage over the others, in terms of higher values of tensile properties. Notwithstanding, the impact energy recorded in TMAIID is much lower than that recorded in the other variants, but one could reflect that the results obtained in TMAIIE are better than the others in terms of tensile strength and impact energy.

Figure 4.23, represents the comparative variation of properties in TMAIII treatments. It is not difficult to observe that TMAIIIC is the best, both in tensile and plasticity values.

It could therefore be concluded that at 8 hours ageing time and 180^0C ageing temperature, TMAIIIC produced the best result when compared with the rest 14 thermomechanical ageing processing routes. The results obtained here are 478N/mm^2 ultimate tensile strength, 404N/mm^2 yield strength, 21% elongation, and 40joules impact energy.

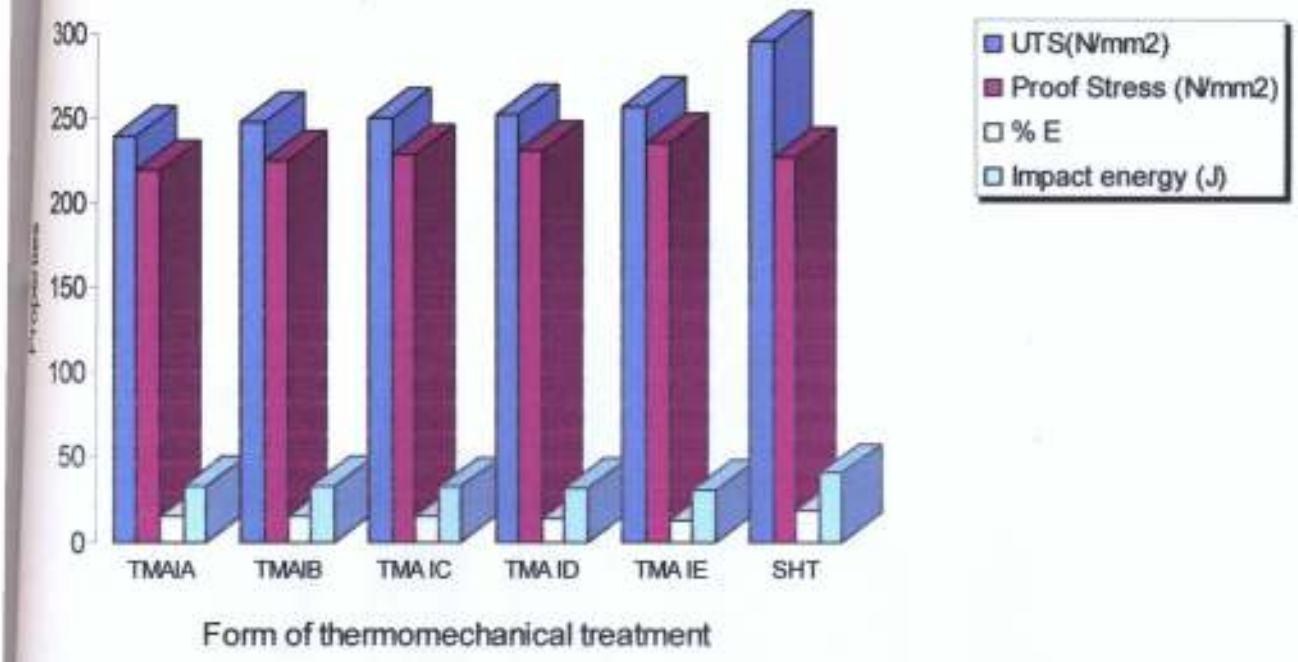

Figure 4.21 Change of Properties in TMA I with increasing degree of deformation at 8hours ageing time.

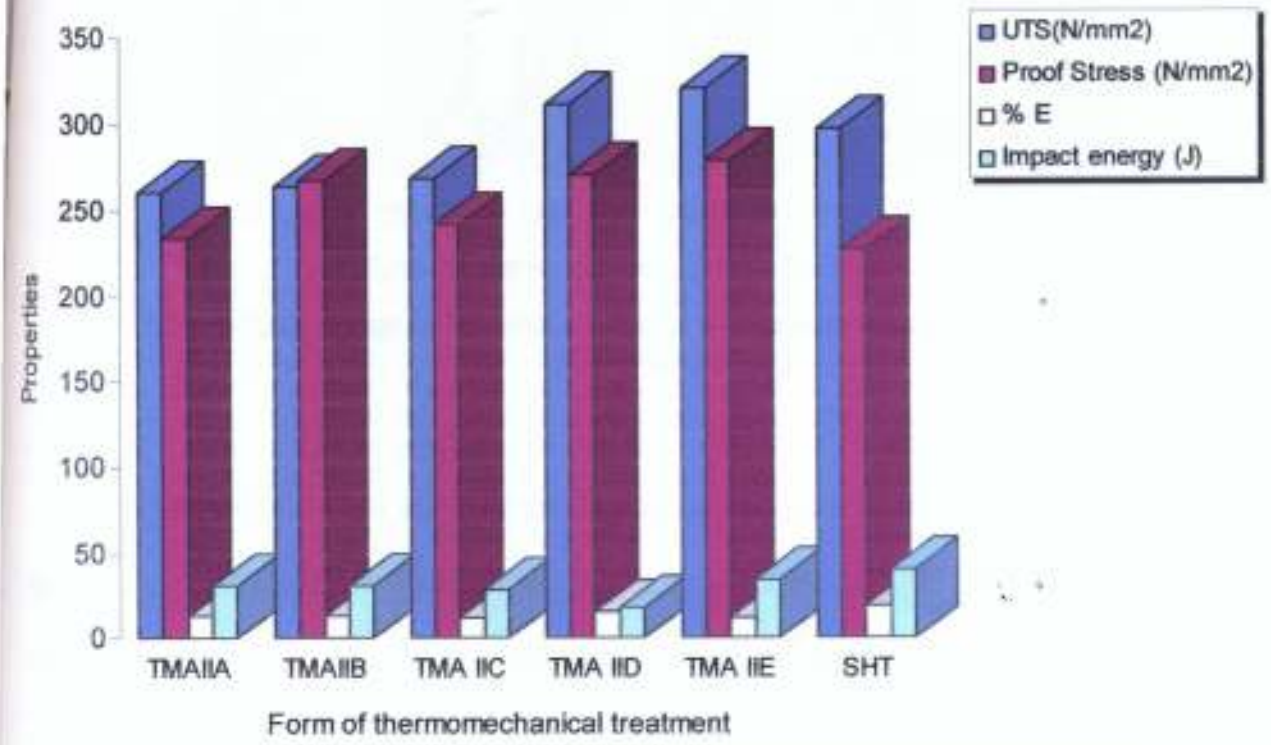

Figure 4.22 Change of Properties in TMAII with increasing degree bof deformation at 8 hours ageing time

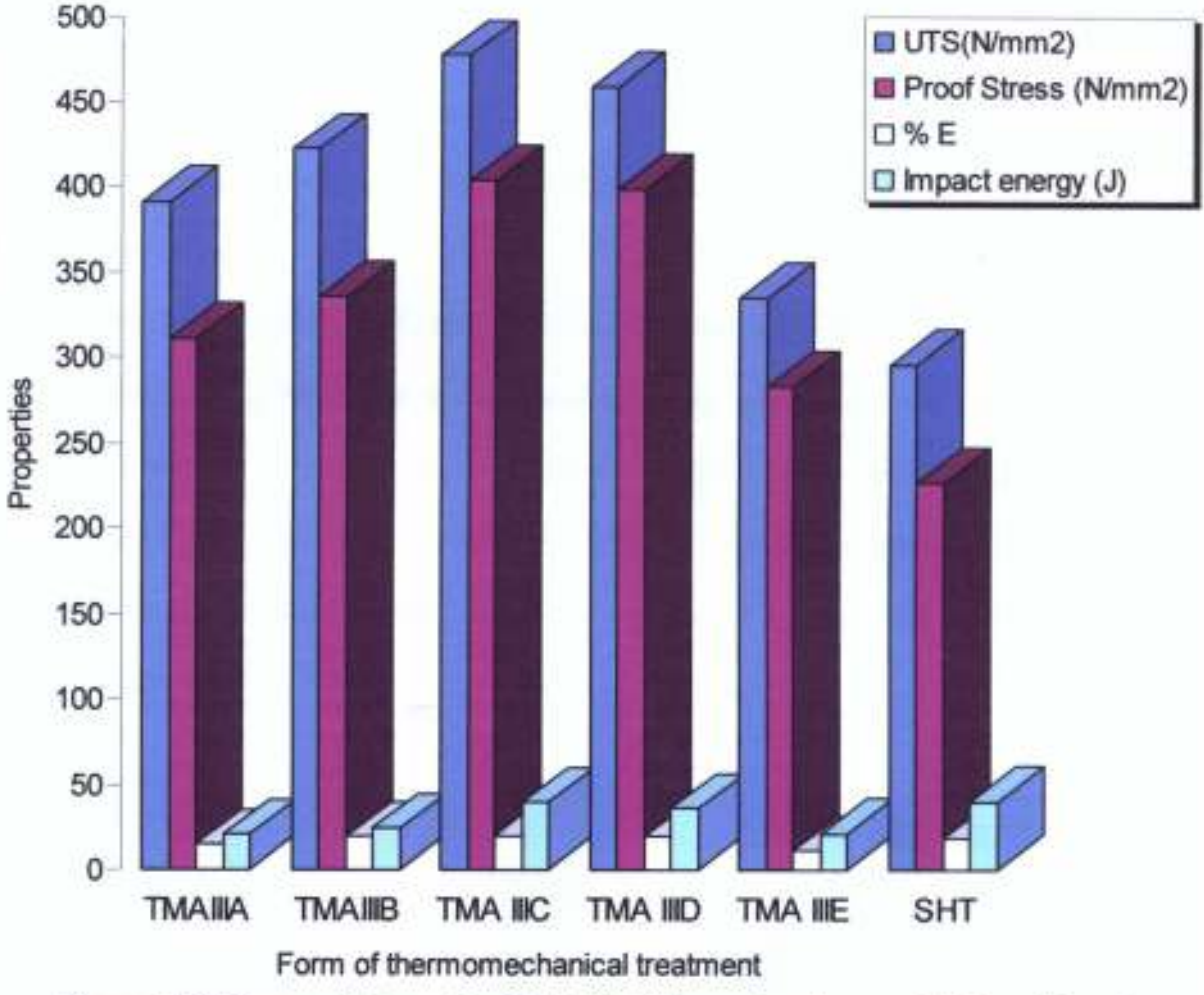

Figure 4.23 Change of Properties in TMAIII with inreasing degree of deformation at 8hours ageing time

Figures 4.24 to 4.28 represent the comparisons of the effects of the degree of pre-ageing on the tensile strength and plasticity of the alloy, at 180^0C ageing temperature and 8 hours ageing time, examined at varying degrees of deformation.

In TMAIA, TMAIIA, TMAIIIA, representing 25% pre-ageing, 50% pre-ageing, and 75% pre-ageing respectively, with a 10% deformation in each case (fig.4.24), it is obvious that 75% pre-ageing treatment produced the best result, even though there is a slight shortfall in the value of the impact energy recorded.

In the processing route TMAIIIA, characterized by 75% pre-ageing, 10% warm deformation at 180^{0}C and final ageing at 180^{0}C for 8 hours, the ultimate tensile strength rises from 335N/mm^2 to 391N/mm^2, the yield strength rises from 272N/mm^2 to 311N/mm^2, while the percentage elongation only increased by 1% and the impact energy decreased by 11 joules.

With increasing degree of plastic deformation (while other processing parameters remained unchanged), the tensile strengths and plasticity indices improved remarkably; hence in TMAIIIC, with 30% warm deformation, higher values of ultimate tensile strength and yield strength of 478N/mm^2 and 404N/mm^2 respectively, were obtained. The corresponding values of percentage elongation and impact energy were 21% and 40 joules respectively (fig.4.26).

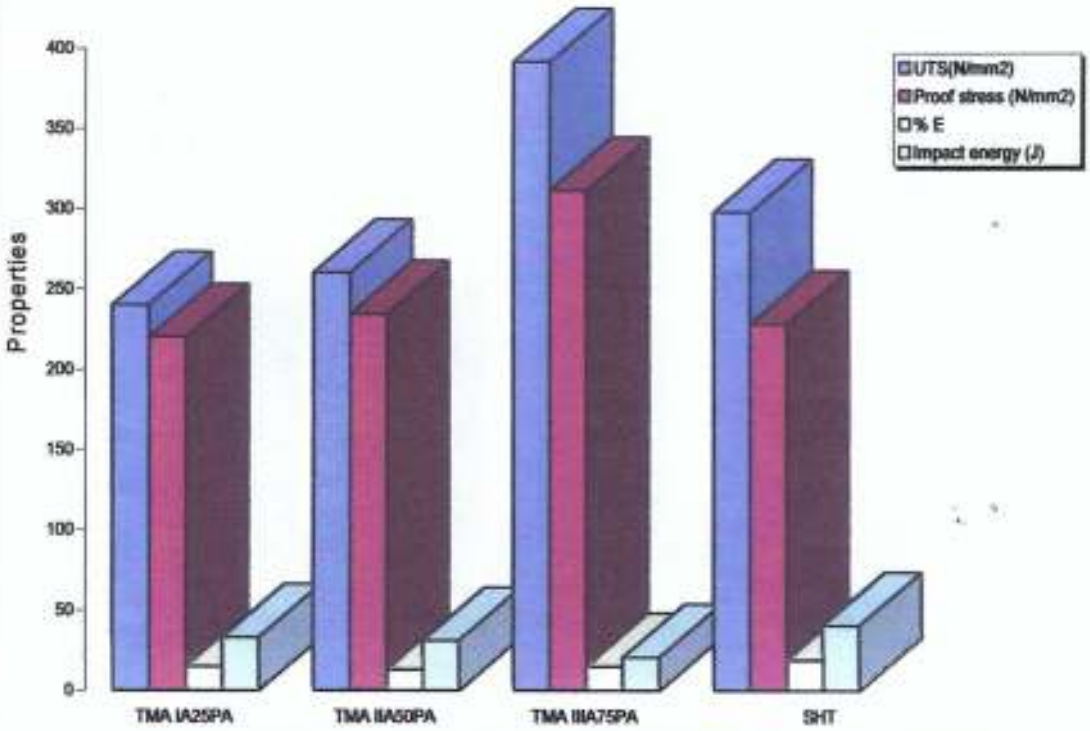

Figure 4.24 Change in Tensile strength and plasticity with increasing Degree of preaging (at 180^{0}C, 10% deformation, 8 hrs Ageing time)

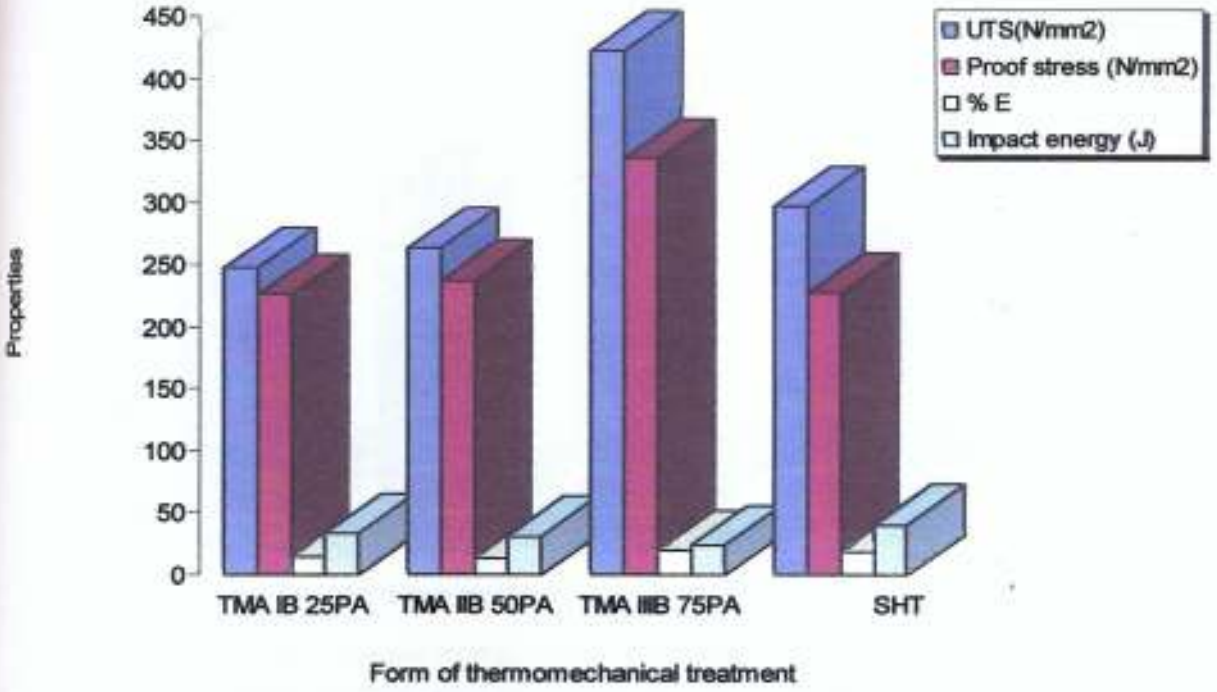

Fig.4.25 Change in Tensile Strength and Plasticity with increasing Degree of Preageing at 20% deformation, 180°C ageing temperature and 8hrs final ageing time.

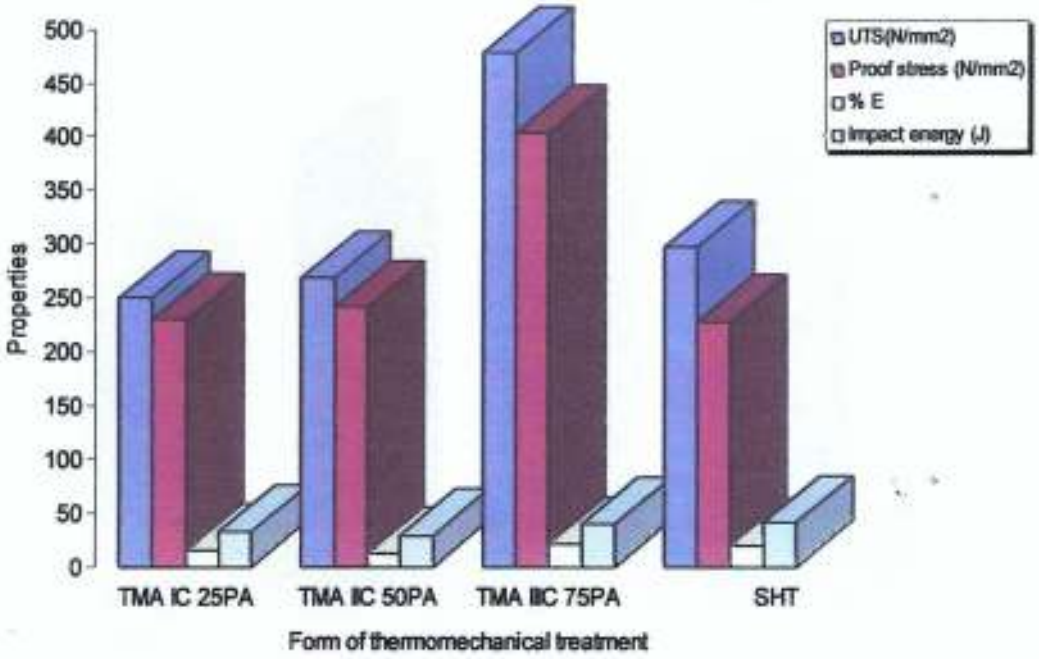

Fig.4.26 Change in Tensile Strength and Plasticity with increasing Degree of Preageing at 30% deformation, 180°C ageing temperature and 8hrs final ageing time

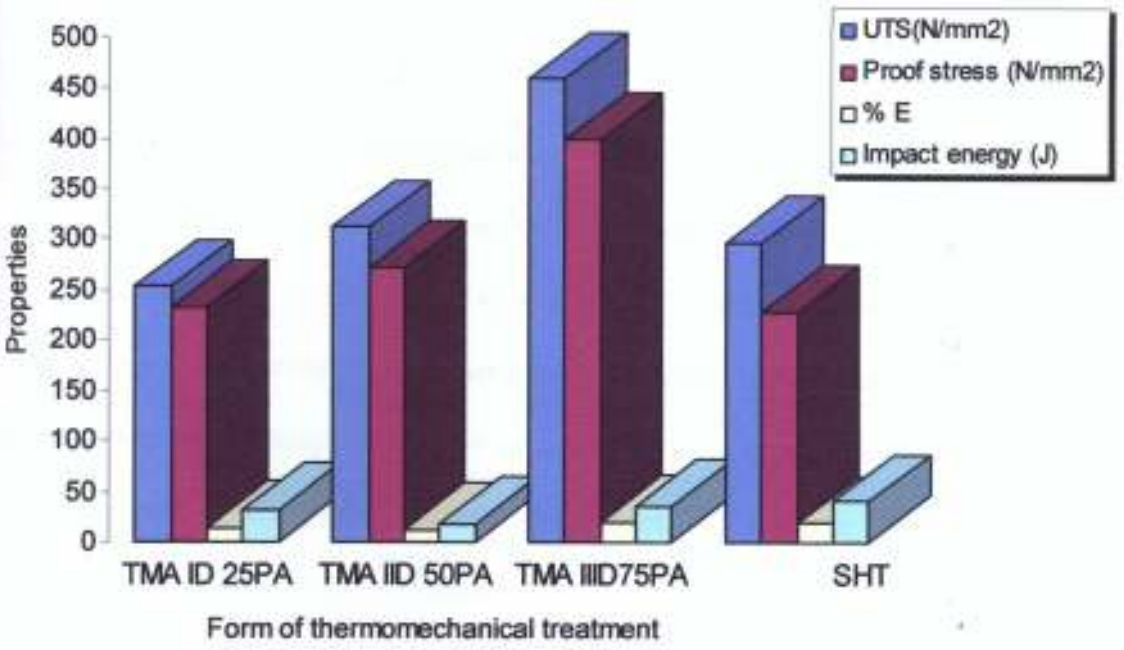

Figure 4.27 Change in Tensile strength and Plasticity with increasing degree of pre-ageing at 180^{0}C, 40% deformation and 8hrs ageing time.

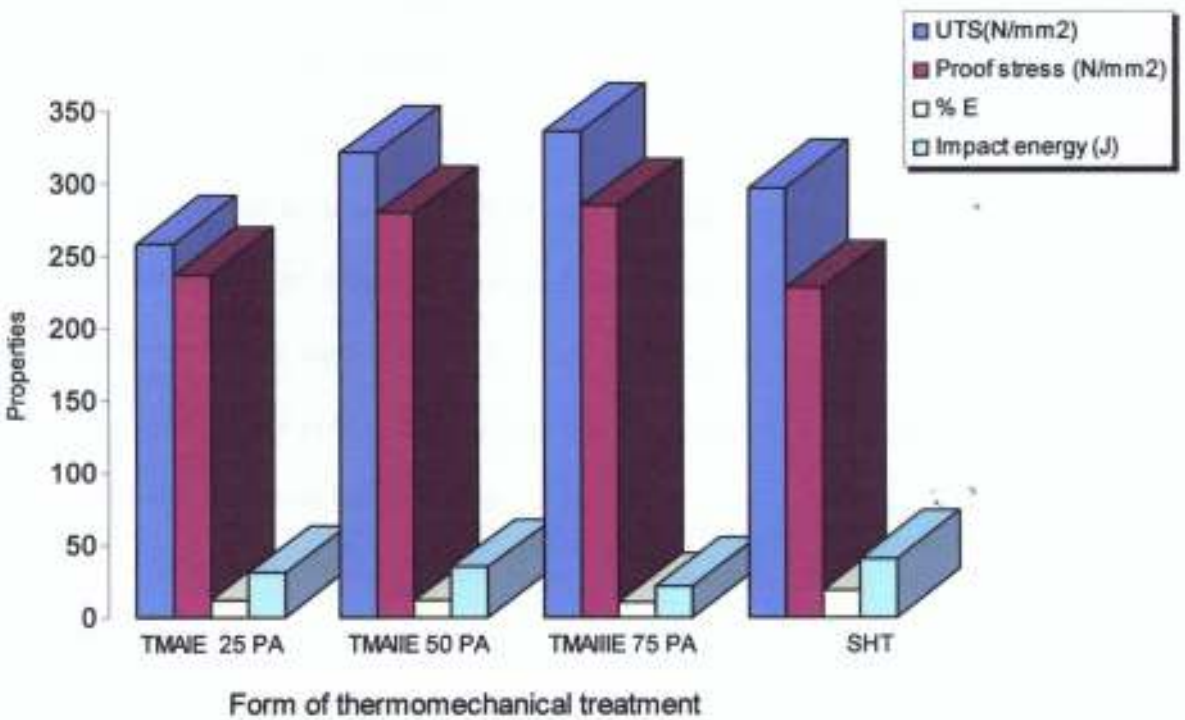

Figure 4.28 Change in Tensile strength and Plasticity with increasing degree of pre-ageing at 180^{0}C, 50% deformation and 8hrs ageing time.

4.3 Discussion of Micrographs.

4.3.1 Macrostructure and Microstructure.

According to Lahktin and Leontiva (1980), structural components of a metal or alloy that can be viewed, by the unaided eye, or under the microscope at a magnification up to x30 or x40 is referred to as macrostructure. In other words, macrostructure is a structure that is large enough to be seen or examined with little or no magnification. While microstructure refer to the structural components of a metal or alloy that can be seen or observed with the aid of a microscope at a magnification not less than x50, and the minimum resolution of such microscope not greater than 2000Å.

For electron microscopes the minimum resolution is about 2 -5Å, and magnification is as high as over x50000. Magnification over x2000 in optical microscopes is of no significance since no new smaller structural details may be observed; only the scale of the image could have changed whereas the resolution which is determined by the light wavelength remain unchanged.

4.3.2 Microstructure of Solution Heat Treated (SHT) 6063 Aluminium Alloy.

The optical micrograph of a typical solution heat treated 6063 Aluminium alloy at a magnification of x250 is shown in Plate 1, which is self explanatory. The solidified particles of Fe_3SiAl_{12} are bold and scriptlike, those of Al_5FeSi are platelike while the Mg_2Si precipitates are small blocky forms, all dispersed in a matrix of Aluminium-rich solid solution (Plate 2). The size and form of these particles do not allow for simultaneous high tensile strengths and plasticity in SHT alloy as compared to the thermomechanically aged alloy with high degree of preageing.

4.3.3 Microstructure of Thermoplastically Worked Al-Mg-Si Alloy.

The micrographs obtained from the thermoplastically worked 6063 Aluminium alloy at varying warm temperatures and degrees of deformation have a number of common structural features. The common phases identified in each of the worked samples are particles of Fe_3SiAl_{12} (script-like forms), and β-phase (lamellar or irregularly shaped rounds), and both particles are dispersed in the α-phase which is the Aluminium-rich matrix (Plates 3-10).

The matrix, Al-rich solid solution, constitutes the prominent phase while the multiple slip, which forms the region of highest misorientation, appears as thin lines (Plate 3), and are also sites of dislocations as reported by Nes et al. (1984).

The particles of Fe_3SiAl_{12}, are formed normally during the solidification of the Al-Mg-Si alloys, while the Mg_2Si (β-phase) are precipitated from the supersaturated solid solution.

In Plates 1 and 2, the particles of the dispersoid Fe_3SiAl_{12}, are many while the equilibrium precipitate particles Mg_2Si, are relatively few. The particles of the dispersoids have been reported to contribute weakly to the strengthening of the alloy especially at low degree of deformation (10%-30%). The strengthening experienced by working the alloy at 28^0C, 160^0C, and 180^0C deformation temperatures and 10-50% degree of deformation is due to increased dislocation density. As the dislocations tangled together, sessile points are created that eventually, translate to increased strength since

Plate 1. Typical microstructure of Al-Mg-Si alloy; as received (SHT) showing particles of Fe_3SiAl_{12} (scriptlike), Al_5FeSi (platelike) and Mg_2Si (small blocky form) in a matrix of Aluminium-rich solid solution. Etched in 0.5 percent HF, 250x.

Plate 1AR. Typical TEM microstructure of the as received Al-Mg-Si alloy showing Fe_3SiAl_{12} particles, dislocations and few β precipitates in a matrix of α-Aluminium rich solid solution.

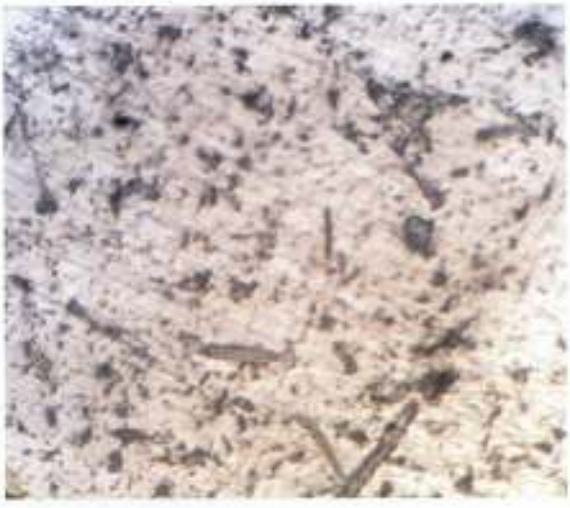

Plate 3. Typical microstructure of Al-Mg-Si alloy;20% deformation at 180^0C, showing particles of Fe_3SiAl_{12} (scriptlike)and Mg_2Si (lamellar or small blocky form) in a matrix of Aluminium-rich solid solution. Etched in 0.5 percent HF,400x.

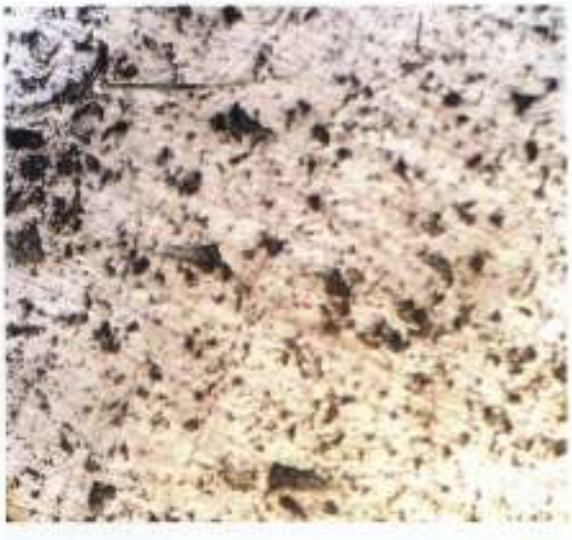

Plate 4. Typical microstructure of Al-Mg-Si alloy; 40% deformation at 180^0C, showing particles of Fe_3SiAl_{12} (scriptlike)and Mg_2Si (lamellar or small blocky form) in a matrix of Aluminium-rich solid solution. Fragmented dispersoids are becoming smaller. Etched in 0.5 percent HF,400x.

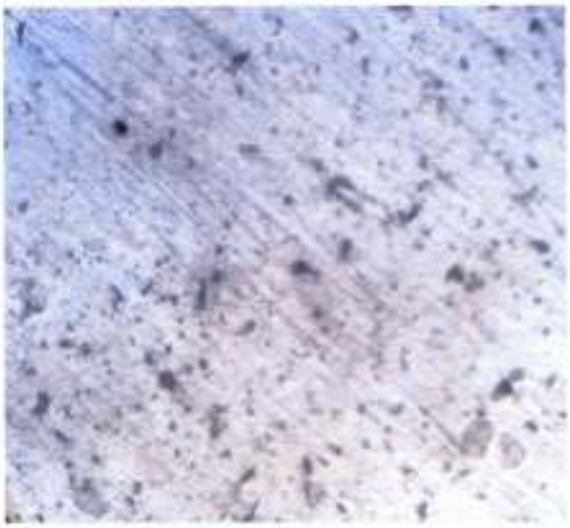

Plate 5. Typical microstructure of Al-Mg-Si alloy; 50% deformation at 180^0C, showing particles of Fe_3SiAl_{12} (scriptlike) and Mg_2Si (small blocky form) in a matrix of Aluminium-rich solid solution. Etched in 0.5 percent HF, 400x.

Plate 6. Typical microstructure of Al-Mg-Si alloy; 20% deformation at 240^0C, showing particles of Fe_3SiAl_{12} (scriptlike) and Mg_2Si (lamellar or small blocky form) in a matrix of Aluminium-rich solid solution. Lamellar forms of Mg_2Si are significantly prominent. Etched in 0.5 percent HF,400x.

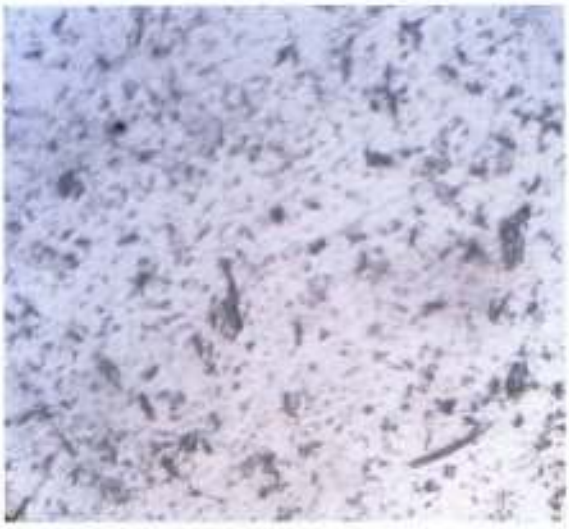

Plate 7. Typical microstructure of Al-Mg-Si alloy; 40% deformation at 240^0C,showing particles of Fe_3SiAl_{12} (scriptlike) and Mg_2Si (small blocky form) in a matrix of Aluminium-rich solid solution. Fewer particles of Mg_2Si compared to that of Fe_3SiAl_{12} dispersoid. Etched in 0.5 percent HF,400x.

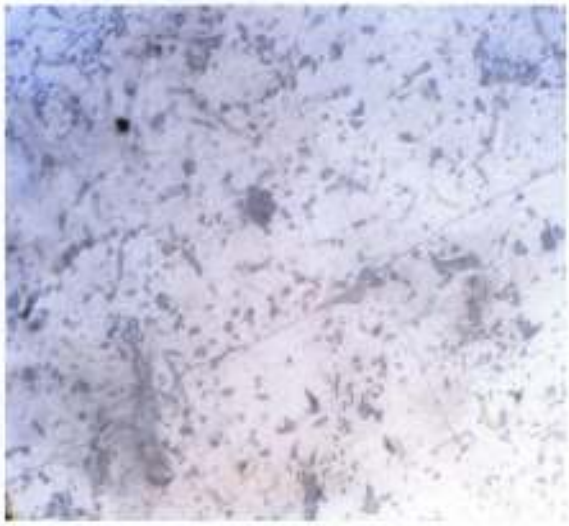

Plate 8. Typical microstructure of Al-Mg-Si alloy; 50% deformation at 240^0C, showing particles of Fe_3SiAl_{12} (scriptlike) and Mg_2Si (lamellar or small blocky form) in a matrix of Aluminium-rich solid solution. Lamellar forms of Mg_2Si are more prominent. Etched in 0.5 percent HF,400x.

Plate 9. Typical microstructure of Al-Mg-Si alloy; 50% deformation at 160^0C, showing particles of Fe_3SiAl_{12} (scriptlike) and Mg_2Si (lamellar, or small blocky form) in a matrix of Aluminium-rich solid solution. Mechanical fibering prominent. Etched in 0.5 percent HF, 400x.

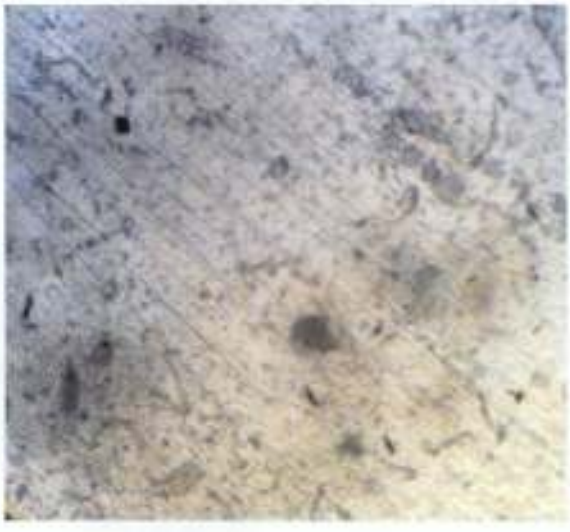

Plate 10. Typical microstructure of Al-Mg-Si alloy; 50% deformation at 220^0C, showing particles of Fe_3SiAl_{12} (scriptlike) and Mg_2Si (lamellar, or small blocky form) in a matrix of Aluminium-rich solid solution. Mechanical fibering evident .Etched in 0.5 percent HF, 400x.

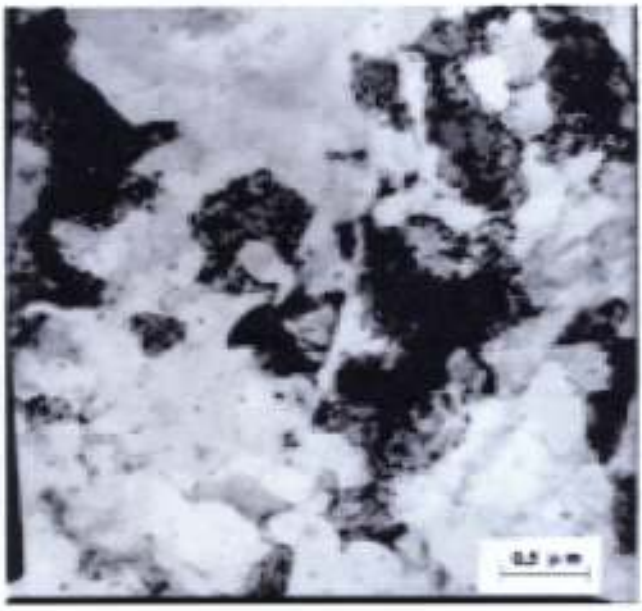

Plate 2TPP Typical TEM microstructure of cold deformed Al-Mg-Si alloy(at 28^{0}C and 20% deformation) showing fragmented Fe_3SiAl_{12} particles, dislocations and few β precipitate in a matrix of α-Aluminium rich solid solution.

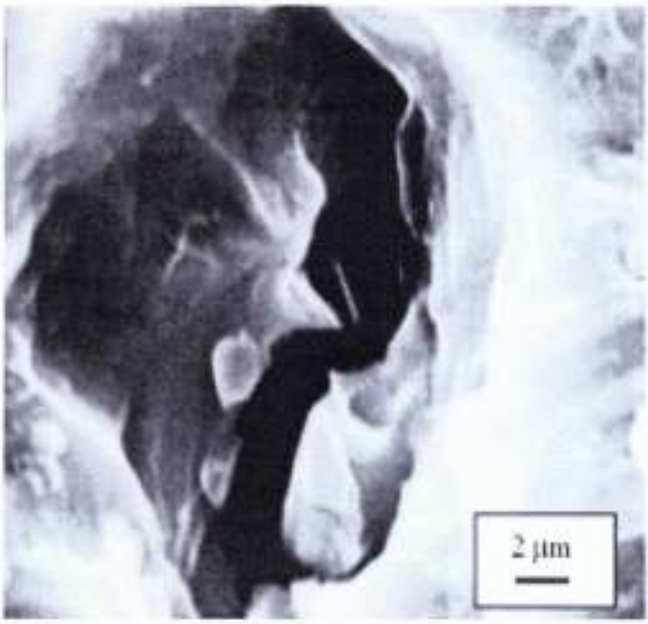

Plate 3TPP Typical TEM micrograph of Al-Mg-Si alloy showing shallow dimples adjacent to a fine microscopic secondary crack in 50% deformed alloy at 220^{0}C.

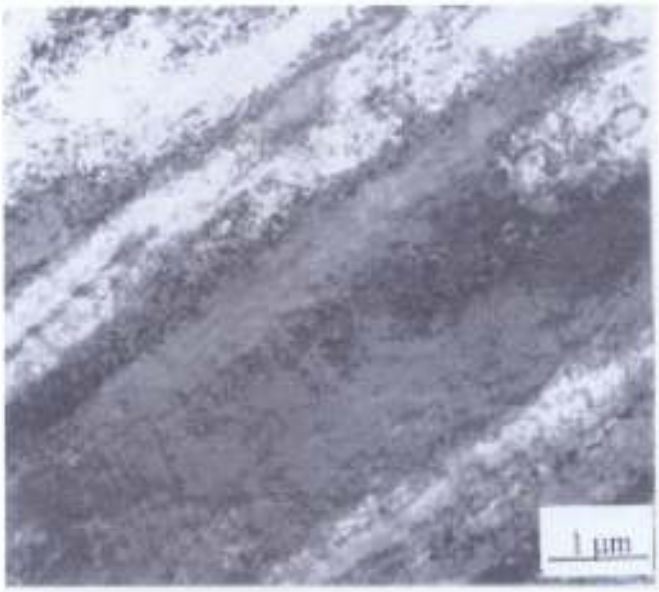

Plate 4TPP Typical TEM microstructures of Al-Mg-Si alloy showing mechanical fibering which are sites of dislocations. No dimples, no annihilations, and few β-phase evident. Alloy deformed by 50% at 160°C.

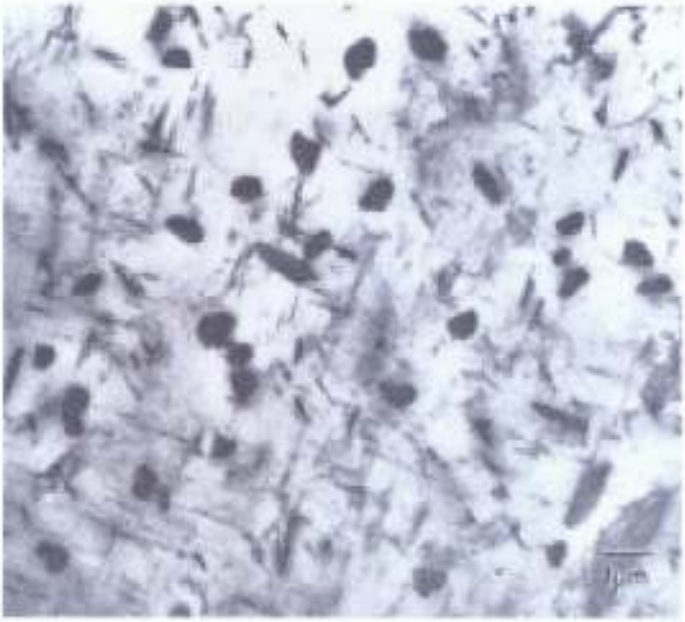

Plate 5TPP. Typical TEM micrograph of Al-Mg-Si alloy, subjected to 50% at 180°C showing several Fe_3SiAl_{12} dispersoids of size 0.1-0.5µm and numerous finely dispersed lamellar-like precipitates of Mg_2Si, in a matrix of α-Aluminium rich solid solution.

higher magnitude of the externally applied load will be required to cause further deformation.

As the degree of deformation increases, for instance above 25%, the higher the tendency for the evolution of more microstructural features. Consequently, in Plates 4,5,10 and 4TPP the presence of multiple slip, forming regions of highest misorientation becomes noticeable and according to Nes et al. (1984) and Khan et al.(2003), these thin lines are sites of dislocations. The greater these multiple slips the more the number of dislocations likely to be present in the deformed alloy, and the larger is the number of sessile points likely to be formed. However, at higher temperatures (in this case above 200^0C) the grain structure of the alloy is continuously reforming due to the process of recovery and recrystallization. Eventually, a dynamic equilibrium is established between the generation of dislocations and their annihilation, which may therefore bring about easy deformation at relatively high deformation temperatures (Plates 7,8,10 and 3TPP).

At lower temperatures of deformation,(28^0C-180^0C), the solidification dispersoids are observed to be more difficult to fragment hence they are coarser than at fairly elevated deformation temperatures,(200^0C-240^0C). When these microstructural features are related to the tensile strength and plasticity indices of the Al-Mg-Si alloy as obtained in this work, one could conclude that deformed 6063 Aluminium alloy obtain its strength from the precipitation of coherent particles and accumulation of dislocations, (Plates 2TPP and 4TPP), which is in agreement with the findings of Jensrud and Pedersen,(1998).

Also, the similarity of the microstructures despite the differences in the applied stresses (different deformation degrees), shows that microstructural evolution does not depend

only on the applied stress, but is the product of complex interactions between the kinetics of dislocation generation and annihilation, nucleation of new phases and zones, and the growth of precipitates (Plates 6 and 5TPP).

Differences in the microstructural evolutions in Plates 3, 4, and 5, showcase the effects of the variation of the degree of deformation at temperatures not greater than 180^{0}C, on the 6063 Aluminium alloy. Plates 6, 7, and 8 reflect the effects of the degree of deformation at temperatures greater than 180^{0}C. A comparison of Plates 5, 8, 9, 10 as well as Plates 3TPP, 4TPP and 5TPP, clearly reflects the effects of the variation of deformation temperature on the microstructure of the alloy. Increasing degree of deformation favours refinement of grains while increasing deformation temperature tend to encourage coarsening of grains resulting in reduced strength.

4.3.4 Microstructure of Artificially Aged Al-Mg-Si alloy.

The microstructure of the aged samples, for each set of ageing time and temperature are essentially similar, only differing in terms of the number and size of the precipitated phases, in particular the non-coherent β-phase (Mg_2Si). The dispersoids also vary in size and shape as the ageing temperature and time change.

Again the common phases identified in each of the aged samples are, Fe_3SiAl_{12}, (scriptlike); Al_5FeSi (platelike); and Mg_2Si (lamellar or small blocky form) precipitates in a matrix of Aluminium-rich solid solution.

The optical micrographs in Plates 11-14, and the transmission electron micrographs in Plates 6AA-9AA, which are representative microstructures of the artificially aged alloy obtained at different ageing times and at 180^{0}C ageing temperature, display the effect of ageing time on the microstructure of the 6063 Aluminium alloy. It is

realized that more precipitates are present in the artificially aged alloy than in the thermoplastically worked samples. However, the dispersoids and precipitates tend to become bigger, the higher the ageing time. In addition, the multiple slip generated in the alloy during the initial primary deformation of the alloy is still discernible, though not as prominent as those observed in the thermoplastically worked samples, which of course have undergone a secondary deformation. The optical micrographs in Plates 15, 16, 17, 18, and 19 reflect the features obtained at different ageing temperatures for a fixed ageing time of 6hrs. These micrographs show clearly that strengthening phases predominate at low ageing time as the ageing temperatures increases. At ageing temperature of 220^0C, peak strength of the alloy is obtained. Plate 20 represents the typical over aged structure characteristic of alloy aged at a temperature greater than 200^0C for ageing time greater than 16 hours. Coarse precipitates are evident and account for the usual low strength of over aged alloys.

As mentioned earlier, the dispersoids only contribute weakly to the tensile strength and plasticity of Al-Mg-Si alloy, hence the presence of another dispersed phase (Al_5FeSi), do not add to the strength of the artificially aged alloy. The initial increase in the tensile strength of the alloy, when aged for a few hours at any temperature is due to the precipitation of a needlelike structure identified as $\beta^{"}$-phase,(Plate6AA), as reported by Marioara, (2000); Urreta et al., (2001); Cai et el., (2004); Gracio et al., (2004); and Garrett et al.,(2005). These $\beta^{"}$ needles are thought to be of composition MgSi, and are shearable as long as are of subcritical size, as they are found at underage and pre-peak age conditions.

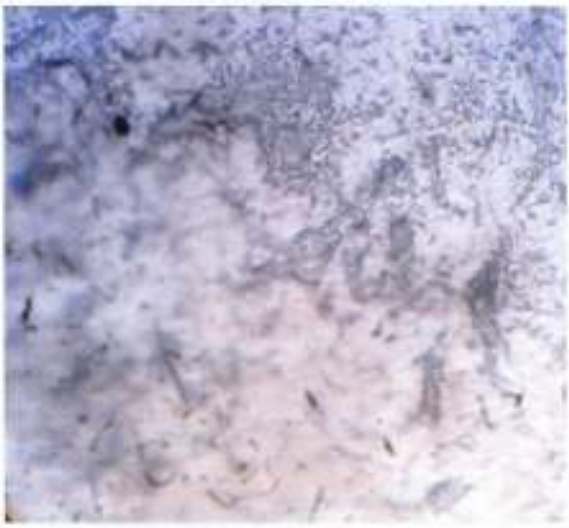

Plate11. Typical microstructure of artificially under-aged (UA) Al-Mg-Si alloy, at 180^0C for 8hrs, showing particles of Fe_3SiAl_{12} (scriptlike), and few precipitates of Mg_2Si (small lamellar/ blocky form) in a matrix of Aluminium-rich solid solution. Etched in 0.5 percent HF, 500x.

Plate12. Typical microstructure of artificially peak-aged (PA) Al-Mg-Si alloy at 180^0C for 12hrs, showing particles of Fe_3SiAl_{12} (scriptlike) and scanty precipitates of Mg_2Si (small blocky form) in a matrix of Aluminium-rich solid solution. Cells formation is visible. Etched in 0.5 percent HF, 500x.

Plate13. Typical microstructure of artificially over-aged (OA) Al-Mg-Si alloy at 180^0C for 16hrs, showing particles of Fe_3SiAl_{12} (modified scriptlike form), and precipitates of Mg_2Si (small lamellar/ blocky form), in a matrix of Aluminium-rich solid solution. Noted here is the clustering of the particles of Fe_3SiAl_{12} dispersoids.. Etched in 0.5 percent HF, 500x.

Plate14. Typical microstructure of artificially strongly over-aged (SOA) Al-Mg-Si alloy, at 180^0C for 20hrs, showing particles of Fe_3SiAl_{12} (modified scriptlike form) and few precipitates of Mg_2Si (small lamellar/ blocky form) in a matrix of Aluminium-rich solid solution. Coarsening of particles is evident. Etched in 0.5 percent HF, 500x.

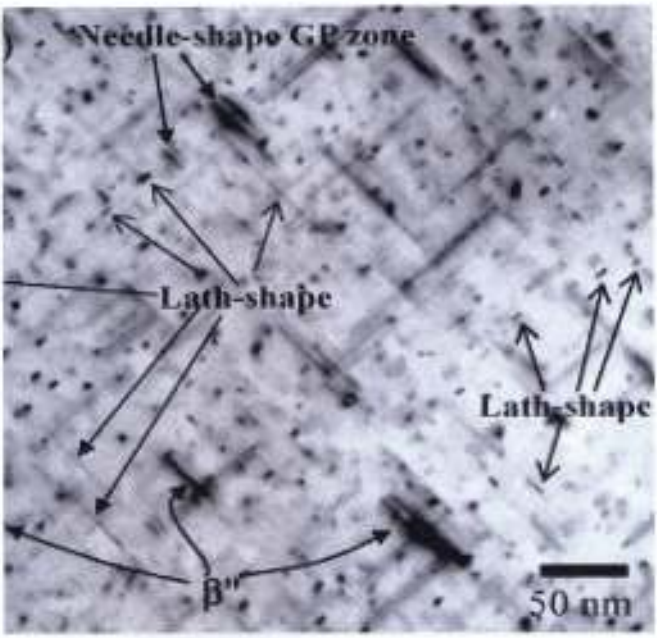

Plate 6AA Typical TEM micrograph of under aged (UA) Al-Mg-Si alloy subjected to conventional artificial ageing (AA) treatment,(at 180^{0}C for 8hrs) showing the needle-shaped GP zones, β'' precipitates, lathe-like β' precipitates (all strengthening particles), and coarse script-like particles of Fe_3SiAl_{12} all in a matrix of α-Aluminium rich solute solution. No pre ageing in this case.

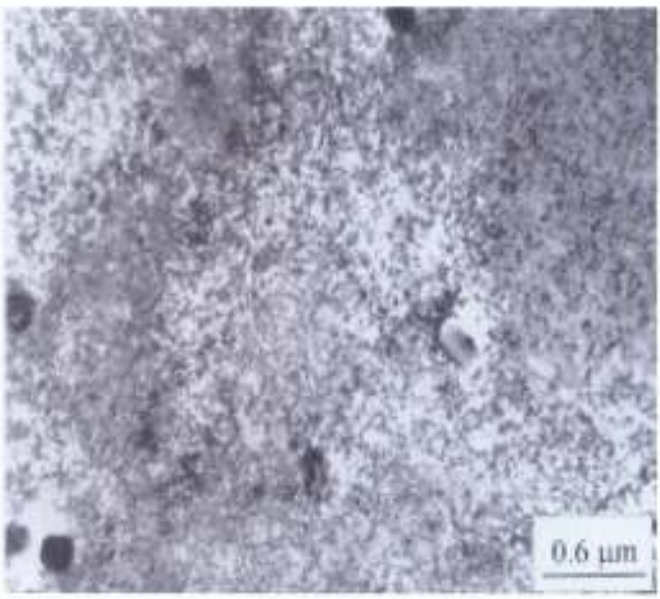

Plate 7AA Typical TEM microstructures of Al-Mg-Si alloy showing peak aged (PA) structure of artificially aged (AA) alloy at 180°C for 12 hrs, few β-phase has started to emerge.

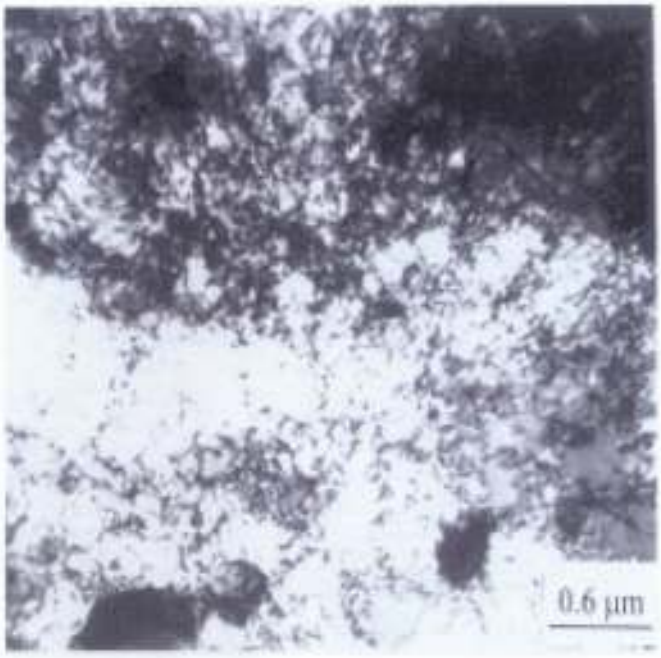

Plate 8AA Typical TEM microstructures of Al-Mg-Si alloy showing overaged (OA) structure of artificially aged (AA) alloy at 180°C for 16hrs. Coarser β-phase and other dispersoids are quite noticeable.

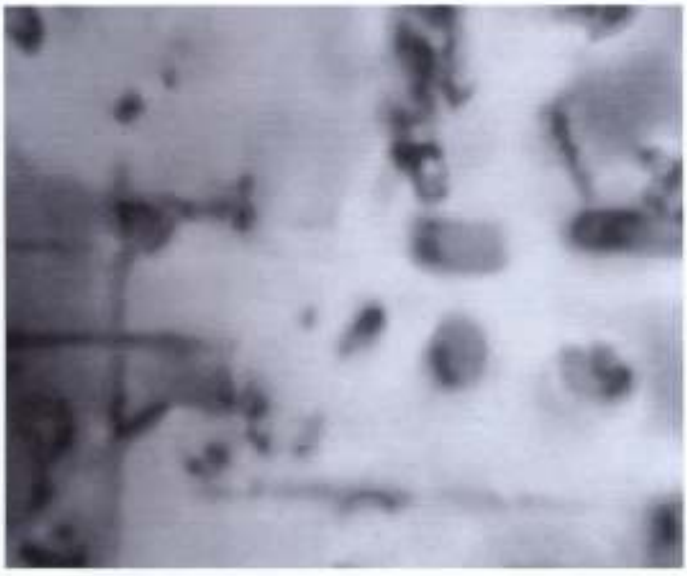

Plate 9AA Typical TEM micrograph of artificially aged Al-Mg-Si alloy in strongly over aged (SOA) condition (at 180°C for 20hrs), showing coarse particles of Fe_3SiAl_{12} and coarse precipitates of the intermediate phases.

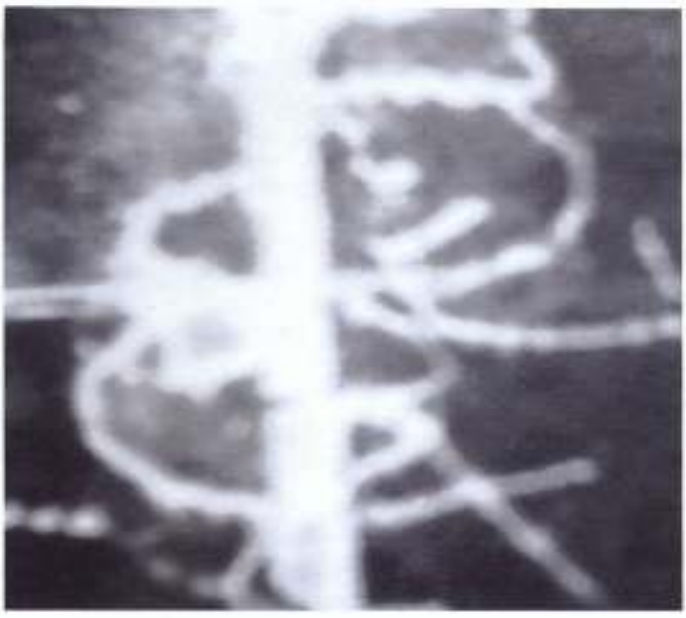

Plate 10AA Typical TEM micrograph of artificially aged Al-Mg-Si alloy in the post peak aged condition (aged for 14hrs at 180^0C), showing the Orowan bypassing mechanism. The vertical 'beam' is one of the larger β' needles, being bypassed by many dislocations (appeared as spiraling around the precipitate).

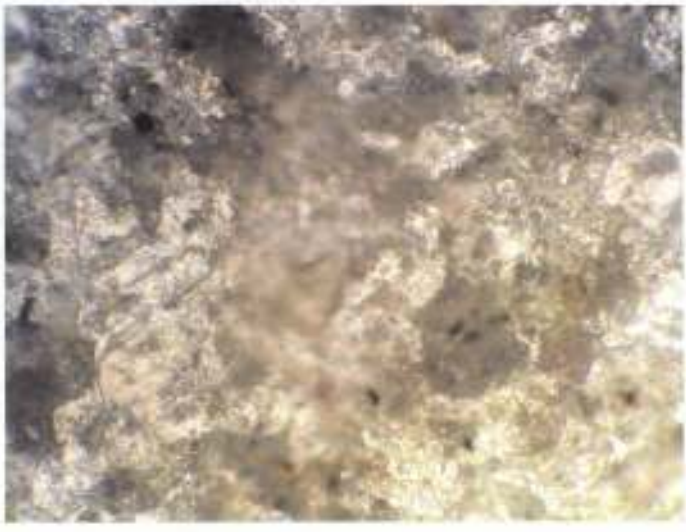

Plate15. Typical microstructure of artificially underaged (UA) Al-Mg-Si alloy at 28^0C for 6hrs, showing particles of Fe_3SiAl_{12} (scriptlike) and precipitates of Mg_2Si (blocky form) in a matrix of Aluminium-rich solid solution. Noted here are clusters of the particles of Fe_3SiAl_{12} dispersoids and very few Mg_2Si phase. Etched in 0.5 percent HF, 500x.

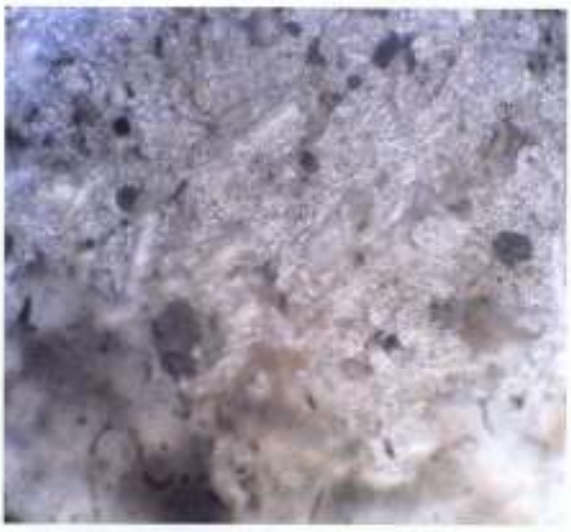

Plate16. Typical microstructure of artificially under-aged (UA) Al-Mg-Si alloy at 160^0C for 6hrs, showing particles of Fe_3SiAl_{12} (scriptlike) and precipitates of Mg_2Si (lamellar/ blocky form) in a matrix of Aluminium-rich solid solution. Noted here are the clusters and the modified forms of the particles of Fe_3SiAl_{12} dispersoids. Etched in 0.5 percent HF, 500x.

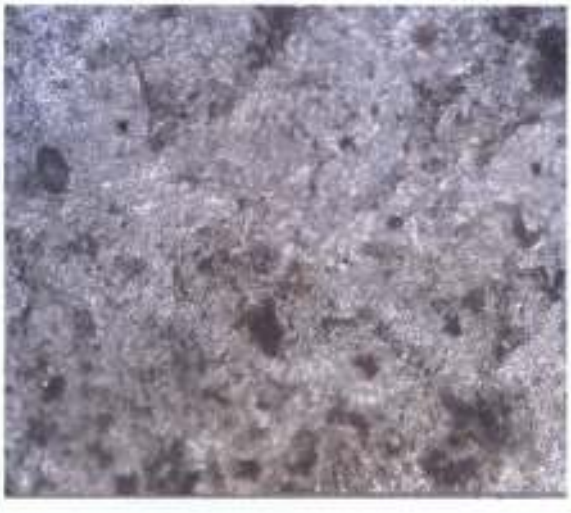

Plate17. Typical microstructure of artificially underaged (UA) Al-Mg-Si alloy at 180^0C for 6hrs, showing particles of Fe_3SiAl_{12} (scriptlike) and insignificantly few precipitates of Mg_2Si (small blocky form) in a matrix of Aluminium-rich solid solution. Noted here are relatively small clusters of the particles of Fe_3SiAl_{12} dispersoids. Etched in 0.5 percent HF, 500x.

Plate18. Typical microstructure of artificially under-aged (UA) Al-Mg-Si alloy at 200^0C for 6hrs, showing particles of Fe_3SiAl_{12} (scriptlike) and very few precipitates of Mg_2Si (small lamellar/ blocky form) in a matrix of Aluminium-rich solid solution.. Etched in 0.5 percent HF, 500x.

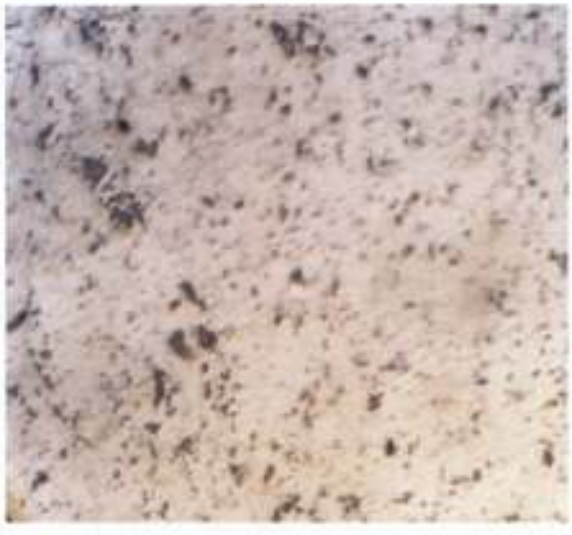

Plate19. Typical microstructure of artificially peak-aged (PA) Al-Mg-Si alloy at 220^0C for 6hrs, showing particles of Fe_3SiAl_{12} (scriptlike) and precipitates of Mg_2Si (small blocky form) in a matrix of Aluminium-rich solid solution. Noted here are relatively smaller forms of the particles of Fe_3SiAl_{12} dispersoids. Etched in 0.5 percent HF, 500x.

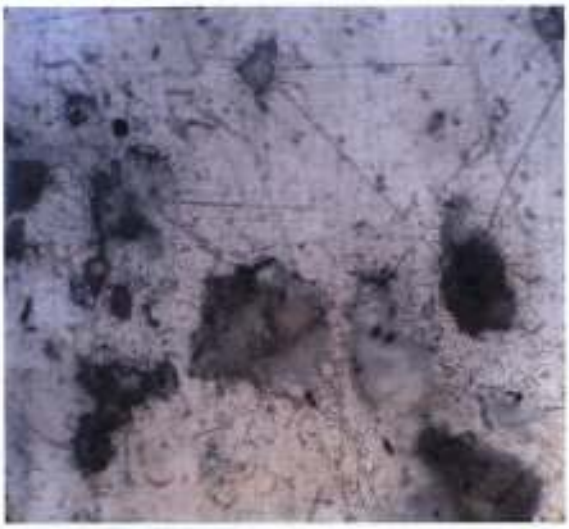

Plate20. Typical microstructure of artificially, strongly over-aged (SOA) Al-Mg-Si alloy at temperatures greater than 200^0C for over 16hrs, showing particles of Fe_3SiAl_{12} (modified scriptlike) and clusters of the precipitates of Mg_2Si (lamellar/ blocky forms) in a matrix of Aluminium-rich solid solution. Etched in 0.5 percent HF, 500x.

These $\beta^{'}$ needles are coherent with the α-Al matrix, which makes them discernible only at high-resolution powers. However, evidences abound in literature that this feature of necessity must be present in substantial number for the alloy to experience any increase in strength at the underage condition. The ageing curves obtained in this work (Figs 4.5-4.6) show increasing strength of the alloy at the underage condition, consequent upon the presence of $\beta^{'}$ needles in the alloy reflected in Plate 6AA.

It is noted that each ageing condition imparts specific mechanical behaviour to the alloy as dictated by the details of the specific microstructural evolutions. The peak age condition has its own characteristic microstructural forms as shown in the optical micrographs in Plates 12, 19 and TEM micrograph in Plate 7AA,

The peak aged alloy has fewer β (Mg_2Si) phase compared to the overaged condition as revealed in Plates 13, 14, 20, 8AA,9AA and 10AA. The α-Al matrix has

dispersed in it particles of Fe_3SiAl_{12}, both coarse and fine forms, as well as platelike particles of Al_5FeSi.

However, all these phases are noted to contribute very little to the enhancement of the tensile strength and plasticity indices of the Al-Mg-Si alloy.

The major phase that enhances the mechanical properties of the Al-Mg-Si alloy is the network of hard, non-shearable coherent β'' needles, homogeneously distributed in the matrix,(Plates 6AA, and 7AA). In a similar work carried out on another composition of Al-Mg-Si alloy by Urreta et al.(2001), TEM micrographs also show clearly the presence of the β'' needles in the peak-aged condition, and showed that a network of hard, fine, non-shearable coherent β'' needles do exist in the aged Al-Mg-Si alloy and are intercepted by dislocations. This precipitate-dislocation interaction was thought to be responsible for the peak values of the tensile properties characteristic of the peak-aged condition. Therefore by analogy the peak tensile properties obtained in the peak age condition in this work can also be thought to arise from the presence of hard, fine, non-shearable and coherent β'' needles, and their interaction with dislocations coupled with the presence of few β'-phase, a semi-coherent rod-like form precipitates.

Also noted in the course of this investigation is the microstructure obtained just immediately after the peak-aged condition. We refer to this as "slightly overaged".

In this circumstance, the β-phase (Mg_2Si) particles are becoming more prominent in size due to the gradual onset of Ostwald ripening. Smaller β'-phase particles that are present in the peak age condition in lesser number than the β'' needles are consumed by the relatively big β-phase particles, such that the latter become bigger. As their number increased, the overage condition tends to deepen. This β-phase is characterized by

relatively low strength because the precipitate-dislocation interaction is thought to take place by the Orowan mechanism,(Fig.2.12,and Plate10AA), which involves by-passing of the precipitates by the dislocations instead of cutting through the precipitates (Frank, 2004; Gracio et al., 2004).

4.3.5 Microstructure of Thermomechanically Aged Al-Mg-Si alloy

(a) Microstructure of Thermomechanically Aged Samples with an initial 25% preageing.

Representative micrographs of samples processed by the TMAI route are shown in Plates 21, 22, 23, 9TMA and 12TMA.

The micrographs show common microstructural features in terms of the second phase dispersoids and precipitates. $Fe_3S_iAl_{12}$, (scriptlike), and Al_5FeSi (platelike), dispersoids and Mg_2Si (lamellar or small blocky form) precipitates in a matrix of Aluminium-rich solid solution, are relatively smaller than for TMAII at lower degree of deformation. However, they tend to reduce in size, but show higher degree of dispersity with increasing degree of deformation. Within the underage region, these second phases in conjunction with GP zones, $\beta^{"}$, and $\beta^{'}$ precipitates coexist (Plates 9TMA–11TMA).

The extent of the evolving microstructural features is guided by the content of the processing parameters. The degree of preageing affects the solute concentration; the higher the degree of preageing, the more the solute content of the solid solution. This leads to higher number of precipitates and a consequent increase in strength due to precipitate-dislocation interaction. The solute concentration of all the samples given 25%

preageing is reflected in the micrographs as light green outlook, and is expectedly similar, but could not be identical by virtue of the varying degree of deformation and final ageing time

The degree of deformation affects the potential sites for precipitation of intermediate phases. Higher degree of deformation leads to greater number of potential sites for precipitation. The more the numbers of fine precipitates or fine particles in a solid solution matrix, the greater the possibility of blockage to dislocation motion and the higher the strength attainable. The peak strength attained by these samples came from the peak aged TMAIE samples, characterized by a relatively more fragmented dispersoids and few Mg_2Si particles as represented by a typical peak aged microstructure (Plates 22 and 24).

The final ageing allows more strengthening precipitates to be formed, hence a higher interaction of precipitate-dislocation network. The longer the ageing time, the higher the number of precipitates; and the higher the ageing temperature, the faster the precipitates are formed. Both factors contributed largely to the improvement in the strength and plasticity of the alloy albeit up to the peak age stage.

The post peak-age stage witnessed a decrease in the strength of the alloy; this is referred to as the overageing stage. As mentioned earlier, this stage is explainable by the Ostwald ripening phenomenon and the Orowan mechanism.

(b) Microstructure of Thermomechanically aged samples with an initial 50% preageing.

Representative micrographs of samples processed by the TMAII route are shown in Plates 25-29.

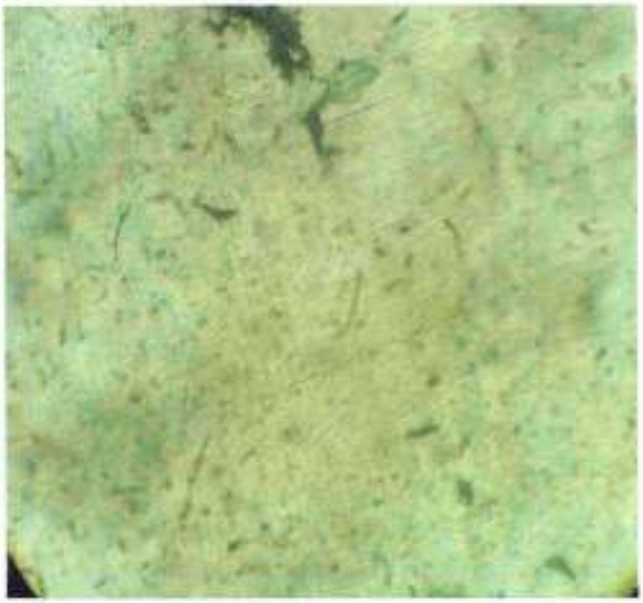

Plate 21. Typical underaged (UA) microstructure of Al-Mg-Si alloy subjected to TMA IA processing route with 10 hrs final ageing time, showing particles of Fe_3SiAl_{12}(scriptlike), and very few precipitates of Mg_2Si (lamellar / small blocky form) in a matrix of Aluminium-rich solid solution. Etched in 0.5 percent HF,400x

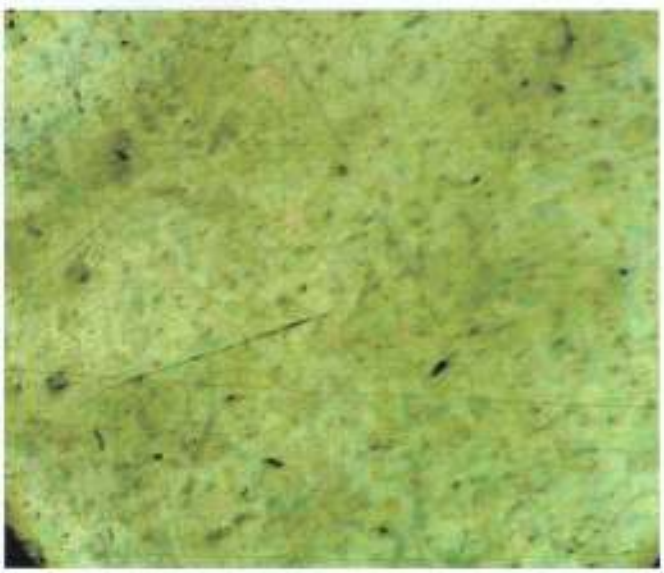

Plate 22. Typical peak aged (PA) microstructure of Al-Mg-Si alloy subjected to TMA IA processing route with 14 hrs final ageing time showing particles of Fe_3SiAl_{12}(scriptlike), Al_5FeSi (platelike), and Mg_2Si (short lamellar/ small blocky form) in a matrix of Aluminium-rich solid solution . The α-Al rich matrix (light green) consists of well dispersed intermediate-phase particles. Etched in 0.5 percent HF, 400x.

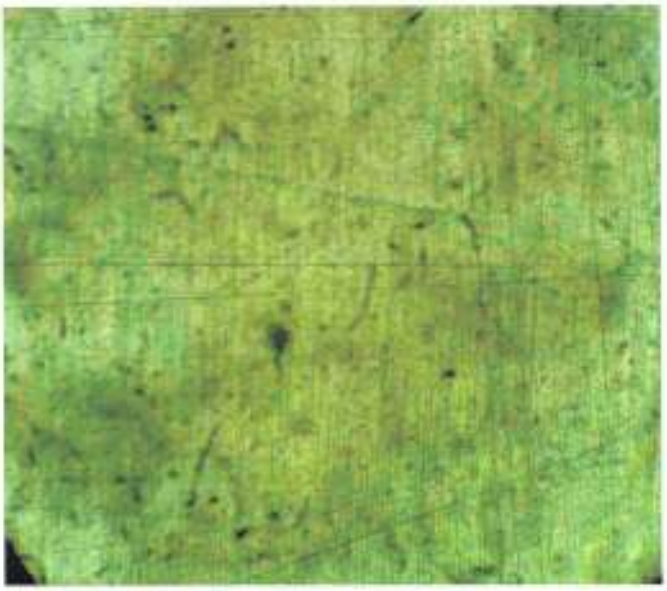

Plate 23 Typical overaged (OA) microstructure of Al-Mg-Si alloy subjected to TMA IA processing route with 20 hrs final ageing time showing particles of Fe_3SiAl_{12}(scriptlike),Al_5FeSi (platelike), and Mg_2Si (lamellar / blocky form) in a matrix of Aluminium-rich solid solution . Etched in 0.5 percent HF,400x

Plate. 24 Typical peak-aged (PA) microstructure of Al-Mg-Si alloy subjected to TMA IC processing route showing particles of Fe_3SiAl_{12}(scriptlike), Al_5FeSi (platelike), and Mg_2Si (short lamellar / small blocky form) in a matrix of Aluminium-rich solid solution . The α-Al rich matrix (light green) has higher solute concentration as a result of 25% preageing. Etched in 0.5 percent HF,400x

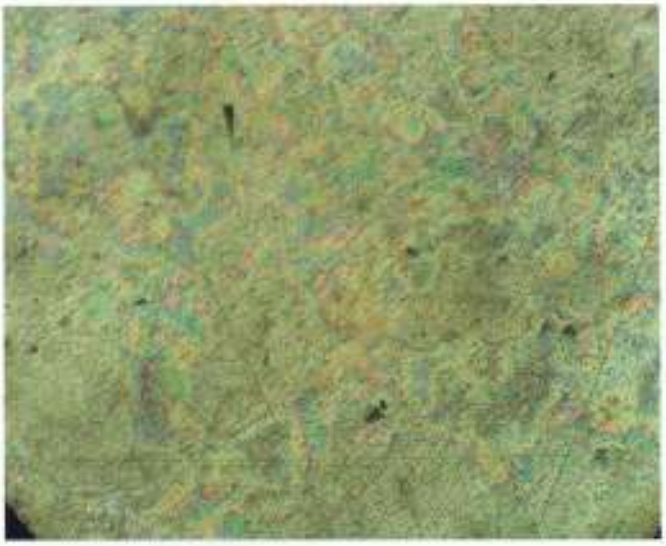

Plate 25 Typical under aged (PA) microstructure of Al-Mg-Si alloy subjected to TMA IIC processing route showing particles of Fe_3SiAl_{12}(scriptlike), and few precipitates of Mg_2Si (small blocky form) in a matrix of Aluminium-rich solid solution . Etched in 0.5 percent HF, 400x.

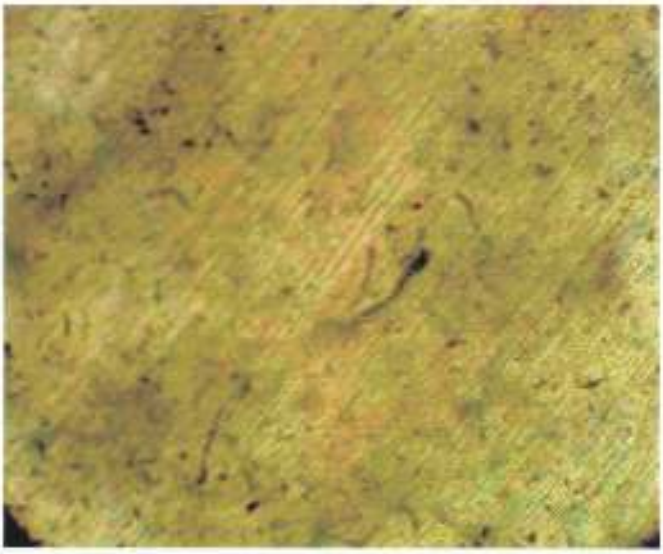

Plate 26 Typical peak aged (PA) microstructure of Al-Mg-Si alloy subjected to TMAIIIC processing route with 10hrs final ageing time, showing particles of redistributed Fe_3SiAl_{12}(scriptlike), and few precipitates of Mg_2Si (small blocky form) in a matrix of Aluminium-rich solid solution . Etched in 0.5 percent HF, 400x.

Plate 27 Typical underaged (UA) microstructure of Al-Mg-Si alloy subjected to TMAIID processing route showing particles of Fe_3SiAl_{12}(scriptlike), and few precipitates of Mg_2Si (small blocky form) in a matrix of Aluminium-rich solid solution . Etched in 0.5 percent HF, 400x.

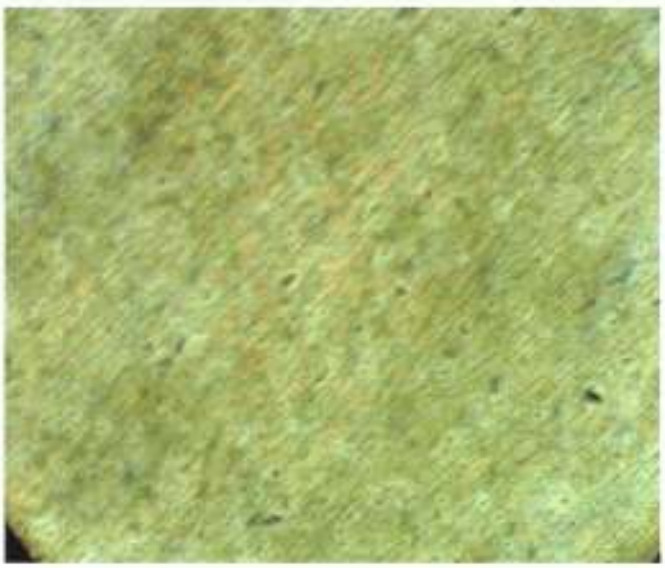

Plate 28 Typical peak aged (PA) microstructure of Al-Mg-Si alloy subjected to TMAIID processing route showing particles of Fe_3SiAl_{12}(scriptlike), and few precipitates of Mg_2Si (lamellar / small blocky form) in a matrix of Aluminium-rich solid solution . Etched in 0.5 percent HF,400x

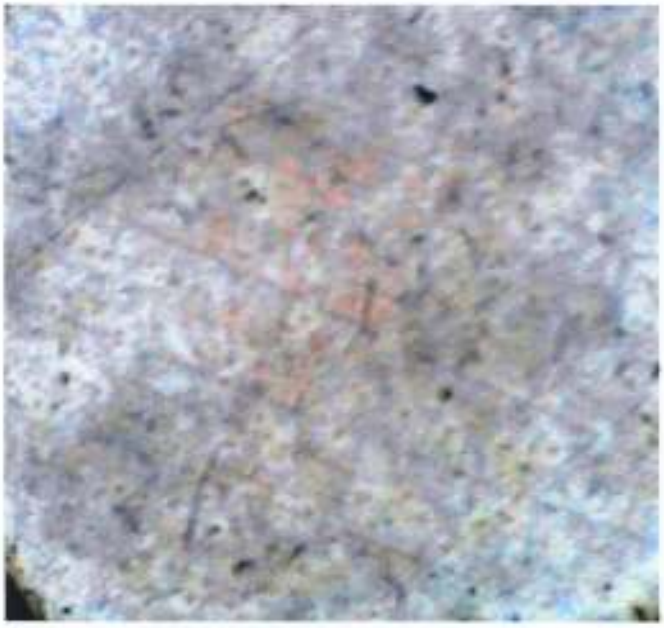

Plate 29 Typical over aged (OA) microstructure of Al-Mg-Si alloy subjected to TMAIID processing route with 20hrs final ageing time, showing particles of Fe_3SiAl_{12}(scriptlike), and precipitates of Mg_2Si (lamella/small blocky form) in a matrix of Aluminium-rich solid solution . Etched in 0.5 percent HF, 400x.

Plate 30 Typical under aged (UA) microstructure of Al-Mg-Si alloy subjected to TMAIIIA processing route showing particles of Fe_3SiAl_{12} (scriptlike) and Mg_2Si (lamellar / small blocky form) in a matrix of Aluminium-rich solid solution. A change in the matrix colouration due to a further increase in solute concentration by virtue of 75% preageing is noted here and for all TMAIII processing routes. Etched in 0.5 percent HF,400x.

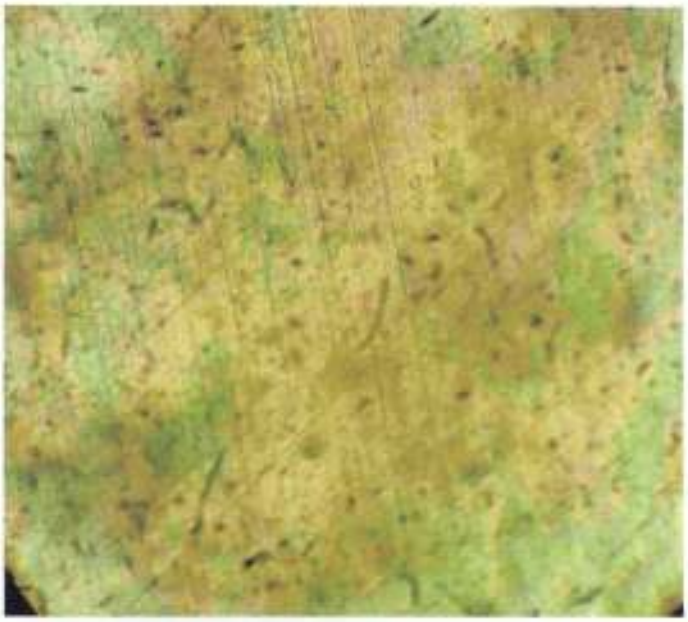

Plate 31 Typical peak aged (PA) microstructure of Al-Mg-Si alloy subjected to TMAIIIA processing route showing particles of redistributed Fe_3SiAl_{12}(scriptlike), and few precipitates of Mg_2Si (lamellar/ small blocky form) in a matrix of Aluminium-rich solid solution . Etched in 0.5 percent HF, 400x.

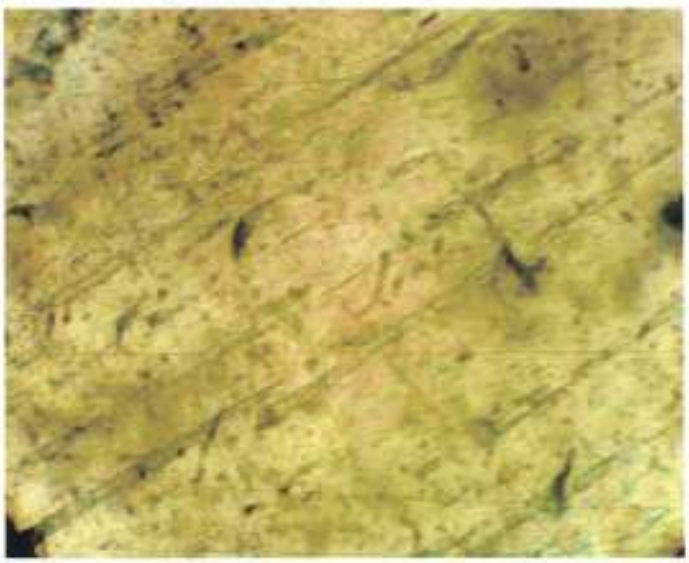

Plate 32 Typical peak aged (OA) microstructure of Al-Mg-Si alloy subjected to TMAIIIA processing route showing particles of Fe_3SiAl_{12} (stretched scriptlike form), and precipitates of Mg2Si (lamellar/ coarse blocky form) in a matrix of Aluminium-rich solid solution. Etched in 0.5 percent HF, 400x.

Plate 33 Typical under aged (UA) microstructure of Al-Mg-Si alloy subjected to TMAIIIB processing route showing particles of redistributed Fe_3SiAl_{12}(scriptlike), and few precipitates of Mg_2Si (small blocky form) in a matrix of Aluminium-rich solid solution . Etched in 0.5 percent HF,400x

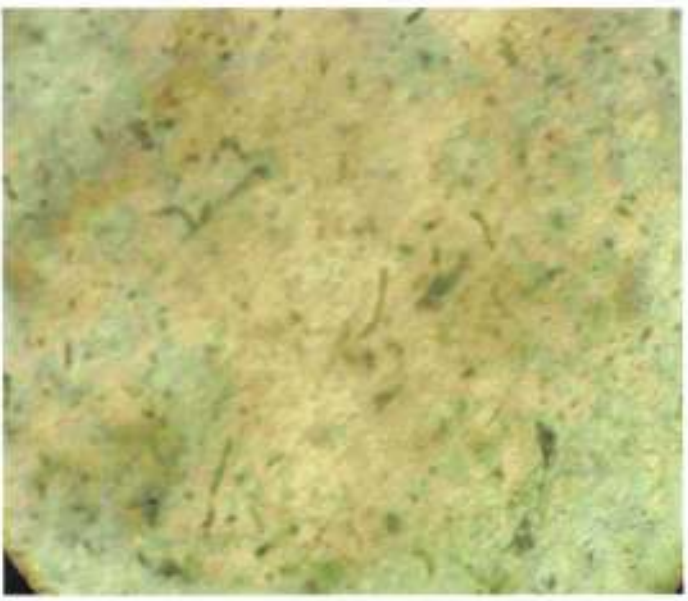

Plate 34 Typical peak aged (PA) microstructure of Al-Mg-Si alloy subjected to TMA IIIB processing route showing particles of Fe_3SiAl_{12}(scriptlike), and few

precipitates of Mg_2Si (lamellar/ tiny blocky form) in a matrix of Aluminium-rich solid solution . Etched in 0.5 percent HF,400x.

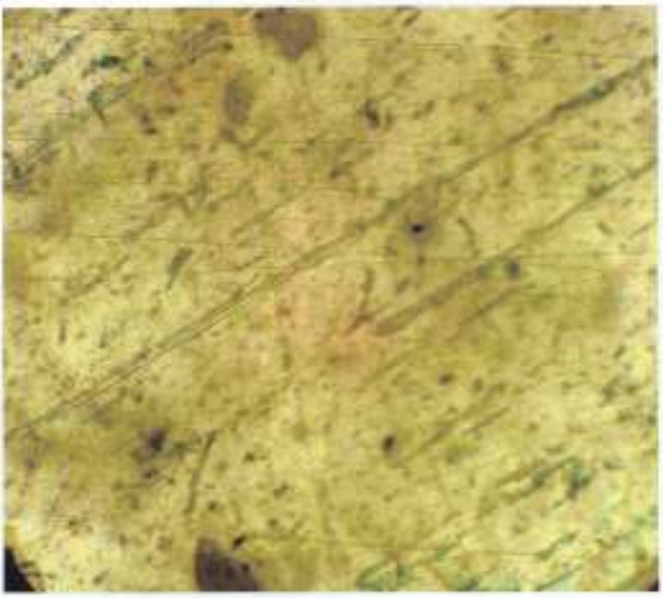

Plate 35 Typical over aged (OA) microstructure of Al-Mg-Si alloy subjected to TMAIIIB processing route showing particles of Fe_3SiAl_{12}(stretched scriptlike form), and precipitates of Mg_2Si (lamellar/ coarse blocky form) in a matrix of Aluminium-rich solid solution . Etched in 0.5 percent HF,400x

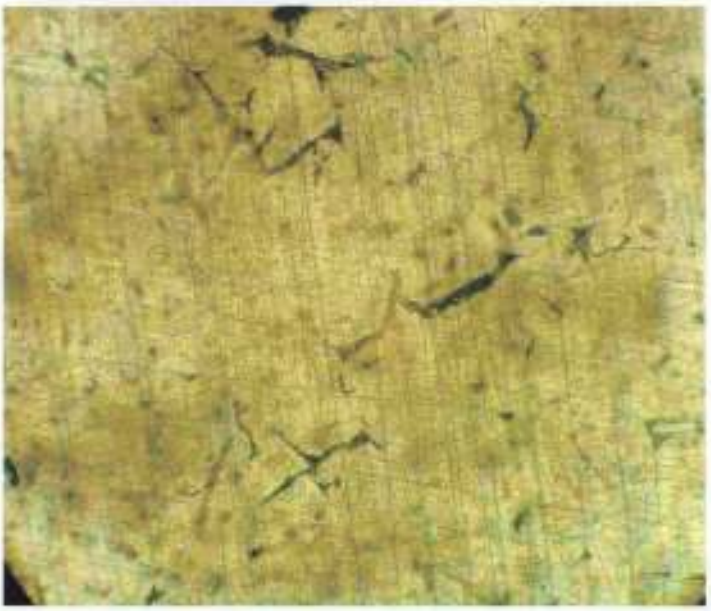

Plate 36 Typical peak aged (UA) microstructure of Al-Mg-Si alloy subjected to TMA IIIC processing route showing particles of Fe_3SiAl_{12}(scriptlike), and few

precipitates of Mg_2Si (small blocky form) in a matrix of Aluminium-rich solid solution . Etched in 0.5 percent HF,400x

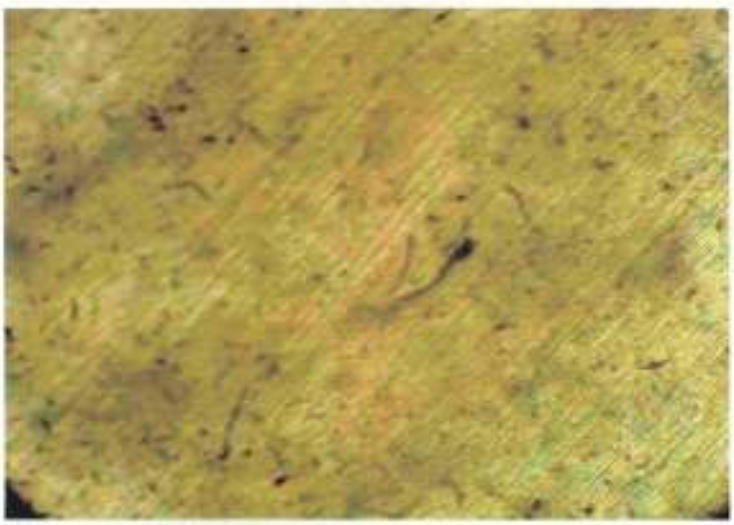

Plate 37 Typical peak aged (PA) microstructure of Al-Mg-Si alloy subjected to TMAIIIC processing route showing particles of redistributed Fe_3SiAl_{12}(scriptlike), and few precipitates of Mg_2Si (small blocky form) in a matrix of Aluminium-rich solid solution . Etched in 0.5 percent HF, 400x.

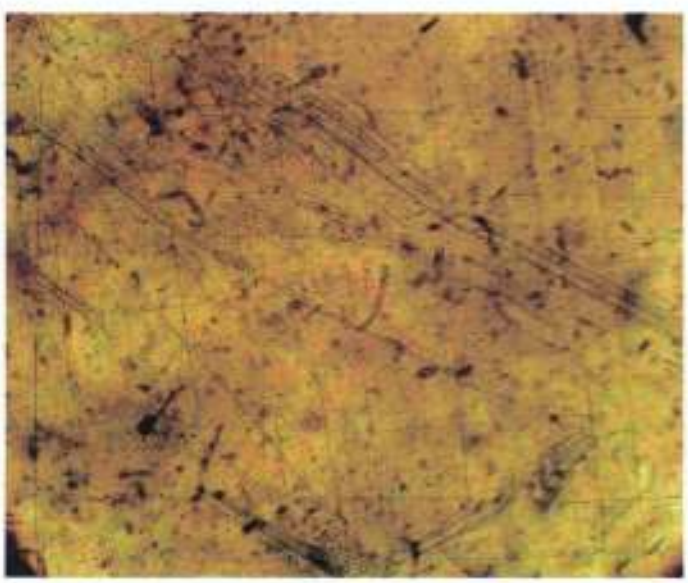

Plate 38 Typical over aged (OA) microstructure of Al-Mg-Si alloy subjected to TMAIIIC processing route showing particles of Fe_3SiAl_{12}(scriptlike), and precipitates of Mg_2Si (lamellar/coarse blocky form) in a matrix of Aluminium-rich solid solution . Etched in 0.5 percent HF,400x

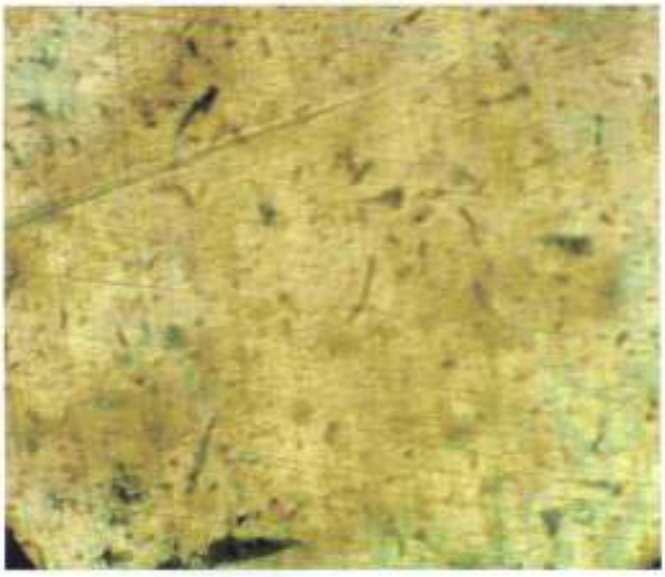

Plate 39 Typical under aged (UA) microstructure of Al-Mg-Si alloy subjected to TMAIIID processing route showing particles of Fe_3SiAl_{12}(scriptlike), and few precipitates of Mg_2Si (lamellar/ small blocky form) in a matrix of Aluminium-rich solid solution . Etched in 0.5 percent HF,400x

Plate 40 Typical peak aged (PA) microstructure of Al-Mg-Si alloy subjected to TMA IIID processing route showing particles of redistributed Fe_3SiAl_{12}(scriptlike), and few precipitates of Mg_2Si (lamellar/ small

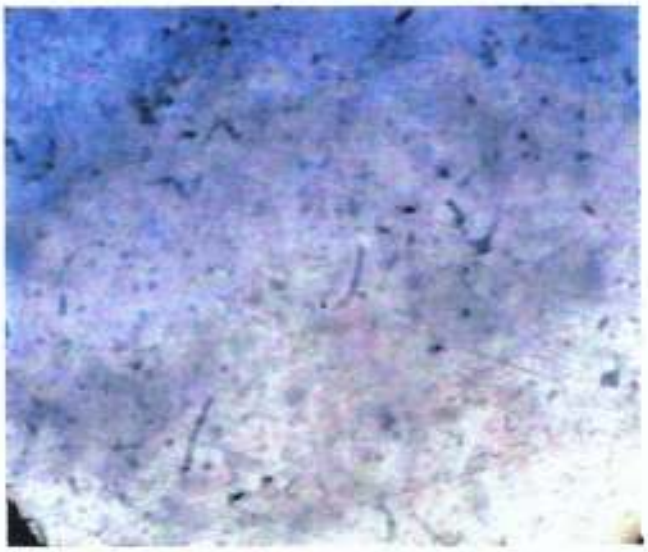

Plate 41 Typical over aged (OA) microstructure of Al-Mg-Si alloy subjected to TMAIIID processing route showing particles of Fe_3SiAl_{12}(scriptlike), and precipitates of Mg_2Si (lamellar/ coarse blocky form) in a matrix of Aluminium-rich solid solution . Etched in 0.5 percent HF, 400x.

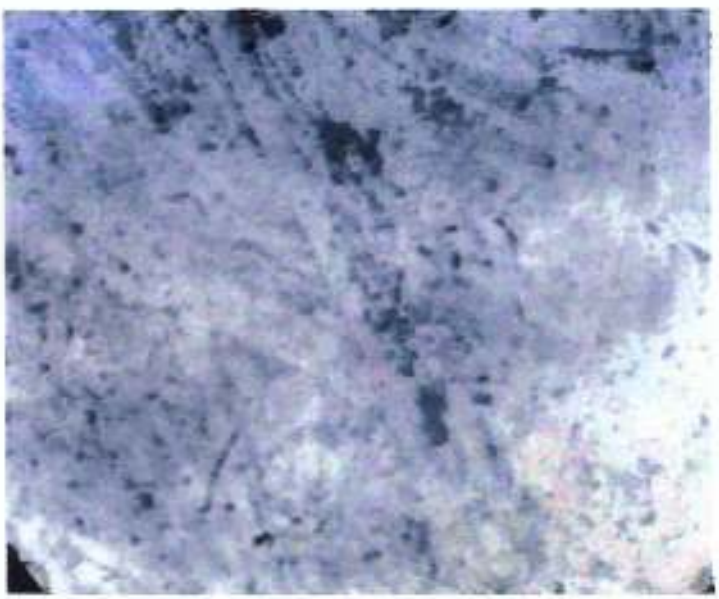

Plate 42 Typical strongly over aged (SOA) microstructure of Al-Mg-Si alloy subjected to TMA IIID processing route showing particles of Fe_3SiAl_{12}(scriptlike), and precipitates of Mg_2Si (lamellar/coarse blocky form) in a matrix of Aluminium-rich solid solution . Etched in 0.5 percent HF, 400x

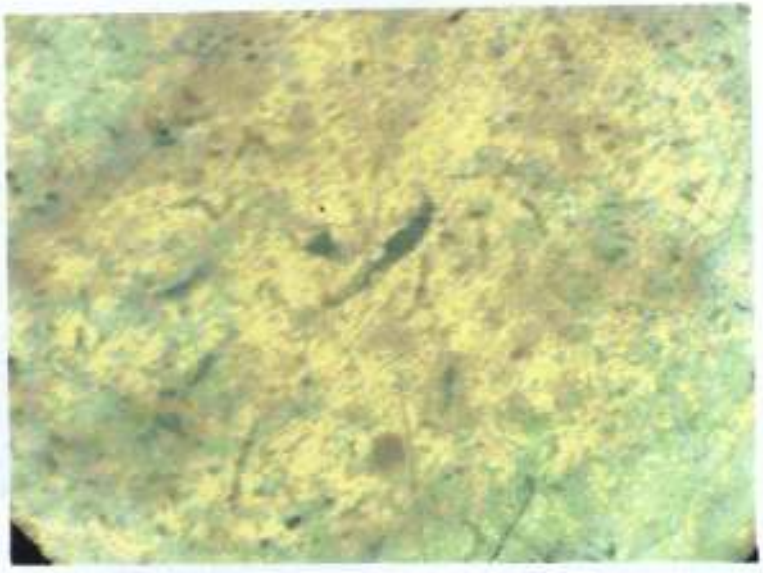

Plate 43 Typical under aged (UA) microstructure of Al-Mg-Si alloy subjected to TMAIIIE processing route showing particles of Fe_3SiAl_{12}(scriptlike), and few precipitates of Mg_2Si (lamellar/ small blocky form) in a matrix of Aluminium-rich solid solution . Etched in 0.5 percent HF, 400x.

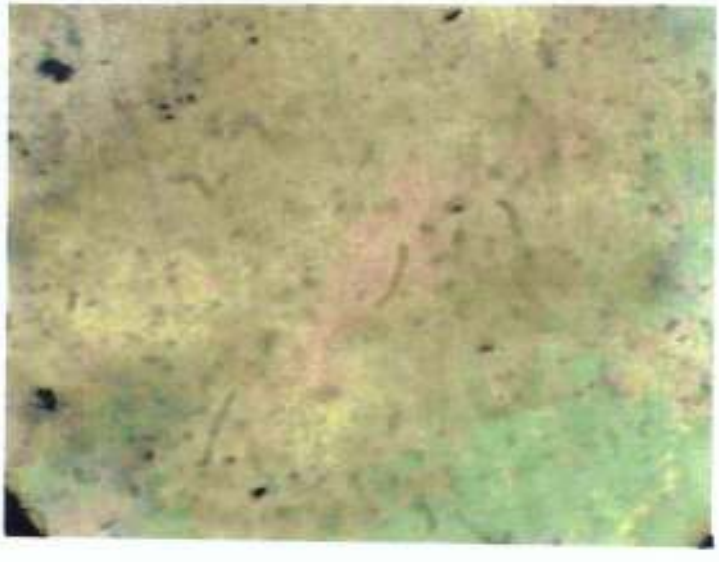

Plate 44 Typical peak aged (PA) microstructure of Al-Mg-Si alloy subjected to TMA IIIE processing route showing particles of redistributed Fe_3SiAl_{12}(scriptlike), and few precipitates of Mg_2Si (lamellar/ small blocky form) in a matrix of Aluminium-rich solid solution . Etched in 0.5 percent HF,400x

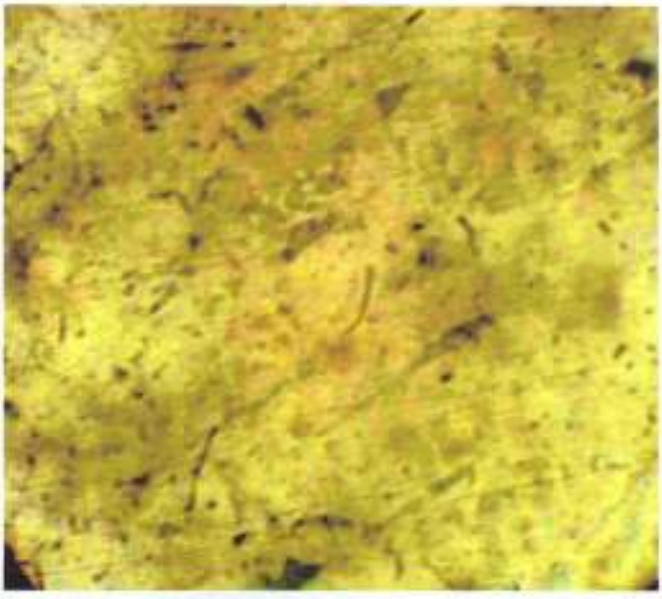

Plate 45 Typical over aged (OA) microstructure of Al-Mg-Si alloy subjected to TMA IIIE processing route showing particles of Fe_3SiAl_{12}(scriptlike), and precipitates of Mg_2Si (lamellar/ coarse blocky form) in a matrix of Aluminium-rich solid solution . Etched in 0.5 percent HF, 400x

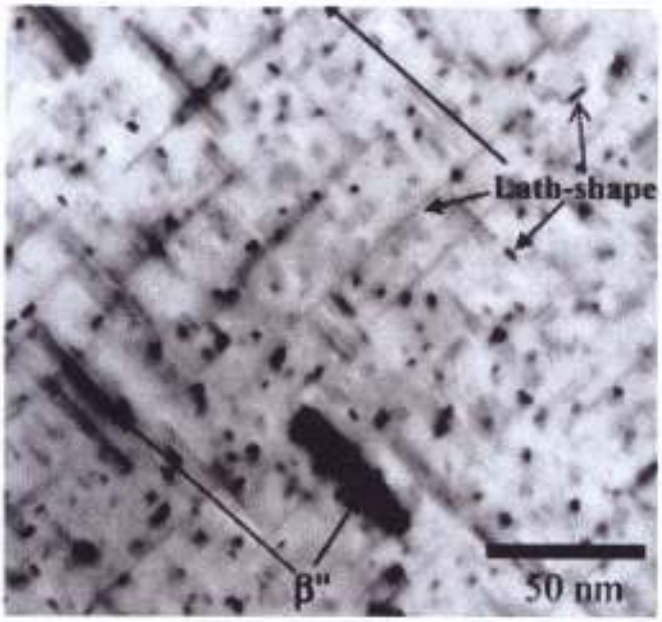

Plate 9TMA Typical TEM micrograph of underaged (UA) Al-Mg-Si alloy subjected to TMA I processing route, showing the GP zones, β", β' precipitates as well as particles of β-phase and Fe_3SiAl_{12} dispersoids all in a matrix of α-Aluminium rich solute solution.

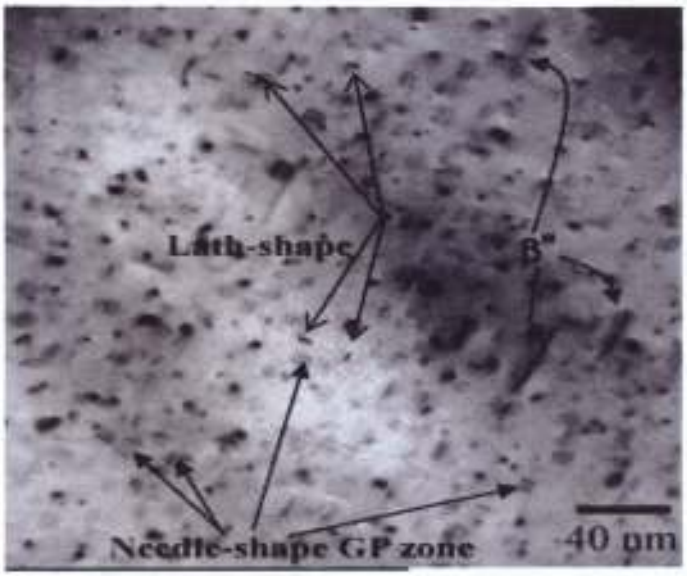

Plate 10TMA Typical TEM microstructures of Al-Mg-Si alloy showing underaged (UA) structure for TMA II alloy at 180°C, 6hrs ageing time and 10%-50% deformation. Needlelike GP zones, β"-phase, and lath-like β'-phase precipitates of high dispersity are noticed. Higher solute content accounts for the fairly dark background. (50% preageing).

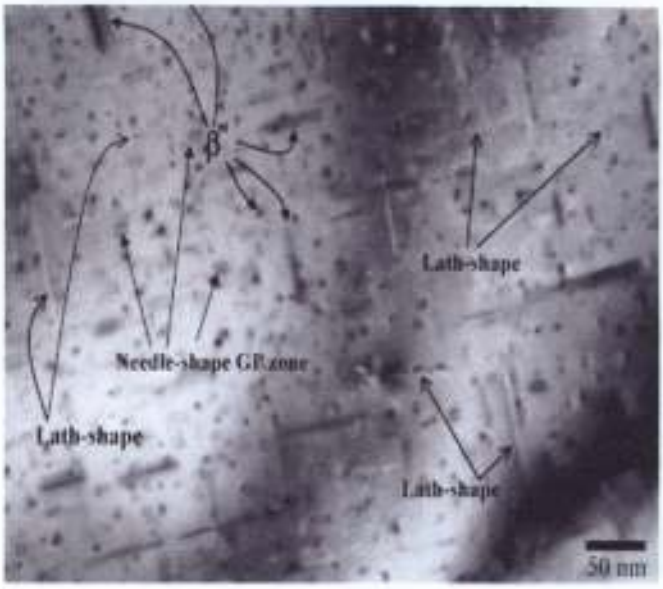

Plate 11TMA Typical TEM microstructures of Al-Mg-Si alloy showing underaged (UA) structure for TMA III alloy at 180°C, 6hrs ageing time and 10%-50% deformation. Needlelike GP zones, β"-phase, and lath-like β'-phase precipitates of high dispersity are noticed. Much higher solute content accounts for the fairly darker background. (75% preageing).

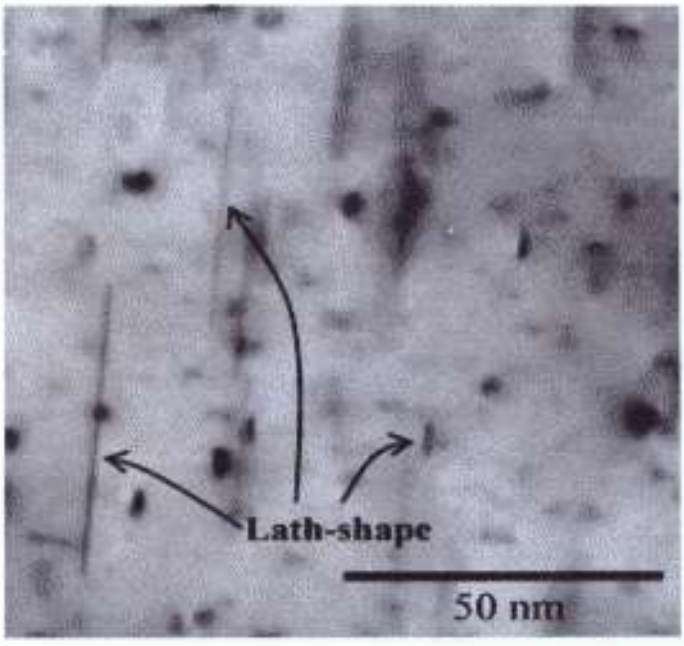

Plate12TMA Typical TEM microstructures of Al-Mg-Si alloy showing few β'-phase (lathlike), Mg_2Si (blocky form) and dispersed Fe_3SiAl_{12} (script-like) particles in peak aged (PA) condition for TMAI. Alloy deformed by 20% at 180°C, aged for 10hrs.

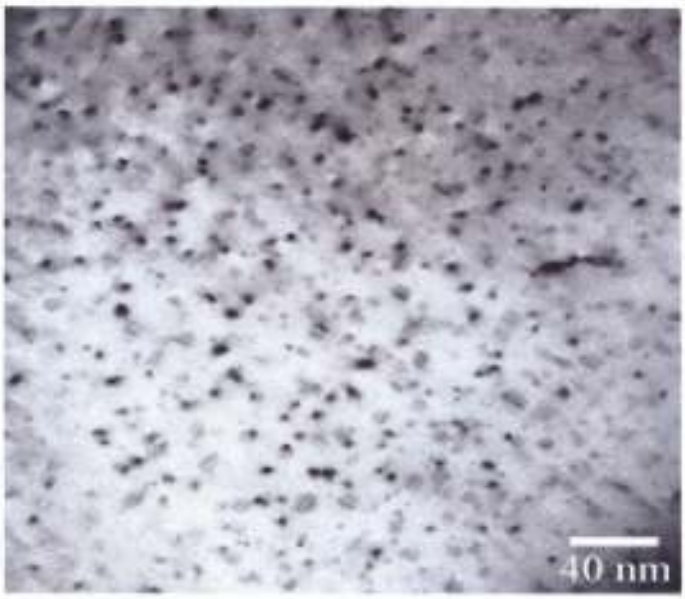

Plate 13TMA: Typical TEM microstructures of Al-Mg-Si alloy showing peak aged (PA) structure for TMA IIIC alloy at 180°C, 10hrs ageing time. Precipitate of β"-phase and β'-phase are observed. They appear as very small lath-like forms and evenly dispersed in the matrix.

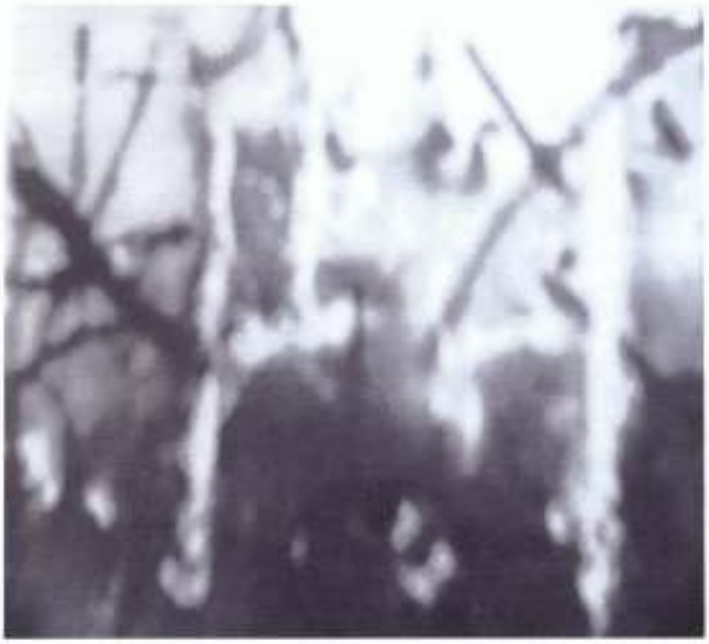

Plate14 TMA. Typical TEM micrograph of Al-Mg-Si alloy subjected to TMAIIIC; 30% deformation at 180°C, aged for 20hrs, showing a dense network of dislocations interfacing with precipitates indicating extensive operation of the Orowan mechanism.

The micrographs show common microstructural features in terms of the second phase dispersoids and precipitates. The average size of Fe_3SiAl_{12} (script like), Al_5FeSi (platelike), dispersoids and Mg_2Si precipitates are comparatively about the same as for TMAI at lower degrees of deformation. However, they tend to reduce in size, but show higher degree of dispersity with increasing degree of deformation. Within the underage region, these second phases in conjunction with GP zones, $\beta^{"}$, and $\beta^{'}$ precipitates coexist,(Plates 21,27,30,33,36,39,43 and 9TMA,10TMA, 11TMA). According to Uan et. al. (2006), the GP zones, $\beta^{"}$ and $\beta^{'}$ precipitates are the phases responsible for the strengthening of the alloy, due to their small size which favour ''shearing mechanism'' of precipitate-dislocation interaction. The dispersoids do not enhance strengthening, but influences improvement in ductility, with little influence on the impact energy.

At the peak aged condition, these microstructural features, with the exception of the GP zones persist (Plates 22,24,25,26,28,31,34,37,40,44,, 12TMA and 13TMA), and more of $\beta^{'}$ precipitates manifest with further increase in ageing time. Beyond the peak age status, the alloy starts to show a downward trend in the amount of $\beta^{"}$ precipitates present, with $\beta^{'}$ and β precipitates taking over alongside the $Al_{12}Fe_3Si$ and Al_5FeSi dispersoids. The β particle is an incoherent equilibrium precipitate which is much larger in size than the $\beta^{"}$ and $\beta^{'}$ precipitates as revealed by both optical and electron micrographs. The β precipitates are too large to give any strengthening effect in the final product.

It is evident from the micrographs, that the solute concentration in the case of 50% preageing is higher than that of 25% preageing. The matrix here shows a deeper grayish appearance, than in 25% preageing. When the alloy becomes strongly overaged, (the strength of the alloy falls), large sizes of varying shapes and distributions, of $Al_{12}Fe_3Si$,

Al_5FeSi, β' and β particles are found in the microstructure, which accounts for the reduced strength. It has been shown by workers such as Urreta et al; (2001), Engler and Hirsch,(2002), Gracio et al; (2004) and Uan et al;(2006) among others, that due to the large size of the particles in overage condition, Orowan mechanism (Plate 10AA) of dislocation-precipitate interaction prevailed, accounting for the reduced strength.

In order for the particle size to remain relatively smaller even in overaged condition, Omotoyinbo et al., (2006), suggested that a large degree of plastic deformation should be employed in a typical thermomechanical processing route.

It is therefore not surprising to find TMAIIE showing the best results (σ_{uts}=321N/mm^2;$\sigma_{0.2}$=279N/mm^2; %ε = 12; toughness =35 J) among the other TMAII processing routes. In TMAIIE, 50% preageing and 50% degree of plastic deformation and 8hrs final ageing time, all at a temperature of 180^{0}C, Plate 28 and 13TMA are representative micrographs of the peak aged structure of TMAII samples, and show a better refined microstructure with mechanical fibering.

(c) Microstructure of thermomechanically aged samples with an initial 75% preageing.

The TMAIII treatments or processing routes consist essentially, 75% preageing, 10%- 50% degree of plastic deformation and a final ageing time, all carried out at 180^{0}C. As expected, the optical micrographs, (Plates 30- 45), all show similar microstructural details.

Each treatment route differs from the other only in the degree of plastic deformation, consequently only differences in the particle size and shape are easily

recognized. 50% deformation shows smaller particle size and better dispersion, thereby giving room for possible dispersion strengthening effect.

In conformity with the composition of the alloy, $Al_{12}Fe_3Si$,(scriptlike), Al_5FeSi,(platelike) dispersoids, as well as very few precipitates of $M_{g2}Si$ are found in the α-Al matrix. With the inception of artificial ageing, GP zones, $\beta^{"}$ particles and $\beta^{'}$ particles precipitate at the underage condition (Urreta et.al. 2001; Uan et.al. (2006), and these precipitates are shown in plate 11TMA.

The peak aged condition reflects the same microstructural features, except that the $\beta^{"}$ and $\beta^{'}$ particles are smaller and precipitated in larger quantities (Plate 13TMA) and these give credence to the peak strength of the alloy at this stage as obtained in each of the figures showing the variation of tensile strength and plasticity with ageing time at 180°C (Figures 4.17-4.20).

The overage condition is characterized by a reduction in the strength of the alloy due to particle coarsening by virtue of prolonged exposure to heat. The $Al_{12}Fe_3Si$, and Al_5FeSi particles tend to coalesce at this moment, with the $\beta^{'}$ and β becoming bigger in size. The $\beta^{"}$ particles at this instance must have dissolved or be engulfed by the bigger particles (Ostwald ripening), (Plates 38, 41, 42, 8AA, and 9AA), which again leads to coarse secondary phase particles and this favours the Orowan mechanism of precipitate-dislocation interaction (Plate 14TMA).

Notwithstanding the fact that large degree of plastic deformation is said to favour greater refinement of grains or particles and higher dislocation density, which in turn is expected to provide higher strength, the results obtained in TMAIIIC (the highest and

best combination of tensile and plasticity parameters obtained in this investigation) show that 30% degree of deformation was better than 50% degree of deformation.

This circumstance is attributable to the fact that the process of dislocation generation is equally accompanied by dislocation annihilation, hence the percentage of dislocation annihilated at the 50% degree of deformation in TMAIIIE is assumed to be large, thereby affecting the effectiveness of the precipitate – dislocation interaction, in terms of strengthening.

It may be concluded from the results of these investigations that improvement or otherwise of the tensile strengths and plasticity indices of the Al-Mg-Si alloy is dependent on the interplay of many processing parameters as well as on the varying interaction of the evolving microstructural features without prejudice to any of the processing variables.

5.0 CONCLUSIONS

Advances in thermomechanical processing techniques have opened a new trend in the development of metallic alloys in the new millennium.

The requirements of Aluminium alloy users are becoming ever more demanding in terms of the need for improved properties, consistency of properties, improved quality and ease of fabrication. To meet these new challenges and remain competitive, Aluminium alloy producers must optimize and tailor the use of thermomechanical processing techniques, improve properties, and reduce cost by adopting the latest process technology.

The overall objective is to maintain the competitiveness of the Aluminium industry in the 21st century by utilizing to the full potential, conventional and new techniques for thermomechanical processing.

In our study of the effects of thermomechanical processing on the microstructure, tensile strengths and plasticity indices of 6063 Aluminium alloy, both conventional and new techniques were explored, and the results obtained compared favourably. The new technique (thermomechanical ageing) portends better prospects for improvement of the processed alloy.

The following conclusions are drawn from the results of this investigation:

1. Thermoplastic working of Al-Mg-Si alloy leads to improved tensile and yield strengths accompanied by a decrease in plasticity indices, especially at low temperatures of deformation (below 200°C).
2. Increase in the degree of deformation and deformation temperature led to a decrease in tensile strength and increase in plasticity indices.

3. It was not possible to increase tensile and yield strengths simultaneously with plasticity indices in any of the thermoplastic working schedules.

4. Microstructural evolutions remarkably affect the tensile and plasticity properties of the alloy.

5. Ageing can be used to improve separately the tensile and plasticity properties of the alloy under specified conditions of heat treatment. Both ageing time and temperature have optimum values for Al-Mg-Si alloy. The optimum ageing temperature is 175°C -180°C, while the optimum ageing time is about 8-10hrs.

6. Ageing time grossly affect the microstructural evolutions in the Al-Mg-Si alloy. Hence, characteristic microstructures are found at underageing, peakageing and overageing conditions, which are dictated by the duration of ageing.

7. Thermomechanical ageing could be used to improve simultaneously the tensile and plasticity properties of Al-Mg-Si alloy under specified processing conditions as obtained in TMA IIIC in this investigation, which happened to produce the best combination of properties,(σ_{uts} =504.03 N/mm^2, σ_y =420.83 N/mm^2, %E= 20.01, impact energy= 35.22 J).

8. Preageing confers higher thermal stability on the alloy, as shown in all the TMA I, TMAII and TMAIII processing routes. In over 85% of the results obtained from the tensile testing of the thermomechanically aged samples, the UTS values are greater than 214N/mm^2.

9. Comparatively, thermomechanical ageing produced results that are slightly superior to the conventional pressure shaping methods.

RECOMMENDATIONS

For the eventual practical application of thermomechanical ageing as an industrial production process more fundamental work is required in terms of mill layout design. However, based on the findings from this research it is recommended that local structural Aluminium alloy producers should endeavour to improve the consistency of the properties of their products by utilizing the technique of thermomechanical ageing, which differs in a number of ways from the conventional method of pressure shaping followed by ageing. This will widen the horizon of the applications of the Al-Mg-Si alloy especially in automobile, machine building, architecture, and civil engineering industries. Acquisition of research facilities in the area of plastic deformation of metallic alloys should be vigorously pursued by the relevant Universities and Research Institutes across the nation in order to encourage meaningful further studies in other aspects of thermomechanical processing of alloys. Facilities such as Electron Probe Analyzer, Scanning/Transmission Electron Microscope and Forming Mills are paramount, if we are to launch into the world of scientific breakthroughs.

REFERENCES

Ashby M.F.Z. (1964). "From Dislocation Mechanisms to New Alloys", Metallkunde. Bd. 55, pp.874-875.

Authier-Martin, M., Forte, G., Ostap, S., and See, J (2001). The Mineralogy of Bauxite for producing Smelter-Grade Alumina. JOM, Vol. 53, No 12 pp.36-40.

Ballufi, R.W., Kehler, G.S., and Simmons R.O. (1963). Recovery and Recrystallization of Metals. Interscience Publ. New York pp.70-75.

Bardossy G. and Aleva G.J.J. (1990). "Lateritic Bauxite" Development in Economic Geology, 27, Amsterdam-Oxford New York; Elsevier. p. 69.

Berstein M.L. (1968). "Thermomechanical Treatment of Metals and Alloys". Journal of Metallurgiya, Moscow. pp.1121-1131.

Beynon J.H. and Sellars C.M. (1992). "Hot Deformation of Aluminium". Iron and Steel Inst. Jpn Int. Vol. 32 No. 3, pp.359-367.

Bielder T.R, Glavicic S.L., and Semiatin S.L. (2002). Using OIM to investigate the Microstructural Evolution of Ti-6Al-4V, JOM, Vol. 54. No. 1, pp.31-36.

Blewitt T.H. Coltman R.R and Redman I.K. (1967). "In dislocation and Mechanical Properties of Crystals". John Wiley, New York pp.335-350.

Boas and Ogilvile G.J. (1954). Deformation of Aluminium and α-Brass crystals. Acta Metal., No 2, pp. 73-76.

Bryant, J.D., (1999). The Effect of preageing treatments on ageing kinetics and mech. Properties in AA 6111 Aluminium autobody sheet, Metall.& Materials Trans.Vol.30A pp. 4125-4135.

Byko Mauren (2002). Aluminium Exhibits its versatility on Art, Life:JOM Vol.52,No.11,p 9.

Cahn R.W. (1974) Ed. Physical Metallurgy. Amsterdam, North-Holand pp. 47-90.

Cai M, Field D.P and Lorimer G.W. (2004). A systematic Comparison of Static and dynamic ageing of two Al-mg-si alloys. Materials Science and Eng. A373 pp. 67-71.

Callister Jr. W.D. (1997). Material Science and Engineering, An Introduction; Arnold Edward Publ. p.507

Celentano, D. J.,(2002): A Thermomechanical model with microstructure evolution for Aluminium alloy casting process. Int. Journal. of Plasticity, 18, pp 1291-1335.

Chalmer, B., and Clark, R. (1954): Bicrystals of Aluminium. Acta Metal, No. 2 pp. 49-60.

Cimenoglu, H.,Sun, Y., and Baydogan, M. (1999): Artificial Ageing of Aluminium Alloys. Mater. Lett. 38, p. 221.

Cornell, R.G., and Bhadeshia, H.K.D.H (1999): "The Aluminum Industry-Annual Review". JOM, Vol. 52, No. 11, p. 4.

Cowdell, R.L. (1986): Aluminium Industry in a Positive Wood. Journal of Metals & Materials, Vol. 2, No.3, p. 123.

Dillamore I.L. and Roberts W.T. (1989): Plastic working effects in Aluminium Alloys. Acta Metallurgy Vol. 12, No.13, pp. 82-85.

Dobatkin V.I. (1965): "On Structural Strengthening of Aluminium alloys". Physical Metallurgy of Light Alloys, MIR Publishers. pp. 85-100.

Duggan B.J. and Roberts W.T. (1975): Dislocations in Deformed Crystalline Solids. Met. Sci. Vol. 9, pp16-24.

Dutkiewicz J. and Litynska L. (2002): The effect of plastic deformation on structure and properties of chosen 6000 series Aluminum alloys. Mat. Sc. & Eng. A 324, pp. 239-243.

Edwards , G.A., Stiller, K., Dunlop, G.L., and Couper, M.J., (1998): Precipitation Strengthening in Metals. Acta Mater. 46. pp. 3893-3904.

El-Baredie Z.M. and El-sayed M. (1996): Effect of double thermomechanical treatments on the properties of 7075 Al. alloy. Journal of Materials Processing Tech. 62, pp. 76-80.

Engler Olaf and Hirsch Jurgen (2002): Texture Control by thermomechanical processing A 336 pp. 249-262.

Frank Ernst (2004): Precipitation Strengthening of Al-Mg-Si. Alloys. Materials Laboratory III, EMSE-290 pp. 1-7.

Fridlander T.N. (1971): Ed. Physical Metallurgy of Aluminium and Aluminium Alloys. Metallurgiya, Moscow p. 352.

Garret R.P., Lin J, and Dean T.A. (2005): An investigation of the effects of solution heat treatment on mechanical properties of AA6xxx alloys. International Journal of Plasticity 21, pp. 1640-1657.

Gaskin A.R.J. (1975): Investigations of the Residual iron-ores of Tonkolili district, Sierra-Leaone. Trans. I.M.M. (Sect. B84, B98-B119).

Gorelik S.S. (1981). Recrystallization in Metals and Alloys, MIR Publishers, Moscow. p. 565

Gracio, J.J., Barlat, F., Rauch, E.F., Jones, P.T., Neto, V.F, and Lopes, A.B. (2004). Artificial Ageing and Shear deformation behaviour of 6022 Aluminium alloy. International Journal of Plasticity, 20, pp. 427-445.

Gulaev A.P. and Leshinskaya R.P. (1980): Kinetics and Sequence of Precipitation on Ageing. Journal of physical metallurgy and Heat treatment Vol. 26, No 9. pp. 71-83.

Gupta A.K., and Lloyd, D.J., in Amberg, L., Lohne, O., Nes, E., Ryum, N., (Eds.), (1992). Precipitation Hardening. Proc. Third Int. Con. on Alloys, No 2, p 21.

Gupta, A.K., Lloyd, D.J., and Court, S.A. (2001). Precipitation hardening processes in an Al-0.4%, Mg-1.3%, Si-0.25% Fe Aluminium alloy. Mater. Sci Eng. A301, pp 140-146.

Hale W.R. (2000): "The Global Light Metals Sector Outlook- A Primary Aluminium Perspective". JOM Vol. 52, No. 11, pp. 26-30

Hasegawa, T. and Yakou, T. (1980): The effect of strain reversal and thermal recovery on stress strain behaviour in Aluminium alloys. Scripta Metall.14, pp1083-1087.

Hatch, J.E., (1984): Aluminium: Properties and Physical Metallurgy. American Society for Metals, Metals Park, OH, USA. pp. 231-233.

Hodgson P.D and Guibbs R.K. (1993): "Thermomechanical Processing of Steel". Iron and Steel Institute Jpn Int. Vol. 32, No. 12, pp. 1329-1338.

Honeycombe R.W.K.(1993): The Plastic Deformation of Metals, Arnold, London. pp.116-300.

Hutchinson W.B. (2000): Effects of Solution Heat Treatment on Mechanical Properties of 6xxx Alloys. Material Science Technology Vol. 5, pp. 118-1127.

Jaoul B. (1967): Dislocation tangles in Solids; J. Mech. Phys. Solids. No. 12, pp. 65-67.

Jensrud, O. (1997): Warm deformation and age hardening response in two Aluminium alloys. Proc. NATA. ASI.,Advance Light Alloys and Composites. Poland. Vol.1, p 90.

Jensrud Ola and Pedersen Ketill (1998): Cold forging of high strength Aluminium alloys and the development of new thermomechanical processing. Journal of Materials Processing Tech. 80-81, pp. 156-160.

John V.B. (1988): Introduction to Engineering Materials. Macmillan, ELBS. pp. 178-179.

Robinson, J.J. (2006): Aluminium, Annual Review. JOM, Vol.92, p. 4.

Jonas J.J. (2000): Thermomechanical Processing of Steel. Metallurgical Review Vol.4, No. 130, pp. 33-43.

Kaczorowskii, M. (1984): "Aluminium" Met.& Mat. Trans. Vol.60, pp.1777-1779.

Kervorkijan V.M. (2002): "Aluminium II". JOM Vol. 51, No 11, pp. 4-10.

Khan, Z.A., Chakkingal, U., and Venugopal, V. (2003): Analysis of forming loads microstructure development and mechanical property evolution during equal channel angular extrusion of a commercial grade Aluminium alloy. Journal of Materials Processing Technology, 135, pp. 59-67.

Kultimann-Wilsdorf D. (1962): Metallographic Analysis. Trans.AIME,Vol. 224, pp.74-92.

Lahktin Yu. M. (1990): Engineering Physical Metallurgy and Heat Treatment, MIR Publishers, Moscow. pp. 371-380.

Marioara, C.D., (2000): TEM study of the precipitates in a 6082 Al-Mg-Si Alloy system. Ph.D Thesis Trondheim, Norway. Pp. 160-168.

Martin, J.W., (1978): Precipitation Hardening 2nd Edition, Butterworths/ Heinemann Oxford p.350.

Matsuda, K., Shimizu, S., Gamada, H., Uetani, Y., Shinagawa F, and Ikeno S. (1999) Thermomechanical Treatment of Steel. Soc. Mater. Sci. Japan 48, pp. 10.

Melvin Tony (1991): Application of Thermal Emission Analysis to Damage Assessmen and Materials Characterization, Ph.D. Thesis, Longhborough University of Technology U.K.

Meyers R.A. (1989): Encyclopedia of Physical Science and Technology, 2nd Edition, Vol. 1 Academic Press Inc. pp. 564-566.

Miao, W.F. and Laughlin, D.E., (1999): Precipitation hardening in Aluminium alloy 6022 Scripta Meterialia. 40, pp.873-878.

Miao, W.F. and Laughlin, D.E., (2000): Effects of Cu content and preageing on precipitation characteristics in Aluminium alloy 6022. Metall. Mater. Trans. A31, pp361-371.

Moons, T., Ratchev, P., Desmet, P., Verlinden, B., and Vanttoutte, P.,(1996): A comparative study of two Al-Mg-Si alloys for automotive applications. Scripta Materialia 35, pp 939-945.

Mott, N.F. (1956): Recrystallization in Deformed Metals. Proc. Phys. Soc, Vol. 64 Part 9 No 381B, pp. 74-92.

MuraYama, M., and Homo, K., (1991): Pre-precipitation clusters and precipitation processes in Al-Mg-Si alloys. Acta. Mater. 47, pp. 1537-1548.

MuraYama, M., and Homo, K., and Laughlin, D.E., (2001): Effect of Cu additions on the precipitation kinetics in an Al-Mg-Si alloy with excess Si. Metall. Mater. Trans. A32, pp. 239-246.

MuraYama, M., and Homo, K., Saga M., Kikuchi, M., (1998): Atom Probe studies on the early stages of precipitation in Al-Mg-Si alloys. Mater. Sci. Eng. A250 pp. 127-132.

Myhr O.R. Grong, Fjaer H.G. and Marioara C.D. (2004): Modeling of the microstructure and strength evolution in Al-Mg-Si alloys during multistage thermal processing. Acta Materialia 52, pp.4997-5008.

Nes, E., (1995): Processes Occurring in Deformed 6xxx Alloys. Scripta. Metal. Mater. 33, p. 225.

Novikov G.I. (1978): Theory of Heat Treatment of Metals. MIR Publishers, Moscow pp. 406-425.

Novikov G.I. and Tiraspolsky V.I. (1970): Phase Transformation in Metals. "Fisika Metalovi metalovidenie Vol. 29, No.4, pp. 45-65.

Ojanuga A.G. (1979): Clay Mineralogy of soils in Nigeria Tropical Savannah Regions. Soil Science Soc. Am. p. 43.

Omotoyinbo J.A., Olorunniwo,O.E, Ogundare, O.,and Oluwole, O.O. (2006): Effect of Degree of Deformation on the mechanical properties of High Temperature Thermomechanically Treated Steel. Journal of Applied Science. 6 (8); pp1762-1765.

Ostap S. (1984): "Effect of Bauxite Mineralogy on its Processing Characteristics" Bauxite (New York: Soc. Mining Eng.) pp. 651-671.

Pavlov. N.N. (1983): Plasticity of Metals and Alloys with peculiar properties. Nauka Academy of Science USSR. Vol. 3, No. 96, pp. 94-98.

Pettersen, T.,Nord-Varhaug, K., and Nes, E.,(1998). Age hardenable Alloys. Proc. Of 6th Int. Conf. on Aluminium Alloys, Vol. 2, p. 751.

Polmear, I.J. (1989): Metallurgy of Light Metals, 2nd Edition, Edward Arnold, Great Britain pp. 50-126.

Polmear, I.J. (1995): Light Alloys-Metallurgy of Light Metals, 3rd Edition, Edward Arnold, London pp. 44-49.

Rabinovich, M.K. (1972): "Thermomechanical Treatment of Aluminium Alloys" Mashinostroenie, MIR Publishers, Moscow pp. 90-115

Rajan, TV. Sharma, C.P. and Sharma, A. (1988): Heat Treatment Principles and Techniques, Prentice-Hall, New Delhi pp. 31-382.

Robert, B.R. (1992): Metallic Materials specification Handbook, 4th Edition, Chapman & Hall, London pp. 10-13.

Seeger, A. (1957): Dislocations and the mechanical properties of crystals, John Wiley, New York pp. 68-98.

Sehnke, E.D. (1996): "World Bauxite and Alumina Production Capacity in the Mid-1990s". Light Metals, ed. W. Hale (Warrendale, P.A. TMS) pp. 115-124.

Sheljaskov, S. (1994): Current level of warm forging technology, J.Mater. Process. Tech, 46, pp 1-2.

Siddique, R.A., Abdullah, H.A., and Al-Belushi, K.R.(2000): Influence of ageing parameters on the mechanical properties of 6063 Aluminium alloy. Journal of Materials Processing Technology, 102, pp. 234-240.

Singh, S. and Goel, D.B. (1990): "Influence of Thermomechanical Ageing on Tensile Properties of 2014 Aluminium Alloy". Journal of Materials Science ol. 25, pp. 3894-3900.

Takeda, M., Ohkubo, F., Shirai, T., and Fukui, K., (1998): Stability of metastable phases and microstructures in the ageing process of Al-Mg-Si ternary alloys. J. mater. Sci. 33, pp 2385-2390.

Thompson, M., and Krammer, M., (1994): Aluminium Alloys for Automobile Bodies. Automatica. 40, p. 1328.

Timmings, R.L. (1989): Engineering Materials, Vol. 1 Longman Group, U.K. p.274.

Uan Jun-Yen, Cho Chi-Yuan, Chen Zhi-Ming and Lin Jun-Kai (2006): Precipitate evolution in underaged Al-Mg-Si alloy during thermal cycling between 250C and 650C. Material Science & Engineering. A419 pp. 98-104.

Urreta, S.E., Louchet, F., and Gharducci, H. (2001): Fracture Behaviour of an Al-Mg-Si industrial alloy. Material Science and Engineering. A302 pp. 300-307.

Usikov, M.P. and Utevsky, R. (1961): Microstructure and Mechanical Properties "Fisika Metalov i Metalovedenie" Vol. 1 No 6. pp 60-70.

Vatne, H.E. Shahani, R, and Nes, E. (1996) "Recrystallization". Acta, mater, Vol. 44 pp. 4447-4461.

Wang, Z.C., and Prangnell, P.B. (2002): Microstructure refinement and mechanical properties of severely deformed Al-Mg-Si alloys. Mat. Sc. and Eng. A328 pp. 87-97.

Webbers, R. and Misra, C. (1987): "Oxide and Hydroxides of Aluminium". Alcoa Technical Paper No 19, Reviewed Version. (Pittsburgh, P.A. Alcoa). p.65.

Weissmann, S., and Hosokawa, N. (1963): "In Recovery and Recrystallization of Metal. New York, p. 78.

West, E.G. (1986): "Aluminium – the first 100 years". Metal and Materials. Vol. 2, No 3, pp. 124-125.

Woodward, Roy (1991): Developments in Aluminium – a review. Metals and Materials, Vol.7, No. 2, pp.96-98.

APPENDIX 1

ble 4.2 Properties of Solution Heat Treated (SHT) 6063 Alloy.

UTS(N/mm^2)	Proof stress (N/mm^2)	%E	Impact energy (J)
297.36	227.76	18.96	40.49

ble 4.3.Variation of Tensile strengths and Plasticity indices with % Deformation at 28°C

Deformation	UTS(N/mm^2)	Proof stress (N/mm^2)	%E	Impact energy (J)
10	241.13	191.35	20	48.2
20	274.09	236.26	18.33	46.08
30	289.04	250.11	15.02	42.25
40	300.22	261	13.85	40.33
50	315.51	272.01	12.11	37.15

ble 4.4. Variation of Tensile strengths and Plasticity indices with % Deformation at 160°C

Deformation	UTS(N/mm^2)	Proof stress (N/mm^2)	%E	Impact energy (J)
10	225	175	14.71	42.66
20	249	210	16.6	49.99
30	255	220	14.18	40.66
40	262	226	10.87	35.55
50	269	232	10.09	32.79

ble 4.5 Variation of Tensile strengths and Plasticity indices with % Deformation at 180°C

Deformation	UTS(N/mm^2)	Proof stress (N/mm^2)	%E	Impact energy (J)
10	238.03	189.13	15.38	56.65
20	254.11	231.15	13.5	55.01
30	260.29	243.32	13.25	32.44
40	269.17	249.02	12.91	25.62
50	269.88	250.09	11.31	20.41

ble 4.6 Variation of Tensile strengths and Plasticity indices with % Deformation at 200°C

Deformation	UTS(N/mm^2)	Proof stress (N/mm^2)	%E	Impact energy (J)
10	237.5	180.14	16.58	58.29
20	258.89	216	14.51	51.03
30	251.07	203	15.08	43.66
40	247.55	198	15.96	45.01
50	238.66	185	16.26	49.78

Table 4.7. Variation of Tensile strengths and Plasticity indices with % Deformation at 220°C

% Deformation	UTS(N/mm^2)	Proof stress (N/mm^2)	%E	Impact energy (J)
10	231	171	17.98	60.56
20	268.5	199	14.66	55..01
30	247.55	181	16.03	44.05
40	201.5	145	14.99	40.63
50	190	145	14.01	42

Table 4.8. Variation of Tensile strengths and Plasticity indices with % Deformation at 240°C

% Deformation	UTS(N/mm^2)	Proof stress (N/mm^2)	%E	Impact energy (J)
10	230	170	18.43	64.01
20	240	185	15.96	58.9
30	168	156	18.76	63.2
40	175	140	19.6	63.4
50	170	131	20.9	65

ble 4.9 Variation of Tensile Strenth and plasticity Parameters with Ageing time at 28°C

eing time (hr)	UTS (N/mm^2)	Proof stress (N/mm^2)	% E	Impact energy (J)
1	264.46	198.66	23.5	51.42
2	275.21	204.98	22.8	48.22
4	286.6	215.12	21	44.95
6	292.29	218.28	19.06	41
8	297.36	227.76	18.96	40.49
10	302.46	228.32	18.43	39.03
12	303.69	228.4	18	37.38
14	306.22	229.68	17.48	35.11
16	310.01	230.93	17	33
20	313.81	233.46	16.4	30.05

ble 4.10 Variation of Tensile Strength and Plasticity Parameters with Ageing time at 160°C

eing time (hr)	UTS (N/mm^2)	Proof stress (N/mm^2)	% E	Impact energy (J)
1	273.32	208.78	23	48.03
2	285.33	215.74	21.2	46.09
4	306.21	231.56	19.1	45.11
6	316.36	245.79	17.5	42.9
8	319.5	259.4	16.1	41.66
10	328.99	265.22	15	40.03
12	331.52	266.35	14.5	40.7
14	334.81	268.89	13.7	38
16	337.85	272.05	13	35.54
20	328.86	266.35	14.6	35.54

ble 4.11 Variation of Tensile Strenth and Plasticity Parameters with Ageing time at 180°C

eing time (hr)	UTS (N/mm^2)	Proof stress (N/mm^2)	% E	Impact energy (J)
1	278.38	213.85	22.5	40.39
2	291.66	227.76	20.5	38.11
4	316.34	253.07	18	37.95
6	328.99	265.73	15.7	35.42
8	335.32	272.05	14.02	32
10	340.38	277.11	13	30.81
12	343	279.01	12.6	30.02
14	339	275	13.8	31.01
16	334.05	272	14.5	33.69
20	322.67	265.72	16.2	36.51

Table 4.12 Variation of Tensile Strenth and Plasticity Parameters with Ageing time at 200°C

Ageing time (hr)	UTS (N/mm^2)	Proof stress (N/mm^2)	% E	Impact energy (J)
1	284.7	221.43	22.1	37.04
2	303.22	246.75	19.8	36
4	341.64	284.7	15.02	35.79
6	347.09	294.19	13.5	32.98
8	354.3	297.43	13.01	30
10	347.97	293.56	12.96	30.88
12	341.64	291.03	13.64	31.22
14	337.22	284.69	16.56	35.6
16	328.97	270.78	18.8	36.08
20	306.85	256.24	19.16	38.66

Table 4.13 Variation of Tensile Strenth and Platicity Parameters with Ageing time at 220°C

Ageing time (hr)	UTS (N/mm^2)	Proof stress (N/mm^2)	% E	Impact energy (J)
1	291.03	240.4	21	26.77
2	316.97	262.56	19.01	26
4	351.14	291.03	14.02	25.04
6	360.62	303.68	12	25.33
8	354.3	291.66	13.4	25.88
10	335.52	284.71	16.66	26.11
12	328.99	274.58	18	26.67
14	316.34	264.46	19.02	26.67
16	310.01	259.4	19.63	27.01
20	296.09	246.74	20	27.25

Table 4.14: Variation of Tensile Strength and Plasticity with Ageing Time for TMA IA Schedule

Ageing time (hr)	UTS (N/mm^2)	Proof stress (N/mm^2)	% E	Impact energy (J)
1	215	175.01	18.4	56.78
2	219.01	195.06	18	56.65
4	226.06	201.09	17.54	48.67
6	234.02	205	16.02	40.56
8	240	220	15.11	33.12
10	251	229.03	14	25.01
12	264.03	240.02	13.39	22.44
14	277	251.01	12	20.32
16	263.04	238	13.5	21.63
20	256.03	224.05	14.02	24.33

Table 4.15 Variation of Tensile Strength and Plasticity with Ageing Time for TMA IB Schedule

Ageing time (hr)	UTS (N/mm^2)	Proof stress (N/mm^2)	% E	Impact energy(J)
1	222	183.01	18.1	56.21
2	228	202	17.82	56
4	233	210	17.2	48.18
6	245	213	15.86	40.15
8	248	226.03	14.96	32.79
10	257.01	234	13.8	24.76
12	279	246.01	11.5	20.12
14	274.02	240	13.26	21.41
16	270	235.05	13.4	22.22
20	265	228.01	13.88	24

Table 4.16 Variation of Tensile Strength and Plasticity with Ageing Time for TMA IC Schedule

Ageing time (hr)	UTS (N/mm^2)	Proof stress (N/mm^2)	% E	Impact energy (J)
1	224	185.01	17.64	55.08
2	231	204.09	17.3	54.88
4	235	212	16.85	47.22
6	246.5	216.5	15.54	39.15
8	250.48	229.5	14.5	32.16
10	260	236.34	13.52	24.26
12	283	248.46	11.2	19.5
14	277.01	242.4	13	20.98
16	272	237.42	13.2	21.77
20	267.65	230.29	13.6	23.52

Table 4.17 Variation of Tensile Strength and Plasticity with Ageing Time for TMA ID Schedule

Ageing time (hr)	UTS (N/mm^2)	Proof stress (N/mm^2)	% E	Impact energy
1	227.03	187.01	17.2	53.7
2	233.5	206.13	16.87	53.5
4	237.56	215	16.43	46.04
6	248.96	219.5	15.15	38.17
8	235	232	14.12	31.35
10	263.02	238.7	13.18	23.6
12	286	251	10.92	19
14	279.78	245	12.68	20.4
16	274.72	240	12.87	21.2
20	270.33	232.6	13.2	22.9

Table 4.18. Varia riation of Tensile Strength and Plasticity with Ageing Time for TMA 1E Schedule

Ageing time (hr)	UTS (N/mm^2)	Proof stress (N/mm^2)	% E	Impact energy (J)
1	231.04	191	16.7	52.2
2	237.6	210.25	15.8	52
4	241.74	219.3	14.65	44.8
6	245.85	224.01	13.66	37.14
8	258.06	236.64	12.6	30.5
10	292.26	256.02	9.5	18.96
12	298	252.5	11.62	19.4
14	285.37	250	13.03	19.84
16	280.21	245.01	13.98	20.63
20	275.74	237.25	12	22.28

Table 4.19: Variation of Tensile strengths and Plasticity with Ageing time for TMA IIA Schedule.

Ageing time(hr)	UTS (N/mm^2)	Proof stress (N/mm^2)	% E	Impact energy (J)
1	228.5	188.22	17.03	52.66
2	232	208.16	16.13	52.43
4	236.66	217.07	15.01	45.12
6	240.5	220.59	14.09	37.4
8	260	240.16	13	31
10	294	252.89	11.5	18.62
12	290.5	250.06	12.4	19.31
14	281.5	247.23	12.97	19.99
16	278	242.2	13.01	20.77
20	274.5	233.78	13.55	22.3

Table 4.20: Variation of Tensile strengths and Plasticity with Ageing time for TMA IIB Schedule.

Ageing time(hr)	UTS (N/mm^2)	Proof stress (N/mm^2)	% E	Impact energy
1	231.93	190.04	16.9	52.23
2	236.08	211.28	16	52.03
4	240.21	220	14.89	44.77
6	244.12	234.04	13.98	37.11
8	264	237.51	12.9	30.76
10	298.41	255	11.41	18.48
12	293.85	253.5	12.3	19.15
14	285.21	250.93	12.89	19.84
16	282.17	245.83	12.91	20.61
20	278	237	13.45	22.13

Table 4.21: Variation of Tensile strengths and Plasticity with Ageing time for TMA IIC Schedule.

Ageing time(hr)	UTS (N/mm^2)	Proof stress (N/mm^2)	% E	Impact energy
1	235.64	195.08	16.5	51.13
2	240	216.46	15.78	51.01
4	244.05	225.32	14.67	44.24
6	249.96	238.87	13.72	36.28
8	268.43	241.31	12.08	28.52
10	304.28	266.58	11.23	18.33
12	299.57	258.93	12.02	19
14	286.76	255.44	12.51	19.68
16	283.66	249.76	12.81	20.45
20	279.12	242.82	13.3	21.98

Table 4.22:Variaton of Tensile strengths and Plasticity with Ageing time for TMAIID Schedule

Ageing time(hr)	UTS (N/mm^2)	Proof stress (N/mm^2)	% E	Impact energy (J)
1	241.45	200	16.1	49.9
2	243.84	219.92	15.41	49.2
4	248.95	228.9	14.32	43.19
6	254.96	242.69	13.39	35.42
8	312.15	271	11.5	17.98
10	304	263.07	11.75	18.25
12	292.03	260	12.25	18.5
14	288	253.75	12.53	19
16	283.58	246.72	12.98	19.96
20	272.74	245.17	11.79	21.4

Table 4.23: Variation of Tensile strengths and Plasticity with Ageing time for TMAIIE Schedule.

Ageing time(hr)	UTS (N/mm^2)	Proof stress (N/mm^2)	% E	Impact energy (J)
1	248	205.31	16.43	52
2	254.58	225.43	15.66	51.3
4	256.08	234.54	14.48	45.29
6	262	248.76	13.5	38.52
8	320.8	278.86	11.98	34.81
10	316.49	269.55	12.08	36
12	300.23	266.41	12.72	38.58
14	295.1	260	12.83	39.9
16	290.75	252.78	13	41.91
20	280.01	251.21	13.44	44

Table 4.24: Variation of Tensile strengths and Plasticity with Ageing time for TMAIIIA Schedule

Ageing time (hr)	UTS (N/mm^2)	Proof stress (N/mm^2)	% E	Impact energy (J)
1	309.69	241.69	19.83	42.77
2	329.79	258.75	19.04	38.33
4	346.46	286.45	18.2	28.68
6	353.57	292.57	17.11	24.81
8	391.32	311.02	15.08	20.7
10	367.47	302.47	17.89	22.59
12	342.39	276.89	17.28	23.68
14	331.11	260.98	18.13	26.4
16	319.26	247.24	19.46	30.06
20	302.59	222.39	20.36	33.88

Table 4.25: Variation of Tensile strengths and Plasticity with Ageing time for TMAIIIB Schedul

Ageing time (hr)	UTS N/mm (N	Proof stress (N/mm^2)	% E	Impact energy (J)
1	352.19	280.19	22.93	45.14
2	375.04	298.37	22.02	41.28
4	391.72	312.83	21.3	30.09
6	410.24	326.73	20.82	26.35
8	422.33	336	20	24
10	443.22	350.01	19.03	21.99
12	414.39	330.67	19.98	25.16
14	386.04	307.56	20.96	28.08
16	365.08	267.44	22.5	32.14
20	347.52	251.74	23.85	35.99

Table 4.26: Variation of Tensile strengths and Plasticity with Ageing time for TMAIIIC Schedu

Ageing time (hr)	UTS (N/mm^2)	Proof stress (N/mm^2)	% E	Impact energy (J)
1	400.51	338	23.4	57.29
2	426.5	359.47	22.76	52.99
4	450.01	370.34	21.98	48.89
6	466.53	391.09	21.24	43.92
8	478	404.05	20.6	39.6
10	504.03	420.83	20.01	35.22
12	471.25	398.3	21	40.67
14	439	366.88	21.89	46.08
16	415.17	340.9	22.99	51.48
20	395.2	324.02	23.73	57.66

Table 4.27: Variation of Tensile strengths and Plasticity with Ageing time for TMAIIID Schedu

Ageing time (hr)	UTS (N/mm^2)	Proof stress (N/mm^2)	% E	Impact energy (J)
1	384.09	324.05	22.9	53.94
2	408.97	341.76	21.99	48.85
4	432.6	362	21	46.03
6	447.19	382.05	20.74	40.33
8	459.44	399.44	19.88	36
10	484.92	404.62	18.52	33.16
12	452.82	385.82	19.01	38.29
14	421.22	353	20.93	42.38
16	397.88	327.08	21.76	48.64
20	378.29	297.01	23	54.01

Table 4.28 Variation of Tensile strengths and Plasticity with Ageing time for TMAIIIE Schedule

Ageing time (hr)	UTS N/mm	Proof stress	% E	Impact energy (J)
1	245.04	195	17.34	41.04
2	258.83	210.38	16.66	36.99
4	261.35	219.04	14.32	32.05
6	274.11	239.61	13	26.22
8	336.07	284.07	11.29	21.55
10	319.43	296	12.48	23.89
12	301.99	248.8	12.99	27.38
14	291.75	229.44	13.07	31.66
16	277.94	211	13.98	36.37
20	255.3	198.03	14.7	38.44

Table 4.29: Change of properties with increasing degree of deformation (at 25 PA, 8 hrs ageing time)

	UTS(N/mm^2)	Proof Stress (N/mm^2)	% E	Impact energy (J)
TMAIA	240	220	15.11	33.12
TMAIB	248	226	14.96	32.79
TMA IC	250.48	229	14.5	32.16
TMA ID	253	232	14.12	31.35
TMA IE	258	236.64	12.6	30.5
SHT	297	227.76	18.96	40.49

Table4.30: Change of Properties with Increasing Degree of Deformation (at 50 PA, 8 hrs Ageing time

	UTS(N/mm^2)	Proof Stress (N/mm^2)	% E	Impact energy (J)
TMAIIA	260	234	13	31
TMAIIB	264	267.51	12.9	30.76
TMA IIC	268.43	241.31	12.08	28.52
TMA IID	312.15	271	15.5	17.98
TMA IIE	320.8	278.86	11.98	34.87
SHT	297.36	227.76	18.98	40.49

Table 4.31: Change of properties with increasing degree of deformation (at 75 PA, 8 hrs Ageing Time

	UTS(N/mm^2)	Proof Stress (N/mm^2)	% E	Impact energy (J)
TMAIIIA	391.32	311.02	15.08	20.7
TMAIIIB	422.33	336	20	24.6
TMA IIIC	478	404.05	20.6	39.6
TMA IIID	459.44	399.44	19.88	36
TMA IIIE	336.07	284	11.29	21.55
SHT	297.36	227.76	18.96	40.49

Table 4.32: Change in Tensile Strength and Plasticity with increasing Degree of preaging (at 180°C, 10% Deformation, 8hrs Ageing Time)

	UTS(N/mm^2)	Proof stress (N/mm^2)	% E	Impact energy (J)
TMA IA25PA	240	220	15.11	33.12
TMA IIA50PA	260	234	13	31
TMA IIIA75PA	391.32	311.02	15.08	20.7
SHT	297.36	227.76	18.96	40.49

Table 4.33: Change in tensile strength and Plasticity with increasing Degree of preaging (at 180°C, 20% Deformation, 8hrs Ageing Time)

	UTS(N/mm^2)	Proof stress (N/mm^2)	% E	Impact energy (J)
TMA IB 25PA	248	226.03	14.96	32.79
TMA IIB 50PA	264	237.51	12.9	30.76
TMA IIIB 75PA	422.33	336	20	24
SHT	297.36	227.76	18.96	40.49

Table 4.34: Change in tensile strength and Plasticity with increasing Degree of preaging (at 180°C, 30% Deformation, 8hrs Ageing Time)

	UTS(N/mm^2)	Proof stress (N/mm^2)	% E	Impact energy (J)
TMA IC 25PA	250.48	229.5	14.5	32.16
TMA IIC 50PA	268.43	241.31	12.08	28.52
TMA IIIC 75PA	478	404.05	20.6	39.6
SHT	297.36	227.76	18.96	40.49

Table 4.35: Change in tensile strength and Plasticity with increasing Degree of preaging (at 180°C, 40% Deformation, 8hrs Ageing Time)

	UTS(N/mm^2)	Proof stress (N/mm^2)	% E	Impact energy (J)
TMA ID 25PA	253	232	14.12	31.35
TMA IID 50PA	312.15	271	11.5	17.98
TMA IIID75PA	459.44	399.44	19.88	36
SHT	297.36	227.76	18.96	40.49

Table 4.36: Change in Tensile Strength and Plasticity with increasing Degree of Preaging (at 180°C, 50% Deformation, 8hrs Ageing Time)

	UTS(N/mm^2)	Proof stress (N/mm^2)	% E	Impact energy (J)
TMAIE 25 PA	258.06	236.64	12.6	30.5
TMAIIE 50 PA	320.8	278.86	11.98	34.81
TMAIIIE 75 PA	336.07	284.07	11.29	21.55
SHT	297.36	227.76	18.96	40.49

APPENDIX II

VISUAL BASIC PROGRAMME TO PREDICT SELECTED TENSILE/PLASTICITY PROPERTY IN 6063 ALLOY

```
Begin VB.Form Form1
  Caption       = "Ultimate Function"
  ClientHeight  = 8010
  ClientLeft    = 60
  ClientTop     = 345
  ClientWidth   = 8745
  LinkTopic     = "Form1"
  ScaleHeight   = 8010
  ScaleWidth    = 8745
  StartUpPosition = 3 'Windows Default
  Begin VB.PictureBox Picture1
    Appearance    = 0 'Flat
    BackColor     = &H80000005&
    ForeColor     = &H80000008&
    Height        = 2055
    Left          = 840
    Picture       = "Modelling (Yield Strength).frx":0000
    ScaleHeight   = 2025
    ScaleWidth    = 7065
    TabIndex      = 14
    Top           = 120
    Width         = 7095
  End
  Begin VB.CommandButton Exit
    Caption       = "EXIT"
    Height        = 495
    Left          = 6000
    TabIndex      = 11
    Top           = 6960
    Width         = 1575
  End
  Begin VB.CommandButton Calculate
    Caption       = "CALCULATE"
    Height        = 495
    Left          = 3600
    TabIndex      = 10
    Top           = 6960
    Width         = 1575
  End
  Begin VB.CommandButton Clear
    Caption       = "CLEAR"
    Height        = 495
    Left          = 1200
```

```
  TabIndex      = 9
  Top           = 6960
  Width         = 1455
End
Begin VB.TextBox Result
  Height        = 375
  Left          = 4080
  TabIndex      = 8
  Top           = 6000
  Width         = 1455
End
Begin VB.TextBox Final
  Height        = 375
  Left          = 5640
  TabIndex      = 7
  Top           = 4920
  Width         = 1335
End
Begin VB.TextBox Initial
  Height        = 375
  Left          = 5640
  TabIndex      = 6
  Top           = 4200
  Width         = 1335
End
Begin VB.TextBox C
  Height        = 375
  Left          = 5640
  TabIndex      = 5
  Top           = 3480
  Width         = 1335
End
Begin VB.TextBox Gamma
  Height        = 375
  Left          = 5640
  TabIndex      = 4
  Top           = 2760
  Width         = 1335
End
Begin VB.TextBox E
  Height        = 375
  Left          = 2520
  TabIndex      = 3
  Top           = 4920
  Width         = 1335
End
Begin VB.TextBox Alpha
  Height        = 375
  Left          = 2520
  TabIndex      = 2
```

```
  Top         = 4200
  Width       = 1335
End
Begin VB.TextBox K
  Height      = 375
  Left        = 2520
  TabIndex    = 1
  Top         = 3480
  Width       = 1335
End
Begin VB.TextBox D
  Height      = 375
  Left        = 2520
  TabIndex    = 0
  Top         = 2760
  Width       = 1335
End
Begin VB.Label Result1
  Alignment   = 1 'Right Justify
  AutoSize    = -1 'True
  Caption     = "A(T)"
  Height      = 195
  Left        = 3360
  TabIndex    = 21
  Top         = 6000
  Width       = 300
End
Begin VB.Label Final1
  Alignment   = 1 'Right Justify
  AutoSize    = -1 'True
  Caption     = "T(Final)"
  Height      = 195
  Left        = 4680
  TabIndex    = 20
  Top         = 4920
  Width       = 525
End
Begin VB.Label Initial1
  Alignment   = 1 'Right Justify
  AutoSize    = -1 'True
  Caption     = "T(Initial)"
  Height      = 195
  Left        = 4680
  TabIndex    = 19
  Top         = 4200
  Width       = 555
End
Begin VB.Label C1
  Alignment   = 1 'Right Justify
  AutoSize    = -1 'True
```

```
  Caption      = "C"
  Height       = 195
  Left         = 5160
  TabIndex     = 18
  Top          = 3480
  Width        = 105
End
Begin VB.Label Gamma1
  Alignment    = 1 'Right Justify
  AutoSize     = -1 'True
  Caption      = "Gamma"
  Height       = 195
  Left         = 4800
  TabIndex     = 17
  Top          = 2880
  Width        = 540
End
Begin VB.Label E1
  Alignment    = 1 'Right Justify
  AutoSize     = -1 'True
  Caption      = "E(O)"
  Height       = 195
  Left         = 1770
  TabIndex     = 16
  Top          = 4920
  Width        = 315
End
Begin VB.Label Alpha1
  AutoSize     = -1 'True
  Caption      = "Alpha"
  Height       = 195
  Left         = 1680
  TabIndex     = 15
  Top          = 4200
  Width        = 405
End
Begin VB.Label K1
  Alignment    = 1 'Right Justify
  AutoSize     = -1 'True
  Caption      = "K"
  Height       = 195
  Left         = 1950
  TabIndex     = 13
  Top          = 3480
  Width        = 105
End
Begin VB.Label D1
  Alignment    = 1 'Right Justify
  AutoSize     = -1 'True
  Caption      = "D(T)"
```

```
    Height        =  195
    Left          =  1740
    TabIndex      =  12
    Top           =  2760
    Width         =  315
  End
End
Attribute VB_Name = "Form1"
Attribute VB_GlobalNameSpace = False
Attribute VB_Creatable = False
Attribute VB_PredeclaredId = True
Attribute VB_Exposed = False


Private Sub Clear_Click()

D.Text = ""
K.Text = ""
Alpha.Text = ""
E.Text = ""
Gamma.Text = ""
C.Text = ""
Initial.Text = ""
Final.Text = ""
Result.Text = ""

End Sub

Private Sub Calculate_Click()

Dim D1 As Double
Dim K1 As Double
Dim Alpha1 As Double
Dim E1 As Double
Dim Gamma1 As Double
Dim C1 As Double
Dim Initial1 As Double
Dim Final1 As Double
Dim Result1 As Double
Dim w1 As Double
Dim x1 As Double
Dim y1 As Double
Dim z1 As Double
Dim R1 As Double

D1 = D.Text
K1 = K.Text
Alpha1 = Alpha.Text
E1 = E.Text
Gamma1 = Gamma.Text
```

```
C1 = C.Text
Initial1 = Initial.Text
Final1 = Final.Text


w1 = D1 ^ (1 - Gamma1)
x1 = K1 * E1
y1 = ((2 * Final1) - Initial1) / Initial1
z1 = (x1 / (K1 + Log(Alpha1 * y1))) ^ Gamma1
R1 = C1 * z1 * w1

Result1 = Round(R1, 4)

Result.Text = Result1

End Sub

Private Sub Exit_Click()

End

End Sub
```